SOLID SOLUBILITY OF SILVER IN THE SUPERCONDUCTING $YBa_2Cu_3O_x$ COMPOUND

by

CHONGMIN ZHANG

B.S.(Ceramics), Shanghai University of Science and Technology, China, 1982

M.S.(Ceramics), Shanghai Institute of Ceramics, Chinese Academy of Science, 1985

A THESIS IN PARTIAL FULFILMENT OF

THE REQUIREMENTS FOR THE DEGREE OF

MASTER OF APPLIED SCIENCE

in

THE FACULTY OF GRADUATE STUDIES

Department of Metals and Materials Engineering

We accept this thesis as conforming

to the required standard

THE UNIVERSITY OF BRITISH COLUMBIA

December, 1991

In presenting this thesis in partial fulfilment of the requirements for an advanced degree at the University of British Columbia, I agree that the Library shall make it freely available for reference and study. I further agree that permission for extensive copying of this thesis for scholarly purposes may be granted by the head of my department or by his or her representatives. It is understood that copying or publication of this thesis for financial gain shall not be allowed without my written permission.

(Signature) _____

Department of Metals and Materials Engineering

The University of British Columbia
Vancouver, Canada

Date Dec 24, 1991

DE-6 (2/88)

ABSTRACT

The solubility of silver in the $YBa_2Cu_3O_x$ compound has been studied. Ceramic $YBa_2Cu_3O_x$ pellets with added silver ranging from 0 to 10 wt% were prepared and characterized by X-ray diffraction (XRD), optical microscopy, scanning electron microscopy (SEM), energy dispersive X-ray spectroscopy (EDX), wavelength dispersive X-ray spectroscopy (WDX), and secondary ion mass spectrometry (SIMS). The lattice parameters were precisely determined by a rigorous X-ray diffraction method and by using a USGS computer program which uses an iterative least square solution to calculate the lattice parameters and the standard deviations. The final precisions are ±0.0005Å for lattice parameters a and b, and ±0.001Å for the lattice parameter c.

Silver appears to be present within the $YBa_2Cu_3O_x$ grains. More intragranular silver was found inside quenched samples than slowly cooled samples. In both cases the silver solubility increased with the nominal silver concentration, which reached a constant level as the nominal silver concentration exceeded 2.5 wt%. The maximum silver solubilities are 0.41 and 0.37 wt% for samples quenched from 950°C and slowly cooled to room temperature, respectively. The intragranular silver concentrations were found to be much lower than the nominal silver concentrations added to the system.

Along with the increasing intragranular silver concentrations, lattice parameters a and c, and unit cell volume of the orthorhombic $YBa_2Cu_3O_x$ phase increased and appeared to reach constant values at higher silver concentrations. Lattice constant b remains relatively unchanged for all silver concentrations. Structural chemistry analyses suggest that the dissolved silver ions may substitute copper ions at Cu(1) sites of the $YBa_2Cu_3O_x$ unit cell. The maximum atomic fraction of Cu substituted by Ag is about 0.023 at room temperature, *i.e.* y~0.023 for $YBa_2Cu_{3-y}Ag_yO_x$. The maximum value of y is about 0.025 for samples quenched from 950°C.

Normalized resistance was also found to increase with the silver concentration, which attained a constant value at higher silver concentrations. Critical temperatures (T_c) are not significantly affected by the silver additions whereas the critical current density (J_c) is marginally improved for the sample with nominal silver concentration of 0.5 wt%.

Table of Contents

List of Figures

List of Tables

ACKNOWLEDGEMENT

It is my sincere pleasure to thank my research supervisor, Dr. Chaklader, for his encouragement and guidance throughout the course of my work on this project. Thanks are also extended to the faculty, staff and fellow graduate students in the Department of Metals and Materials Engineering, especially to Dr. Alina Kulpa and Mr. Glenn Roemer for their many valuable discussions and help.

The financial support from the department in the form of research and teaching assistantships is sincerely acknowledged.

The J_c measurement provided by Mr. Reinhold Krahn in Department of Physics is gratefully acknowledged.

My special thanks are to my wife, Xiyi, for her understanding, support and patience throughout my graduate study, and for her sharing the happiness and hardships in the past years.

1 INTRODUCTION

1.1 The Breakthrough of Copper Oxide High T_c Superconductors

The discovery of high-temperature superconductivity in Ba-La-Cu-O ceramic oxides with a critical temperature (T_c) at 30K by Nobel laureates Bednorz and Müller[1] in 1986 and the subsequent confirmation and extension of this discovery by several groups in USA, China, and Japan triggered large scale research efforts worldwide. Superconductivity at temperature about 90K, which breaks down the temperature barrier of liquid nitrogen (77K), was reported in March 1987 in the Y-Ba-Cu-O system[2]. The general formula of these new high-temperature superconducting compounds is $RBa_2Cu_3O_{7-x}$, where R is a rare earth element which is most commonly Y and it is usually also referred to as 123 compound as it is known because of the stoichiometric ratio of its cations. Achievement of superconductivity at such a high temperature has had two important consequences. First, this discovery has acted as a catalyst in re-opening the interest of the scientific community and stimulated basic research across a broad spectrum of disciplines and applied research. The interest arises out of the fact that the discovery, contrary to earlier predictions by many theorists, demonstrates that superconductivity can occur not only at high temperature but also in a wide range of oxides whose concentration of charge carriers is low. Second, and most importantly, this discovery has re-kindled the interest of industrial community in the development and applications of high temperature superconducting materials. Previously, the widespread use of superconducting materials was limited by the necessity of using expensive liquid helium (at $4 per liter) as the cryogen. With the development of new copper oxide superconducting materials which can be operated by cooling with inexpensive liquid nitrogen (at 25¢ per liter), the economic viability of superconductors' applications has dramatically improved. Moreover, liquid nitrogen has an exceptional high latent heat of evaporation. In an

hour one watt of heat will evaporate 1.4 liters of liquid helium but only 0.016 liters of liquid nitrogen. This effect in large scale applications of superconductors is obvious and the cost to maintain a cryogenic system has been reduced to 1/1,400, excluding the reduction in thermal insulation, by using high temperature superconducting materials.

Although several claims of superconductivity in the Y-Ba-Cu-O system at temperatures near 270K have been reported[3], most measurements indicate that only a small portion of a specimen exhibits superconductivity at the higher temperature. Furthermore, the apparent high-temperature superconductivity disappears over time[4]. Two other notable oxide superconductors: $Bi_2Sr_2CaCu_2O_8$ (T_c=110K) and $Tl_2Ba_2Ca_2Cu_3O_{10}$ (T_c=122K) were discovered subsequent to the discovery of $YBa_2Cu_3O_x$. Figure 1 shows the critical temperatures of historic superconductors *versus* their discovery year. This illustrates the dramatic progress triggered by Bednorz and Müller.

There are two interesting features of these ceramic superconductors. First, wide chemical substitutions for certain transition elements can be made without seriously degrading the critical temperature. Second, all of these ceramic superconductors have a layered structure derived from the perovskite structure. Table 1 lists the critical temperatures of the $RBa_2Cu_3O_x$ group, where R is given. Another large group of ceramic superconductors is of the type $(AO)_mM_2Ca_{n-1}Cu_nO_{2n+2}$, where the A cation can be Tl, Bi, Pb or a mixture of them. The value of m is 1 or 2, and the M cation is Ba or Sr. The superconducting compounds in this family and their critical temperatures are shown in Table 2. In these layered structure compounds, Cu-O layers (also called basal planes) are the essential parts of the layer structure and the oxygen ordering in the Cu-O layers is crucial to the superconductivity of these ceramic superconductors. Unlike other transition elements in these ceramic superconductors, Cu can only be partially

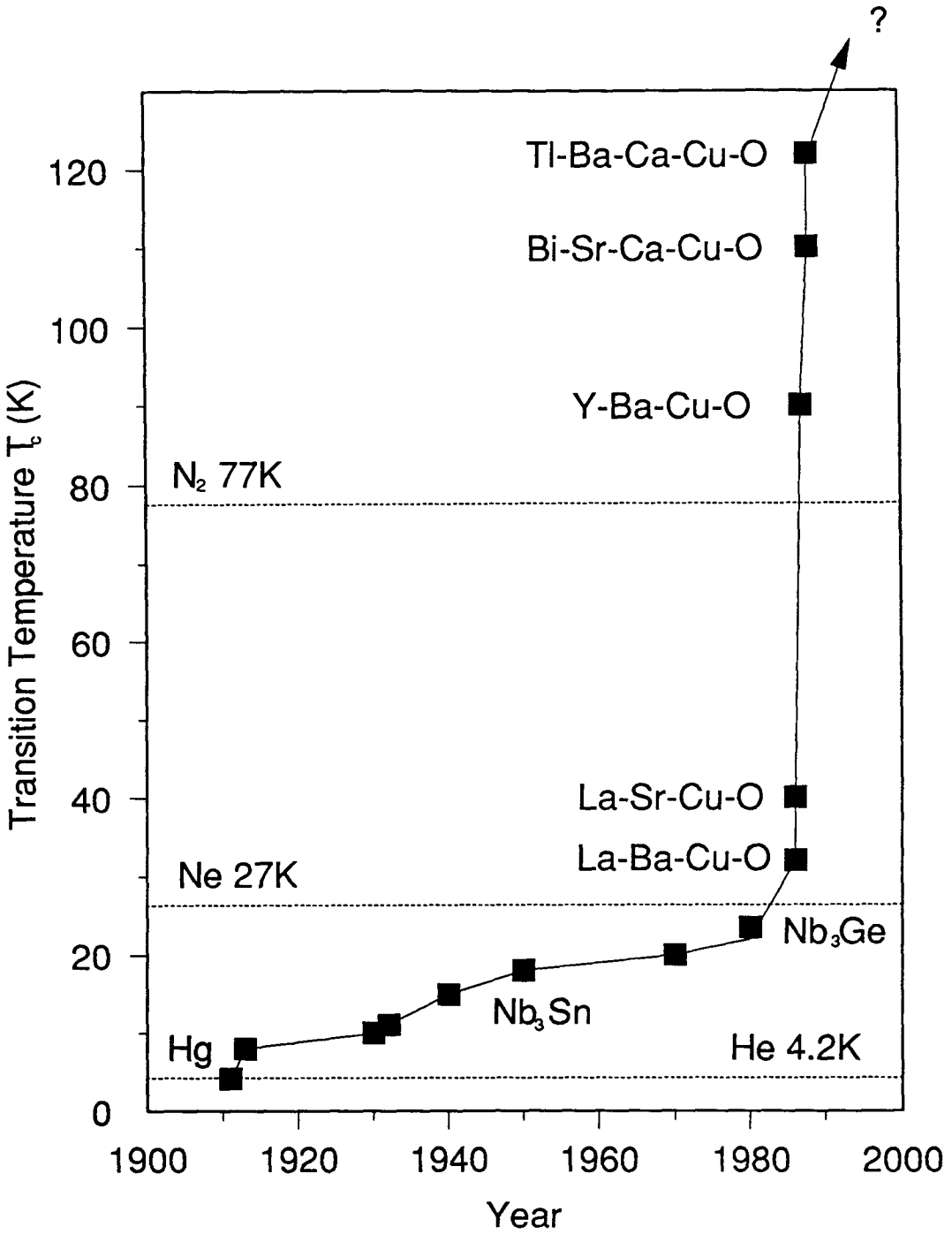

Figure 1 The time evolution of the superconducting transition temperature.

Table 1 Critical Temperatures of $RBa_2Cu_3O_x$ Group[5]

R	T_c (K)
Eu	94
Nd	92
Gd	92
Y	91
Dy	91
Tm	91
Er	91
Ho	91
Sm	88
Lu	88
Yb	86

Table 2 Compounds and Critical Temperatures of $(AO)_mM_2Ca_{n-1}Cu_nO_{2n+2}$ Family[5]

Compound	T_c (K)
$TlBa_2CaCu_2O_7$	90
$TlBa_2Ca_2Cu_3O_9$	110
$TlBa_2Ca_3Cu_4O_{11}$	122
$(Tl,Bi)Sr_2CuO_5$	50
$(Tl,Bi)Sr_2CaCu_2O_7$	90
$(Tl,Pb)Sr_2CaCu_2O_7$	90
$(Tl,Pb)Sr_2Ca_2Cu_3O_9$	122
$Tl_2Ba_2CuO_6$	90
$Tl_2Ba_2CaCu_2O_8$	110
$Tl_2Ba_2Ca_2Cu_3O_{10}$	122
$Tl_2Ba_2Ca_3Cu_4O_{12}$	119
$Bi_2Sr_2CuO_6$	12
$Bi_2Sr_2CaCu_2O_8$	90
$Bi_2Sr_2Ca_2Cu_3O_{10}$	110
$Bi_2Sr_2Ca_3Cu_4O_{12}$	90

substituted by other elements otherwise the superconductivity would be destroyed. Due to the second feature described above these superconductors, including La-Sr-Cu-O compounds, are also known as high T_c cuprates.

Perovskite structure (Figure 2), originated from the mineral perovskite ($CaTiO_3$), is one of the typical structures for ABO_3 compounds. In this structure, large cations A and anions O combine to form a close-packed cubic structure with the smaller, more highly charged B cations in the octahedral interstices. The coordination numbers are 12 and 6 for A cations and B cations, respectively. The unit cell of $YBa_2Cu_3O_x$, as illustrated in Figure 3, contains three distorted perovskite building blocks, in which Y and Ba cations are at A sites, and Cu at B sites. For the orthorhombic phase of $YBa_2Cu_3O_x$, O5 sites are empty and O1 sites are filled orderly by oxygen whereas in the tetragonal phase of $YBa_2Cu_3O_x$, O1 and O5 sites are either disorderly occupied or empty. The structures of bismuth- and thallium-containing superconductors (Figure 4) consists of perovskite-like units containing one, two, or three CuO_2 planes sandwiched between Bi-O or Tl-O bilayers. For the thallic compounds, these CuO_2 planes can also be separated by Tl-O monolayers.

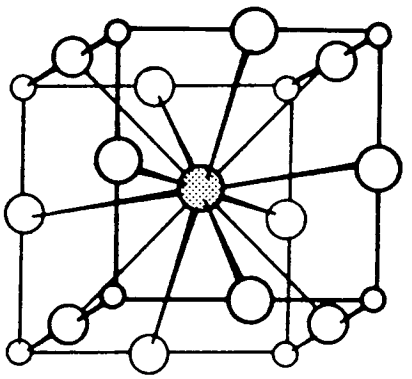

Figure 2 The perovskite structure for ABO_3 compounds. Large open circles represent O ions, the shaded circle A, and the small circles B ions.

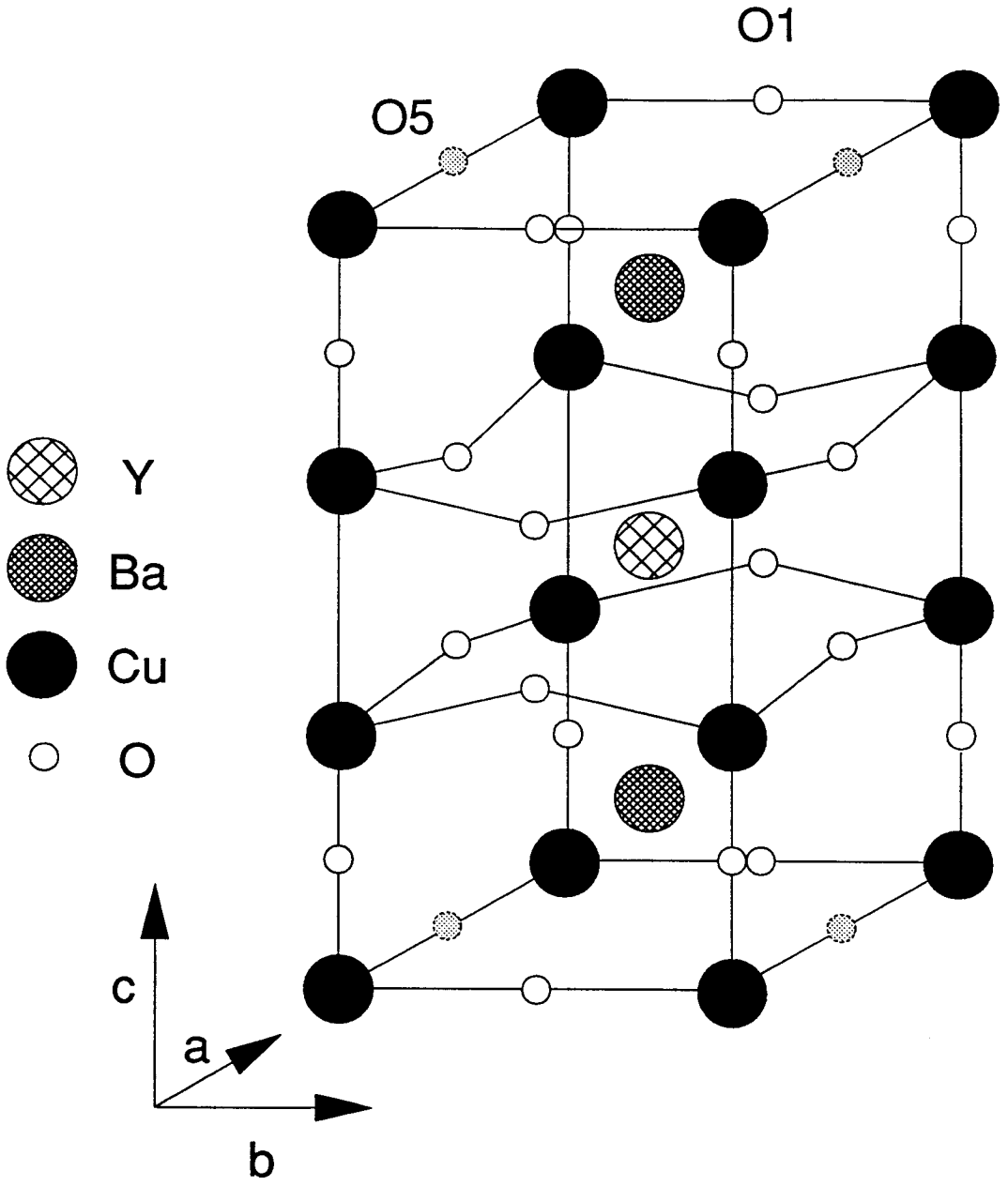

Figure 3 Crystal structure of $YBa_2Cu_3O_x$.

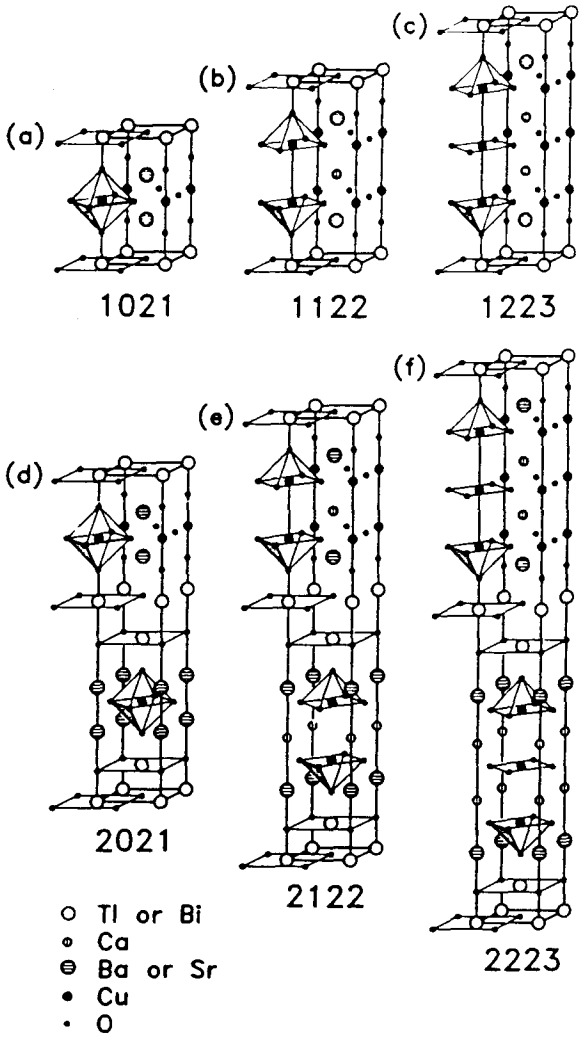

Figure 4 Nominal unit cells for the bismuth- and thallium-containing superconductors. Only the 2021, 2122, and 2223 structures form in the Bi-Ca-Sr-Cu-O system, whereas all six structures form in the Tl-Ca-Ba-Cu-O system.

For the purposes of this study, only the $YBa_2Cu_3O_x$ compound was considered. There are several reasons for this. The $YBa_2Cu_3O_x$ compound has only one superconducting phase and is the easiest to synthesize. This is contrasted to bismuth compounds which form multi-phase

components much more easily. Although one of the phases has a critical temperature of 110K, it is difficult to separate this phase from other phases which have lower critical temperatures. The $YBa_2Cu_3O_x$ phase is safe to handle without special precaution because although barium and copper compounds are generally toxic if ingested, they are not volatile. Thallium and many of its compounds including Tl_2O_3 are extremely toxic. Particularly, the toxin can readily pass through unbroken skin. Also, $YBa_2Cu_3O_x$ has been extensively investigated and such things as phase diagrams, crystal structures and physical properties are well documented. Moreover, among these ceramic superconductors, $YBa_2Cu_3O_x$ has one of the highest flux melting temperatures under a given applied magnetic field.[6]

1.2 Applications for High Temperature Superconductors

The possibility of superconductivity above the temperature of liquid nitrogen holds, of course, tremendous promise for their future applications. The applications can be roughly grouped into three categories: electronics, magnets and electric power applications.

Though currents in electronic devices are small, due to restricted dimensions, current densities are similar to those in large machines. However, magnetic fields are generally small. On the other hand, thin films, as would be required for fabrication of a variety of electronic devices, have already demonstrated their ability to meet the required current density.

1.2.1 Josephson Junctions and SQUIDs

A large number of superconducting devices are based on the properties of Josephson junctions. These junctions are formed by two superconducting films separated by a very thin insulating layer so that they are only weakly coupled. A simple Josephson junction is a switch which can be switched from the superconducting to the resistive state through the

electron tunneling effect which was discovered by Giaever in 1960.[7] The switch can be operated either by the application of a voltage or by exceeding the critical junction current. The critical junction current is very strongly affected by small magnetic fields and therefore the junction can sense very small changes of magnetic flux (on the order of 10^{-19} Wb). Single Josephson junctions can be used as (i) switches with a gate switching time of 10^{-12} second, (ii) SIS mixers to convert frequencies for millimeter-band receivers with extremely low noise, (iii) detectors for electromagnetic radiation over a very broad range of frequencies, (iv) voltage standards, etc. A two-junction device, in which two Josephson junctions are connected in parallel, is called a SQUID (superconducting quantum interference device) whose critical current of the junction is very sensitive to the magnetic flux that threads the junction and, in fact, is modulated with the period of a flux quantum ($\varphi_0=2.07\times10^{-15}$ Wb). SQUID devices can be used as voltmeters with sensitivities on the order of 10^{-15}V, sensitive magnetometers for biological as well as geophysical applications and instruments useful for physicists to search for magnetic monopoles and gravity waves.

1.2.2 MRI Devices

Magnetic resonance imaging (MRI) is used for noninvasive imaging of soft tissues without the need for exposure to radiation. MRI, which probes the nuclear magnetic resonance (NMR) characteristics of the hydrogen nuclei in the body, can distinguish between the various chemical environments in which the hydrogen atoms reside in various tissues of the body. The key element in making this technique work is the large superconducting magnet that provides both the bias magnetic field and the magnetic field gradient. MRI is currently the dominant market of superconducting materials and devices.

1.2.3 Superconducting Magnets

Another potential application of superconducting magnets is for the separation of magnetic materials from nonmagnetic matrices or even the separation of materials by their degree of magnetism, *e.g.* removal of impurities from food and industrial raw materials. The principle on which this method is based is that the force on a weakly magnetic particle is proportional to the product of its magnetic susceptibility and the gradient of the magnetic field. Superconducting magnets offer the possibility of high fields and high field gradients and therefore could provide very efficient separation.

The superconducting magnetic energy storage (SMES) system is another notable application of superconducting magnets. The concept is simple; the energy is stored in the magnetic field of a rather large, underground solenoid or toroid. For a persistent current level I in the SMES inductor L, stored energy is $LI^2/2$. The SMES is inherently low-loss, with ~95% efficiency expected. Small SMES systems could be used by industries, hospitals, office complexes, and shopping centers to reduce electricity costs during peak demand periods. It might also be used as a power backup to protect sensitive equipment, such as large computer or telecommunication systems, against sudden power failures.

Other superconducting magnet applications include magnets used to reduce the size or to increase the energy of accelerators for high energy physics, high power motors and generators, magnetic levitation for fast ground transportation systems and airplane runways, etc.

1.2.4 Electric Power Applications

Electric power applications include power transmission and distribution. The transmission of electrical energy over long distances with very small losses is an important problem for power industry. Superconducting AC and DC transmission lines are certainly ideal for this purpose. The major impact of the new high temperature superconductors would be in terms of low refrigeration energy cost due to the use of liquid nitrogen instead of liquid helium.

1.3 Difficulties of Practical Applications of Bulk $YBa_2Cu_3O_x$ Compounds

Despite the impressive progress in high temperature superconductors, researchers have soon realized that there are many tough problems which must be solved before the commercialization of ceramic superconductors is possible. The complexities of the problems dampened almost all enthusiasms of study on the bulk materials, at least by the physicists, who have now turned their research activities to thin films. These problems are left to the ceramic community to handle.

1.3.1 Low Critical Current Density

There had been much hype in the media about these materials which was initially directed towards increasing the critical temperature (T_c) at which these ceramics become superconducting. However, it has become clear that the critical current density (J_c) is the limiting factor for their applications and not the T_c. The relatively low J_c in the polycrystalline, bulk superconductors and its significant deterioration in weak magnetic fields[8] have been the major roadblocks to the rapid technical advancement towards commercialization. For large scale applications such as high-field magnetic coils, the materials must be fabricated

in the form of wires or tapes with critical current densities (J_c) of the order of 10^5 A/cm^2 in magnetic fields higher than 10T at 77K.[9] Measurements on the thin films indicates that at 77K, critical current densities (J_c) as large as 10^6 A/cm^2 in zero field are possible.[10] However, the best ceramic polycrystals have J_c values at least two orders of magnitude lower than that of thin films or single crystals. Usually, it is only about 100 A/cm^2 for ceramic samples without any specific treatment during processing. The poor J_c of bulk $YBa_2Cu_3O_x$ is the result from a combination of several factors associated with this material.

The $YBa_2Cu_3O_x$ compound is very anisotropic. It is virtually a two dimensional conductor. Measurements on single crystals of $YBa_2Cu_3O_x$ showed that the J_c in the crystal's a-b plane was at least an order of magnitude higher than that along the c axis.[11] Because of this anisotropy, it is expected that the J_c will be poor in three dimensions for bulk ceramic $YBa_2Cu_3O_x$ materials in which the crystals are randomly oriented.

One of the important parameters of superconductivity is the coherence length (ξ). The coherence length may be thought of as a measure of the maximum distance between members of a Cooper pair which carries supercurrent. Within the coherence length, the electrons or holes are said to be "correlated", and one may think of ξ as being the "size" of the Cooper pair. The value of ξ of $YBa_2Cu_3O_x$ was measured to be approximately 13Å and 2Å in the a-b plane and in the c direction, respectively.[12-13] These are extremely short compared to the values of the order of 1,000Å for conventional metallic superconductors. Since ξ is the distance over which coherence can be maintained across a normal state region, it is a measure of the scale at which lattice interruptions can disrupt the supercurrent. The inherent characteristic is that even grain boundaries or twinning planes (twins are abundant in the superconducting $YBa_2Cu_3O_x$ phase) may have sufficiently large dimensions, *i.e.* widths, to act as weak links in the superconducting state and, therefore, hinder the movement of Cooper

pairs resulting in a poor transport J_c in bulk materials. Direct measurements of critical current densities of individual grain boundaries in thin films as a function of their relative misorientation were reported.[14] The result (Figure 5) showed that the critical density across a grain boundary fell rapidly with misorientation angle, until it had fallen by about a factor of 50 for $\theta>15°$ relative to the intragranular J_c.

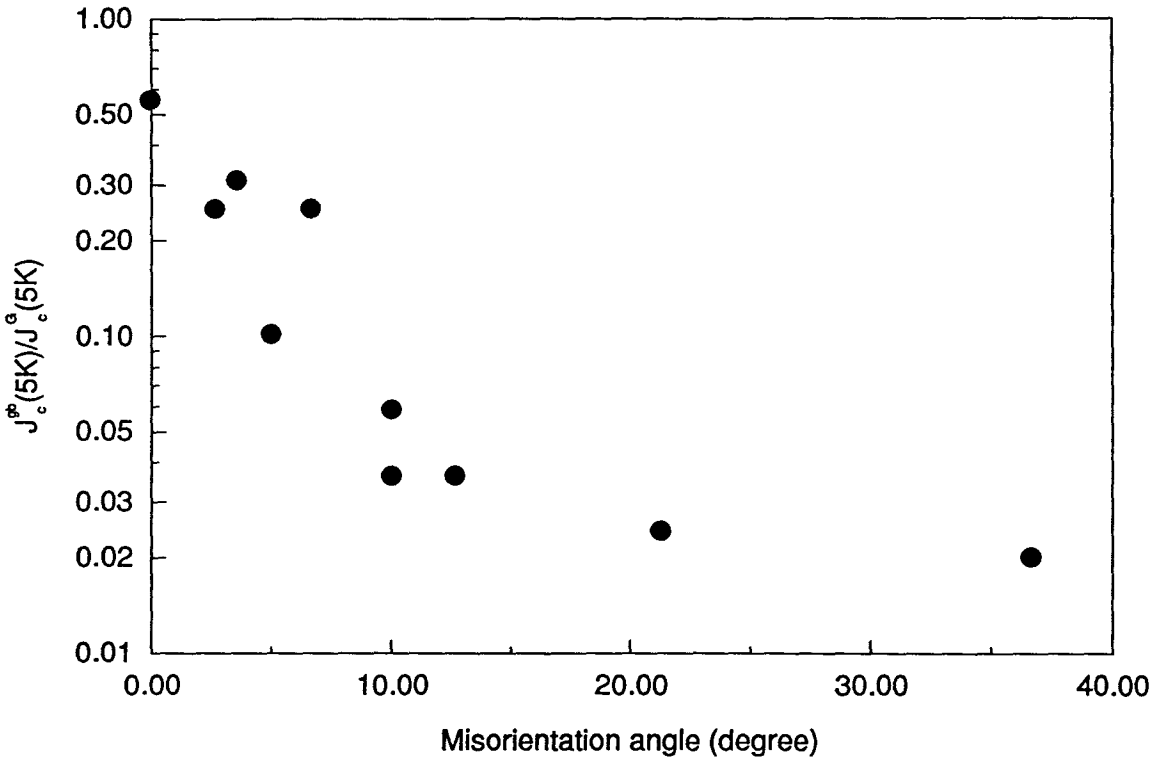

Figure 5 Ratio of the grain boundary critical current density to the average value of the critical current density in the two adjacent grains as a function of the misorientation angle in the basal plane. Measurements were made at 5K.[14]

$YBa_2Cu_3O_x$ is virtually a point compound at any particular oxygen potential (Figure 6). Any deviation from its stoichiometrically cationic composition will lead to non-

superconducting phases. These phases usually segregate in grain boundaries forming weak links and limiting the J_c values. The worst case is that these insulating phases form a continuous film coating each individual superconducting grain and severely deteriorating the J_c.

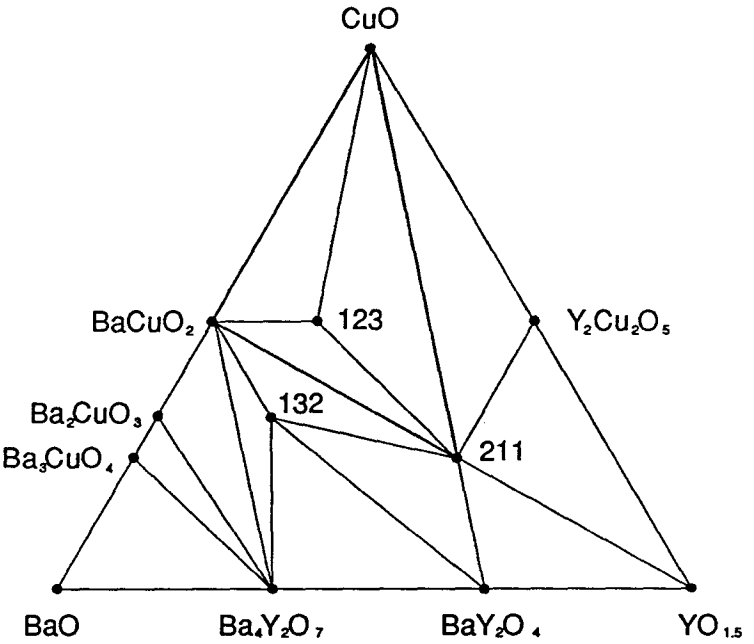

Figure 6 $Y_{1.5}O$-BaO-CuO phase diagram at 950°C.[15]

1.3.2 Brittleness and Weakness

The applications of superconductors often require the materials to have a sufficient flexibility to be fabricated into complex shapes, *e.g.* wound into a solenoid. Unfortunately, brittleness is an inherent characteristic of ceramics. It has been found to be exceptionally difficult to fabricate $YBa_2Cu_3O_x$ into structurally sound bulk forms such as tapes, wires, or more intricate configurations while maintaining a high J_c. Compared to other ceramic materials, $YBa_2Cu_3O_x$ is very weak in terms of fracture toughness (~1 $MPa \cdot m^{1/2}$). The

material is usually porous with only about 85% of theoretical density. Lower sintering temperature is responsible for such a high porosity. As shown in Figure 7, $YBa_2Cu_3O_x$ melts peritectically at a temperature of 1,015°C to form a liquid (of approximate composition $Y_{0.01}Ba_{0.25}Cu_{0.74}O$) and the crystalline phase Y_2BaCuO_5. Both of them are non-superconducting although the presence of the liquid phase can enhance the sintering. To avoid the formation of insulating phases, the sintering temperatures typically employed are low and lie in a range between 925 and 975°C, yielding poor density in the final compact. So far, no sintering aid which does not affect the superconducting properties of the material has been found. High porosity not only gives low strength but also generates poor electrical connections between individual grains. There is a contradictory requirement about the grain size: good mechanical properties require fine grains but finer grains are accompanied by a larger amount of non-superconducting grain boundaries (even without a liquid phase), *i.e.* poorer J_c values.

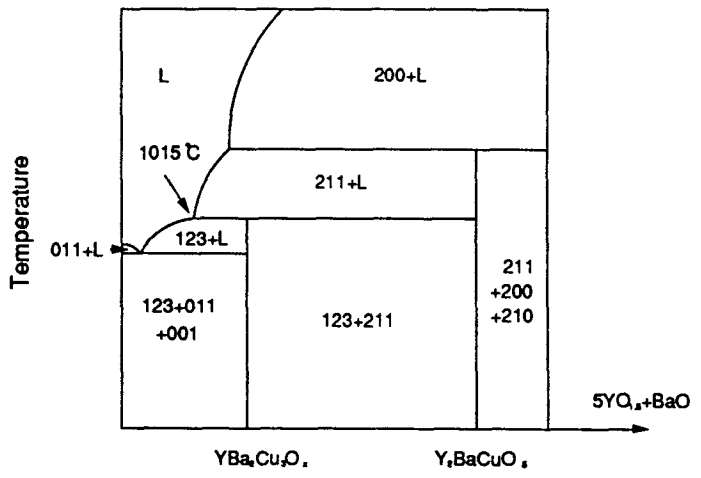

Figure 7 Section through the ternary phase diagram along the join $YBa_2Cu_3O_x$-Y_2BaCuO_5. Positions of all lines are approximate, except for the incongruent melting point of $YBa_2Cu_3O_x$.[16]

Highly dense $YBa_2Cu_3O_x$ samples can be produced by applying external forces on the samples during sintering such as hot-pressing[17], sintering-forging[18] and hot isostatic pressing (HIP).[19] Densities over 90%, even 99.3% of theoretical, were reportedly achieved. But as will be discussed in the next section, another serious problem will arise for samples with low porosity.

1.3.3 Oxygenation Behavior

According to Gallagher and others[20-23], $YBa_2Cu_3O_x$ will go from non-superconducting to superconducting and to non-superconducting again as oxygen is removed or added to the structure. This phenomenon is associated with the orthorhombic↔tetragonal phase transformation. Those materials with x=6.38 are non-superconducting and tetragonal, and when x>7.1 they also are non-superconducting. The best superconductors, which must be orthorhombic, were found with x=6.98. X is a function of both temperature and oxygen partial pressure.

The control of oxygen content in a $YBa_2Cu_3O_x$ sample is very important. As the oxygen content, x, decreases, critical temperature, T_c, decreases as well. This is shown in Figure 8. Both orthorhombic and tetragonal phases show a monotonic decrease in oxygen content with temperature above 400°C. This has allowed the use of thermogravimetric analysis (TGA) to determine the x values of $YBa_2Cu_3O_x$ samples. It has been demonstrated[20] that the weight loss experienced by $YBa_2Cu_3O_x$ upon heating is due solely to changes in oxygen stoichiometry. A TGA trace of orthorhombic $YBa_2Cu_3O_x$ heated and cooled under 1 atmosphere of oxygen is shown in Figure 9. It can be seen that at high temperature the value of x is low (about 6.2 at 950°C) and the $YBa_2Cu_3O_x$ phase is tetragonal. This indicates that the sintering of the $YBa_2Cu_3O_x$ compound is always performed in the tetragonal region.

Since the samples are totally tetragonal after sintering these samples must be converted to the orthorhombic phase, which is superconducting at lower temperatures, by oxygenation. From the same figure (TGA trace) it can also be seen that oxygen stoichiometry is completely reversible. This provides a processing window to regain high oxygen content, which is required for good superconductivity, by annealing the samples in an oxygen atmosphere.

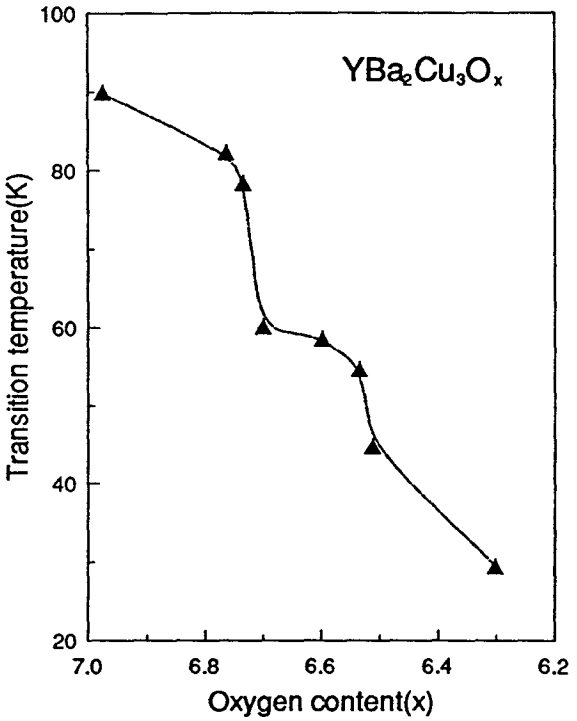

Figure 8 Transition temperature versus oxygen content of $YBa_2Cu_3O_x$.[21]

To ensure an oxygen content around 6.98 for the $YBa_2Cu_3O_x$ compound, the material must be annealed in an oxygen atmosphere. Annealing temperature is usually below about 500°C since the orthorhombic phase is stable until ~600°C[22-23]. The diffusion of oxygen into the structure is limited by the low temperature and a very low diffusion coefficient of 10^{-14} cm^2/sec at 500°C.[24] It was found experimentally that a 1 mm thick specimen could

be completely oxygenated in several days at 600°C[15] otherwise the interior of each grain was tetragonal, *i.e.* non-superconducting. For samples of larger dimensions and high density, the time requirement for complete oxygenation would be impractical. An additional complication encountered is the finding that the activation energy for oxygen diffusion into $YBa_2Cu_3O_x$ is dependent on the oxygen stoichiometry of the material such that the greater the oxygen content the lower the oxygen diffusion. Specifically, Tu, *et al.*[25] found that the activation energy was only ~0.5eV for a composition $YBa_2Cu_3O_{6.62}$ and rose to ~1.3eV for the fully oxygenated composition $YBa_2Cu_3O_7$. Reoxidation of bulk material is, therefore, believed[24,26] to require open porosity so that the necessary oxygen diffusion path is shorter. But this is contrary to the higher density requirement to promote the critical current density J_c and to obtain good mechanical properties.

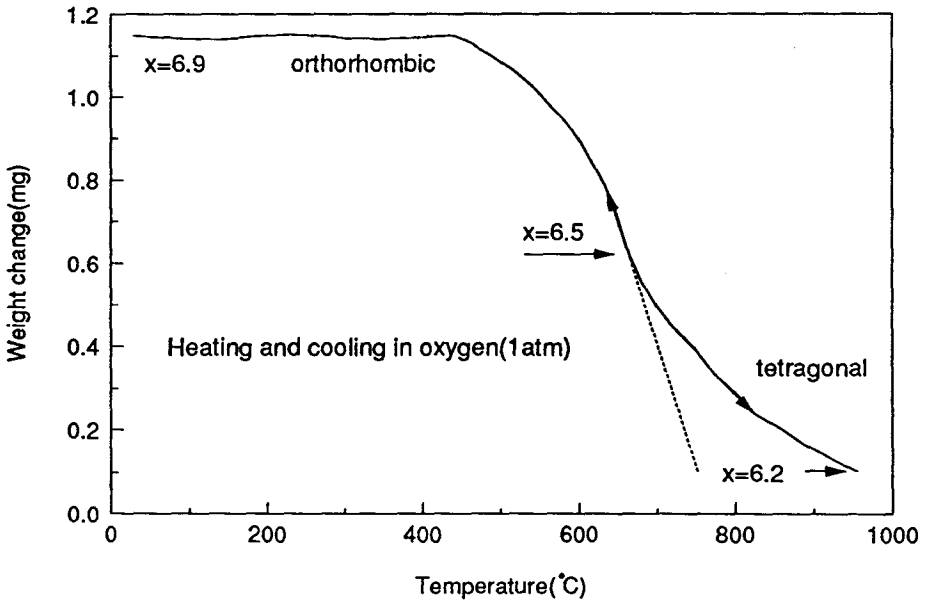

Figure 9 TGA trace for $YBa_2Cu_3O_x$ heated and cooled under 1 atmosphere oxygen, showing orthorhombic-tetragonal phase transformation and completely reversible stoichiometry.

1.3.4 Weak Flux Pinning

One of the most fundamental properties of superconductors which was discovered by Meissner and Ochsenfeld in 1933 is that magnetic fields do not penetrate into a superconducting sample, *i.e.* a perfect diamagnetism, if the external magnetic field is lower than the critical magnetic field (H_c) of the sample. This is known as the Meissner effect. Since zero resistivity is, of course, impossible to be measured in an absolute sense, reports of new superconductors must meet Meissner effect criterion prior to acceptance by the scientific community. Superconductors can be divided into two broad categories: Type I and Type II. Type I superconductors are generally pure metals which exhibit perfect diamagnetism below H_c. Most compound or alloy superconductor, including the $YBa_2Cu_3O_x$ compound, are Type II superconductors. As illustrated in Figure 10, Type II superconductors allow additional magnetic flux penetration without losing the ability of carrying supercurrent between their lower critical field H_{c1} and upper critical field H_{c2}. When an electrical current is passed through a Type II superconductor which contains magnetic flux, the current creates a Lorentz force ($\mathbf{J}\times\mathbf{B}$) which acts on the flux lines. The movement of the flux lines under the Lorentz force causes dissipation of the energy of the current, resulting in a lower critical current density J_c. The movement of flux lines may be pinned by the presence of impurities and defects.

Tinkham[27] theoretically analyzed the critical currents in high T_c superconductors and argued that high T_c materials may have an intrinsic weakness of flux pinning due to a variety of unfortunate parametric combinations. To further improve the critical current density of the $YBa_2Cu_3O_x$ compound, intragranular pinning is necessary. Oxygen point defects are believed to be the most important pinning sites in the $YBa_2Cu_3O_x$ compound, and the critical

density is higher in more oxygen-disordered crystals.[28]

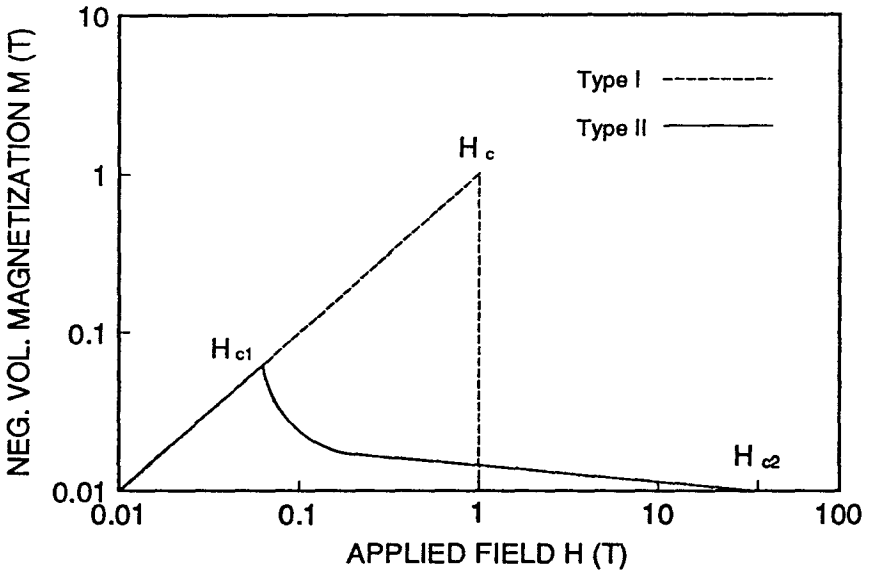

Figure 10 Plot of magnetization M versus magnetic field H. The values of H_{c1} and H_{c2} are typical for high-T_c superconductors.

1.4 Approaches to Overcome the Problems

To overcome these difficult and contradictory problems, two approaches have been explored. One is to develop microstructural textures so that the grains are connected by predominantly low-angle grain boundaries. The methods reported are mechanical alignment under uniaxial pressure such as hot forging,[9,29] melt texturing[30] and alignment of $YBa_2Cu_3O_x$ powders in the presence of a magnetic field.[31] Another method is to add a certain amount of silver into $YBa_2Cu_3O_x$. The latter method will be reviewed in detail in the next section.

1.5 Previous Work on Silver Addition to the $YBa_2Cu_3O_x$ Compound

Because silver addition may provide a large number of beneficial effects to $YBa_2Cu_3O_x$ it has been extensively studied, especially to improve the mechanical and superconducting properties of the $YBa_2Cu_3O_x$ compound. Only noble elements can be used, as other elements reduce or remove oxygen from the system.

1.5.1 Improved Mechanical Properties by Silver Addition

For most practical applications, both good superconducting (high critical temperature, current density and magnetic field) and mechanical properties (strength and fracture toughness) are desirable. Previous authors have observed that $YBa_2Cu_3O_x$ specimens are very brittle, with unacceptably low strength.[32-33] This owes not only to the intrinsic nature of ceramics but also to the unavoidable presence of porosity. To overcome this, silver was employed as a reinforcement by a number of authors.

Mechanical and electrical properties of rectangular bars and thin tapes of $YBa_2Cu_3O_x$-Ag composites with 10-30 vol% of Ag or Ag_2O were reported by Singh, *et al.*.[34] The addition of 20 vol% Ag resulted in an increase in strength from 40 to 75 MPa and a twofold increase in critical current density from 150 to 300 A/cm^2 at 77K in the absence of an applied magnetic field was observed. They believed that these results were primarily due to the increased density (ρ_{th} up to 98%). Silver phase was also believed to relax residual stresses resulting from the expansion anisotropy of grains and to provide increased resistance to crack propagation by pinning the propagating cracks. The strength was increased further to 87 MPa by an addition of 30 vol% Ag, while the elastic modulus was improved from 75 to 117 GPa and hardness from 137 to 243 kg/mm^2. But the critical current density dropped

to 50 A/cm^2 for samples containing 30 vol% Ag whereas the critical temperature was unaffected. In samples with high silver content, a continuous silver phase was formed. This continuous, non-superconducting phase may be responsible for the low critical current density in these samples. No difference between Ag and Ag_2O additions was found by these authors.

Nishio, *et al.*[35] prepared composite superconductors by sintering a mixture of $YBa_2Cu_3O_x$ and Ag powders at various proportions (0-95.1 wt%) and were able to enhance the mechanical strength up to 226 MPa from 42 MPa for sintered pure $YBa_2Cu_3O_x$ samples without seriously lowering the critical temperature. It was surprising that the porosity of these samples was high (25% for samples without silver and 16% for samples containing 25.9 wt% Ag) while still attaining high strengths. They claimed that silver did not react with $YBa_2Cu_3O_x$ at all and reported that for samples containing even 50 vol% silver, fine $YBa_2Cu_3O_x$ grains formed continuous networks around homogeneously distributed silver particles, which was contrary to the observation of Singh, *et al.*

A $YBa_2Cu_3O_x$-Ag composite tape with 13 vol% silver was reportedly fabricated by tape casting technique followed by appropriate sintering.[36] The deformation strain could be up to 2% without breaking, as compared with a typical pure $YBa_2Cu_3O_x$ material, which fractured at a strain of ~0.1-0.2%. The silver addition did not adversely affect the superconducting properties of the composite tapes. Small changes of critical temperature were demonstrated and actual change on critical current density was not reported.

A most recent report from the University of Houston[38] shows that by the refinements of grain size and porosity, in addition to the control of silver morphology and distribution, a fracture toughness of 3.6 MPa·m$^{1/2}$ could be obtained from $YBa_2Cu_3O_x$/Ag composites for

silver composition near 20%. This is the highest bulk fracture toughness value published to date. This value is comparable with many structural ceramic materials. The superconducting properties of these composites are not mentioned in this paper.

Although the data about the mechanical properties of silver reinforced $YBa_2Cu_3O_x$ composites are scattered, the reinforcing effect is not questionable. The introduction of a ductile second phase can certainly enhance the material as a result of crack blunting and crack arrest mechanisms.[37] The problem is how to improve the mechanical properties while maintaining good superconducting properties.

1.5.2 Enhanced Critical Current Density by Silver Addition

As mentioned in previous sections, the transport supercurrent density of bulk $YBa_2Cu_3O_x$ is limited by non-superconducting grain boundaries. These grain boundaries are also called weak links. A weak link in a superconductor generally means a junction between two bulk superconductors. The supercurrent carrying capacity across such a junction is generally lower than that in bulk materials and depends on the material at the interface.[39] The interfacial material can be an insulator (I), a normal conductor (N) or even a second superconductor (S') which has a lower critical temperature.[39] Thus S/I/S, S/N/S and S/S' weak links may be formed. In a polycrystalline material, in order to transport a current through the bulk of the material, supercurrent must pass through these weak links. Therefore the properties of grain boundaries are of vital importance to the critical current density. Since the maximum critical current is inversely proportional to the normal state resistance of the S/I/S junction,[40] and silver can scavenge the impurities at the grain boundaries and thereby reduce the thickness of non-superconducting grains,[41] silver was

introduced into the $YBa_2Cu_3O_x$ compound by a number of researchers under the hypothesis that silver can reduce grain boundary resistance and improve the coupling condition of the weak links at the grain boundaries.

It is necessary to clarify that there are two different methods of J_c measurements. One is the DC four-lead method which will be described in detail in Section 2.5.1. This method is a direct method and the critical current density measured by this method is called transport J_c. Another method is an indirect one, which uses a magnetometer to measure the magnetization (M) versus Magnetic field (H) hysteresis loop. The critical current density is calculated through the Bean model using the following equation:[42]

$$J_c = 30\Delta M/d$$

where ΔM is magnetization hysteresis loop width in A/cm and d is the particle dimension in cm perpendicular to the applied H. Average grain size is usually used as d. The J_c values from this method are called magnetization currents. Usually magnetization currents are much higher than transport currents because magnetization currents are not limited by the grain boundaries. But the magnetization currents may be affected by microcracks and twin walls within the grains.

Attempts of adding silver to enhance the critical current density of the $YBa_2Cu_3O_x$ compound can be divided into two groups according to the starting composition formulas used: $YBa_2Cu_3O_xAg_z$ and $YBa_2(Cu_{3-y}Ag_y)O_x$. The first one is a $YBa_2Cu_3O_x$+Ag composite and the second one is a substitutional solid solution.

Most researchers prepared samples in the form of composites. The optimum content of silver for enhancing the critical current density given in published papers are very controversial, ranging from 0.8 to 20 wt%. The best transport critical current densities with

silver vary from 215 to 700 A/cm^2 at 77K without any applied magnetic field. The best magnetization currents reported are from 1.24×10^4 to 10^5 A/cm^2. These published data are listed in Table 3, and also data measured by the same authors from the samples without silver (if provided) are also included for comparison.

Although almost all authors claimed that critical current densities of $YBa_2Cu_3O_x$ with silver were enhanced, the data were in apparent contradiction. Overall, most authors agreed that a small portion of silver would be beneficial to the critical current density. The only paper that claimed that silver had no substantial enhancement in critical current density was published by Jin, *et al.*.[52] They mixed 25 wt% Ag_2O powders with $YBa_2Cu_3O_x$ powders followed by normal sintering and annealing processes. They found the magnetization current was 4,800 A/cm^2 for the composite whereas it was 5,200 A/cm^2 for the sintered sample without silver.

Some authors[53-56] substituted copper by various amount of silver in the form of $YBa_2(Cu_{3-y}Ag_y)O_x$ and got similarly contradictory results. For example, Motsumoto, *et al.*[55] believed that the best critical current density was obtained at y=0.3 although they noticed that silver could not completely substitute copper when y>0.1. Gangopadhyay and Mason[56] argued that critical current densities were nearly unchanged for y up to 0.12.

Most of the authors stated that silver did not have any reactivity with $YBa_2Cu_3O_x$ and no silver was detectable within $YBa_2Cu_3O_x$ grains although they did not provide sufficient evidence about that. In the cases of substitution, the content of silver which truly substituted at the copper sites was not checked by most of the authors. Only a few authors[56-57] inferred that there was a certain amount of silver really existing within $YBa_2Cu_3O_x$ grains. Weinberger, *et al.*[57] examined the microscopic composition inside the grains of

Table 3 Summary of the Data on Critical Current Densities of $YBa_2Cu_3O_x$+Ag Composites and $YBa_2Cu_3O_x$ at 77K and Zero Magnetic Field

Optimum Ag (wt%)	J_c (A/cm^2)			Reference
	transport	magnet.	pure 123	
0.8	300		150	[43]
5	215		105	[44]
5		12,400		[37]
5		10^5		[45]
7	450		50	[46]
10	700		450	[47]-[48]
10		52,480	20,000	[49]
15		22,000	6,000	[50]
20	300		150	[34]
10-50	250-350		2 orders lower	[51]

$YBa_2Cu_3O_{7-x}$/Ag samples by WDX and found the compositions for $YBa_2Cu_3O_x/Ag_{0.1}$ and $YBa_2Cu_3O_x/Ag_{1.0}$ samples to be $YBa_{2.02}Cu_{2.86}Ag_{0.037}O_x$ and $YBa_{2.11}Cu_{3.09}Ag_{0.050}O_x$, respectively. This result indicates that the silver content within the grains is lower than the nominal content. These authors also claimed that the Cu (1), *i.e.* Cu^{3+}, was substituted by silver based on the information that the length of Ag-O bond was found to be 2.0±0.1Å from extended

X-ray absorption fine structure (EXAFS) measurements. However, there are several Cu(1)-O and Cu(2)-O bonds ranging from 1.931 to 1.955Å in the $YBa_2Cu_3O_x$ lattice. Hence, this experimental result is insufficient to support their claim. Recently, Gangopadhyay and Mason[56] have made an attempt to determine the silver solubility in $YBa_2Cu_3O_x$ by using electron probe microanalysis (EPMA). The nominal composition of the samples they used was $YBa_2Cu_{3-x}Ag_xO_{6+y}$ (x up to 0.75). They also found that the silver content within the grains is lower than the nominal content. Their EPMA results are shown in Figure 11. However, silver can be either in the form of precipitates or within the $YBa_2Cu_3O_x$ lattice. They just assumed that the silver substituted copper in $YBa_2Cu_3O_{6+y}$ and did not provide any evidence for it.

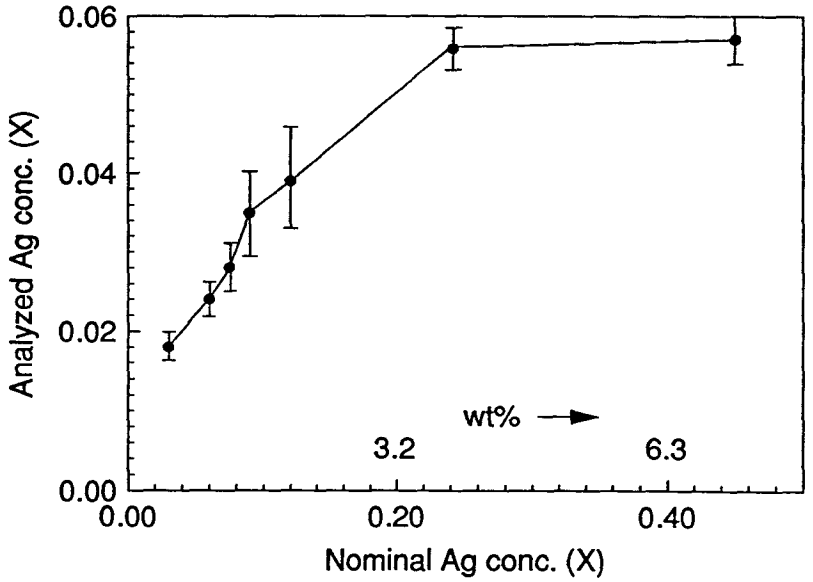

Figure 11 Electron probe microanalysis (EPMA) Ag contents in 123 vs. doping in $YBa_2Cu_{3-x}Ag_xO_{6+y}$ (re-plotted from Gangopadhyay and Mason[56]).

1.5.3 Improved Flux Melting Temperatures by Silver Addition

Critical temperature of a superconductor is also limited by a magnetic field (H). As the applied magnetic field increases, temperatures lower than T_c are required to maintain a lower thermodynamic state, i.e., the superconducting state. The variation of the critical magnetic field, H_c with temperature for $T<T_c$ is empirically shown to approximate a parabola. If $H_c(0)$ is the critical field at absolute zero temperature, a useful approximation of H_c at temperature T is:

$$H_c = H_c(0)\left\{1-\left(\frac{T}{T_c}\right)^2\right\}$$

If the applied field is greater than $H_c(0)$, it is impossible to produce a superconducting state even at absolute zero temperature. As the applied magnetic field increases, temperatures lower than T_c are required to maintain a lower thermodynamic state, *i.e.*, the superconducting state. A critical temperature under a specific magnetic field lower than $H_c(0)$ is called the flux melting temperature (or flux depinning temperature), $T_c(H)$, at this magnetic field.

The influence of silver addition to the $YBa_2Cu_3O_x$ compound on fluxline dynamics was studied by Sayer, *et al.*.[58] They reported that the flux melting temperatures of $YBa_2Cu_3O_x \cdot Ag_y$ samples were substantially improved for y=0.38. Their results are summarized in Table 4.

Table 4 Flux Melting Temperatures of $YBa_2Cu_3O_x$·Ag_y Samples[58]

Magnetic field (Tesla)	Drive current (mA)	Flux melting temp.(K)		
		y=0	y=0.38	y=0.77
1	0.2 1.0	74 74	83 80	83.5 80
2	0.2 1.0	71 71	81 78	
3	0.2 1.0	70 70	80 78	

1.5.4 Other Studies on Silver Addition to $YBa_2Cu_3O_x$

The effect of silver addition on flux pinning was observed by some researchers[45-51, 59] from the same group headed by M.K. Wu, who discovered the first 123 sample, in their magnetic studies of $YBa_2Cu_3O_x$-Ag composites. Large magnetization and hysteresis were found to be present in samples containing 2.2, 3.1 and 5.1 wt% silver.[45] This was believed to be the main evidence of the existence of strong pinning forces. But such a strong pinning force was not observed in the sample containing 14% silver by the same authors because it contained too much silver. Similar results were also reported by Huang, *et al.*.[59]

Another observation found in silver-containing $YBa_2Cu_3O_x$ samples is the significant grain growth promoted by the presence of silver. Although the microstructure of a ceramic material depends on the processing conditions, the silver-promoted grain growth was commonly reported by a number of authors who used various processing routes and different amounts of silver additions.[59-66] The promotion of the grain growth results from the

increased amount of liquid phase present at high temperature. It has been reported that silver addition causes partial melting of the $YBa_2Cu_3O_x$ phase above 931°C where the silver leaches copper from $YBa_2Cu_3O_x$ resulting in its decomposition.[67]

It has also been reported that silver addition improves normal state resistance[49, 51, 62, 64, 68] and resistance to water[44, 36], and silver acts as an internal oxygen donor[69] and a faster diffusion path for oxygen.[68,70]

In summary, the role of silver addition to $YBa_2Cu_3O_x$ compound is multifold.

1) Silver can improve the mechanical properties of $YBa_2Cu_3O_x$ by filling the pores and voids among $YBa_2Cu_3O_x$ grains and forming a dense composite .

2) Silver may reduce the resistance of the junctions, *i.e.* grain boundaries, between superconducting grains to enhance J_c since the maximum J_c in a weak link is inversely proportional to the junction resistance. Silver can also scavenge the impurities at the grain boundaries and therefore reduce the thickness of non-superconducting regions.

3) The raw material of Ag_2O for silver addition can act as an internal oxidant to supply the necessary oxygen to form the orthorhombic phase. Silver can also provide a faster diffusion route of oxygen as well as act as a catalyst to promote the low temperature decomposition of the barium carbonate species added as raw material for synthesis of $YBa_2Cu_3O_x$.

4) Dissolved and precipitated silver within $YBa_2Cu_3O_x$ grains can pin magnetic flux lines and therefore increase J_c. It may also increase flux melting temperature.

1.6 Objective of Present Study

Silver additions to the $YBa_2Cu_3O_x$ compound have already been extensively studied. The data published in the improvement of the mechanical properties of $YBa_2Cu_3O_x$ compounds are convincing because the reinforcing effects of silver in $YBa_2Cu_3O_x$ compounds are primarily intergranular. However, published data on silver enhanced electrical and magnetic properties of $YBa_2Cu_3O_x$ compounds are in an apparent contradiction. Since the electrical and magnetic properties can be affected by the presence of both intergranularly and intragranularly silver, the fact that the contradiction is existing may suggest that not only the quantities, but also the distribution of silver may have a significant effect on the properties of bulk $YBa_2Cu_3O_x$ compounds. Published papers predominantly assert that silver does not have any reaction with $YBa_2Cu_3O_x$ compounds and all silver added is intergranular. Little attention has been paid to the interaction between the $YBa_2Cu_3O_x$ compound and silver at the molecular level, and its effect on the intragranular and intergranular properties. The questions of whether silver may go into the $YBa_2Cu_3O_x$ lattice, to what extent silver may enter and which site silver may occupy are still unclear. Moreover, because silver has been widely employed as the cladding material in the fabrication of $YBa_2Cu_3O_x$ wire, tape, etc, it is of extreme importance to know the reactivity between the $YBa_2Cu_3O_x$ compound and silver, and the solid solubility of silver in the $YBa_2Cu_3O_x$ compound.

To shed some light on these issues, attempts were made to study the solid solubility of silver in the $YBa_2Cu_3O_x$ compound. This is carried out by studying a number of silver doped $YBa_2Cu_3O_x$ samples using X-ray diffraction (XRD), optical microscopy, scanning electron microscopy (SEM), energy dispersive X-ray spectroscopy (EDX), wavelength dispersive X-ray spectroscopy (WDX) and secondary ion mass spectrometry (SIMS). In addition, precise lattice

parameter determination of $YBa_2Cu_3O_x$ samples with and without silver may allow the identification of sites within the unit cell, which may be occupied by silver ions. And also, the critical current density (J_c), normal state resistance and the critical temperature (T_c) of the silver-containing $YBa_2Cu_3O_x$ samples are measured.

2 EXPERIMENTAL PROCEDURE

2.1 Sample Preparation

In this study a number of samples were prepared with nominal silver content from 0 to 10 % which was added using two separate routes-wet and dry mixing. All silver concentrations referred to in this thesis, unless otherwise noted, are in weight percent. Two batches of the samples were made for the purpose of testing the reproducibility of experimental data. A commercial powder of $YBa_2Cu_3O_7$ (particle sizes: 2μm - 6μm provided by SSC, Inc., Seattle, U.S.A.) was used as the raw material. A silver nitrate ($AgNO_3$) solution and a silver oxide (Ag_2O) powder were used as the starting materials of silver addition for wet and dry mixing, respectively.

The wet mixing method was employed to produce samples with nominal silver concentrations of 0.5, 1.0, 1.5 and 2.5%. An appropriate quantity of analytical grade $AgNO_3$ crystal was dried in air at 120°C for two hours, weighed and dissolved completely in a small amount of distilled water for each nominal silver concentration. The aqueous solutions were then diluted by an appropriate amount of denatured alcohol. These solutions were mixed thoroughly with the $YBa_2Cu_3O_x$ commercial powder by manual stirring to form homogeneous slurries. The slurries obtained were put into a dryer at 120°C. The dried powder was pulverized and reground by pestle and mortar.

In the sample preparation route of dry mixing, a silver oxide powder was added to the samples in the nominal concentration of 5 and 10%. Raw powders of Ag_2O and $YBa_2Cu_3O_x$ were dry mixed in a vibratory mixer for 20 minutes. The mixed powders were ground manually and repeatedly. The final powders from both wet and dry routes were subsequently pelletized

into discs under an uniaxial force about 300 MPa. The pellets were about 9.5 mm in diameter and 1g in weight. These pellets were sintered in air at 950°C for 24 hours followed by an annealing process at 500°C in pure O_2 for the same amount of time for the purpose of reoxygenation. After the annealing process, samples were furnace cooled to room temperature.

In order to study the silver solubility at higher temperature, one sample of each of the Ag nominal concentrations was sintered in a suspended crucible in a vertical tube furnace and quenched by dropping it into liquid nitrogen immediately from 950°C after sintering. The flow chart of the sample processing procedure is illustrated in Figure 12.

The commercial powder used in this study was produced by decomposition of organometallics and contains a significant amount of residual carbon[71]. This carbon contamination could deteriorate the transport properties of $YBa_2Cu_3O_x$ by reducing the oxygen content in areas of high carbon to the point where the material may be locally non-superconducting. To overcome this problem, raw $YBa_2Cu_3O_x$ powders were synthesized using Y_2O_3, $BaCO_3$ and CuO powders as precursors and calcining. The samples processed through this route were used for electrical property measurements.

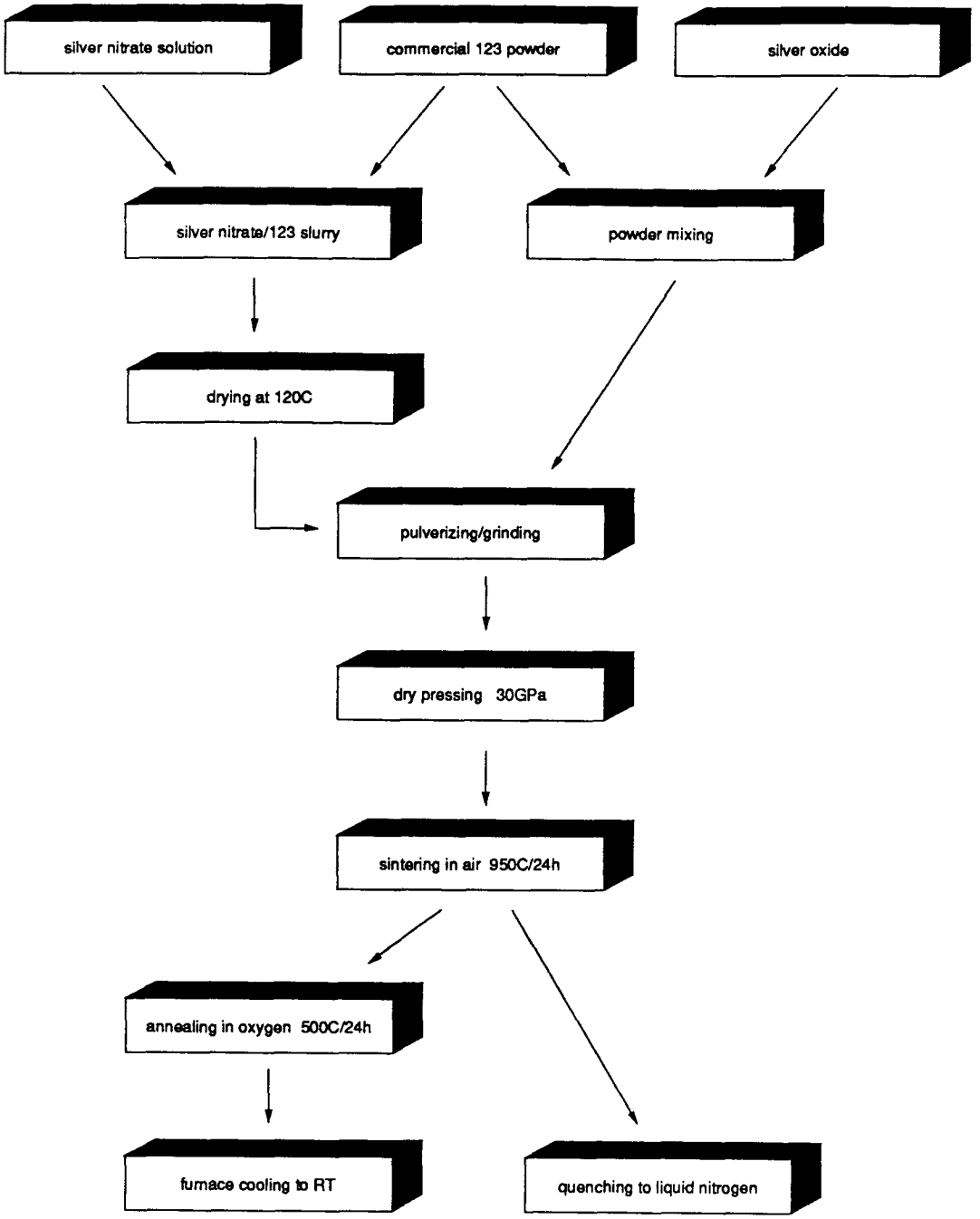

Figure 12 Flow chart of the processing steps for sample preparation.

2.2 Scanning Electron Microscopy

A scanning electron microscope (SEM) with both energy dispersive X-ray spectroscopic (EDX) and wavelength dispersive X-ray spectroscopic (WDX) attachment was used to examine silver doped $YBa_2Cu_3O_x$ samples. The SEM scans the surface of a sample with a beam of electrons which produces secondary electrons, backscattered electrons, X-ray photons, etc. from the surface layer of the sample which is detected. From the detected secondary electron density an image of the surface can be generated. In this investigation, the backscattered electron imaging technique was also used to enhance the contrast between $YBa_2Cu_3O_x$ and silver phases. X-ray signals generated by the bombardment of the sample with incident electrons were used to identify the silver phase and determine the quantity of silver dissolved and/or precipitated within $YBa_2Cu_3O_x$ grains. EDX is suitable for a quick qualitative examination of the samples whereas WDX is more sensitive and can do the quantitative analysis more precisely. The sensitivity of WDX varies element by element, and depends on the operating conditions and the standard chosen. X-ray emission obeys the statistical rules of random processes. In this study the detection sensitivity for silver was estimated at about 0.05% by using the following equation[75]:

$$C_1 = C_{st}\frac{3\sqrt{B}}{P-B}$$

where C_1: detection sensitivity (in mass%);

C_{st}: concentration of analyzed element in a standard (in mass%);

P: total peak counts;

B: total background counts.

SEM samples were polished by diamond powders down to 1μm and carbon-coated. Pure Y, Cu, and Ag metals, and a $BaSO_4$ crystal were employed as the standards for quantitative analysis by wavelength dispersive X-ray spectroscopy. The SEM equipment with the WDX detector was operated at 20kV. The counting time was 10 seconds. In order for the X-ray emitting efficiency of silver to be high enough and detectable, a constant beam current of 40 nA, which was the standard beam current for analyzing silver, was used. The diameter of the incident beam was about 0.3 μm. But the area where the X-ray signal was generated was larger. Castaing[72] suggested that the spot size can be estimated by following equation:

$$S(\mu m) = 0.033(V^{1.67} - V_c^{1.67})\frac{A}{\rho Z}$$

where V: accelerating voltage (kV);

V_c: critical exciting voltage (kV);

A: atomic weight (g/mol);

Z: atomic number;

ρ: density (g/cm^3).

Since A/Z is approximately constant, from the Monte Carlo calculation of Bishop,[73] Reed[74] gave the following general expression for deducing the lateral extent of the X-ray distribution:

$$S(\mu m) = \frac{0.077}{\rho}(V^{1.5} - V_c^{1.5})$$

In this experiment, V was 20 kV and V_c was 3.8 kV for silver $L\alpha_1$. Assuming x=6.9 for the $YBa_2Cu_3O_x$ compound and taking the lattice parameters obtained from X-ray diffraction in this study, the theoretical density (ρ) of $YBa_2Cu_3O_x$ was estimated to be 6.34 g/cm^3. By substituting

these numbers into Reed's equation, the resulting S was about 1 μm. This was small enough compared to the width of elongated $YBa_2Cu_3O_x$ grains, which was about 5 to 10 μm, so that the grain boundaries where the silver segregated would not be stricken by the bombardment of incident electrons during the quantitative analysis. For the data of quantitative analysis by WDX to be statistically reliable, at least 25 grains of various morphologies were analyzed from each sample. Computerized ZAF corrections were applied to the concentrations of Y, Ba, Cu and Ag in the area analyzed.

2.3 Secondary Ion Mass Spectroscopy

Secondary ion mass spectroscopy (SIMS) is mainly a surface analytical technique which was used in this study to detect the existence of silver within the $YBa_2Cu_3O_x$ grains. Sputtering is the physical process on which SIMS analysis is based. A beam from an ion gun is directed to a point on the sample surface. The high energy ions strike the surface causing atoms and ions of the surface material to be ejected from the surface. These secondary ions are collected and passed through a mass spectrometer which separates the ions of different mass numbers. The number of ions at each mass number are measured over a given time period. The mass number identifies the ion, and the measured number of ions is related to the concentration of that element in the sample.

In this investigation, the SIMS data was collected by using a V.G. SCIENTIFIC LTD. QUADRUPOLE MASS SPECTROMETER mounted on a Micro Lab MK II chamber. The system was fitted with a gallium liquid metal ion gun (LMIG), with an angle of incidence to the sample of 50° off normal and an MM12-12 quadrupole mass spectrometer with one atomic mass unit (a.m.u.) resolution. The primary ion used was Ga^+ and $^{89}Y^+$ was used as the internal standard. The instrument was operated with an accelerating voltage of 10 kV and a beam current

of 2 nA. The mass span was set from 106 to 112 and the scan time was 40 minutes. For the same reason given in the WDX analysis, the magnification was set at 20,000 to avoid the grain boundaries being hit by primary ions. Because SIMS is mainly a surface analytical technique and the current interest in this research was in the bulk solubility of silver within $YBa_2Cu_3O_x$ grains, the surface of each sample was sputtered off before the sample was used for detection.

2.4 Precise Determination of Lattice Parameters

The lattice parameters of the samples were determined by X-ray powder diffraction at room temperature on a Philips diffractometer (type 1011/80). Copper radiation filtered with nickel was used at the setting of 36 kV and 30 mA. The divergent, scattering and receiving slits used were 1, 0.1 and 1 degree, respectively. The wavelength used for calculation was λ=1.5405Å. Diffraction spectra were scanned between 2θ of 14° and 70° at the speed of 0.25 degree per minute using the maximum time constant. The diffraction spectra were recorded on a chart recorder and the chart speed was set at 10 mm per minute. The combination of slow scanning and fast chart speeds set here was to improve the resolution of the 2θ values measured from the diffraction peaks.

By differentiating the Bragg Law, $2dsin\theta=\lambda$, with respect to θ, the following equation is obtained.

$$\Delta d/d=-\Delta\theta\cdot\cot\theta$$

As shown in Figure 13, since $\cot\theta$ approaches zero as θ approaches 90°, the calculated lattice parameters from the various lines on the diffraction pattern approach the true value more closely as 2θ increases. Unfortunately, for the $YBa_2Cu_3O_x$ compound the line with the highest 2θ and known index is (026) for which 2θ is ~68.8°. This was the reason why the scanning was stopped at 2θ=70°.

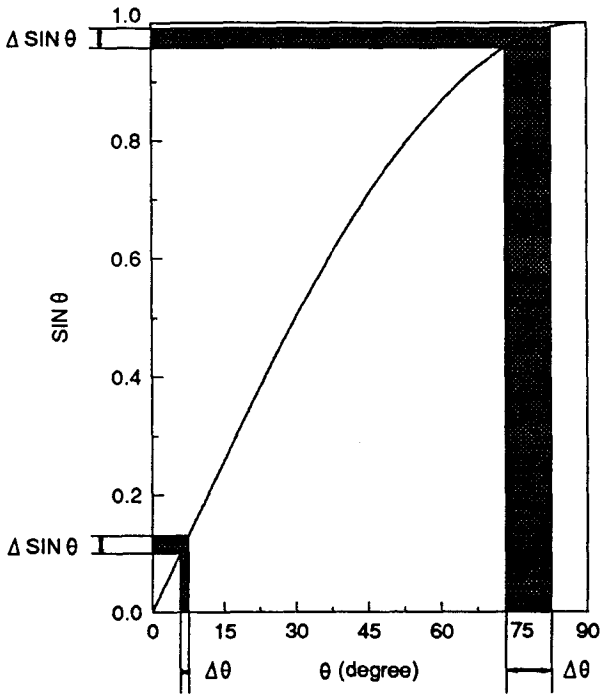

Figure 13 θ-sinθ relationship

The main systematic errors in the measurement of interplanar spacing, d, by a diffractometer are the following:

1) Displacement of the sample from the diffractometer axis;

2) Misalignment of the instrument;

3) Use of a flat sample instead of a sample curved to conform to the focusing circle.

These systematic errors can be minimized by using an internal standard material for calibration. The selection of an internal standard is normally based on the following considerations:

1) Its d values are well known and reliable;

2) Its peaks do not overlap or interfere with the peaks of the sample to be measured;

3) It does not react significantly with the sample at the experimental temperature.

The standards typically employed in X-ray diffraction are silicon, rocksalt, diamond, quartz, fluorophlogopite, etc.[76] In this study, an analytical grade and crystallized NaCl (rocksalt) powder was chosen as the internal standard because it was of the least overlapping with the samples under analysis. NaCl powder was mixed with $YBa_2Cu_3O_x$ powder by the weight ratio of 1:3 in the experiments.

In addition to the systematic errors mentioned above, extra caution was needed for the slow scanning and fast chart speeds which were used in the experiments. It was found during the experiments that the scale on the chart paper sometimes deviated away from its nominal scale. The deviation was very small, for example, 0.5 mm short for a length of 300 mm (<0.2%), which might be due to the uneven shrinkage of the paper during manufacturing. But in this study, over 2 meters of the chart paper was used to record the diffraction spectrum in each experiment. Hence the cumulative error from it could not be ignored in order to get highly precise lattice parameters. In each X-ray experiment a calibration curve was constructed by plotting $\Delta(2\theta)$, the peak shift from its theoretical value, against 2θ of NaCl lines measured from the experimental spectrum. The curves were used to correct the peak positions, *i.e.* 2θ values, of the $YBa_2Cu_3O_x$ phase. It was found that these curves were not always horizontal. Two of them are shown in Figure 14 on the following page.

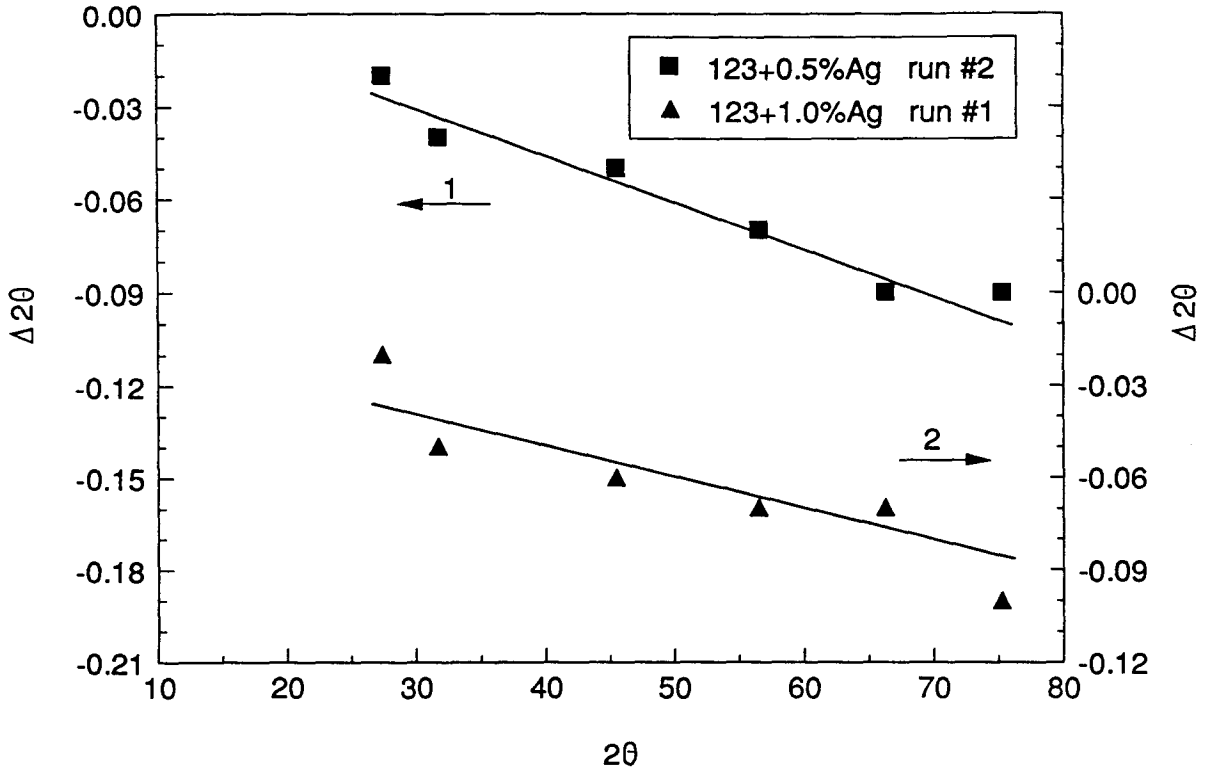

Figure 14 Calibration curves for 2θ measurements of X-ray diffraction

Because of the use of slow scanning and fast chart speeds diffraction peaks were broadened. For the diffractometer method, there are several factors (*e.g.*, absorption of X-ray by the sample and vertical divergence of the X-ray beam) which affect the peak profile asymmetrically. Due to this inherent nature, broadened peaks are usually obviously asymmetrical. The methods usually used to determine the positions of these broadened and/or asymmetrical peaks are[76-79]:

1) Use of $dI/d\theta=0$ (θ_1);

2) Extrapolating the linear portions of a peak and taking the intersection point as the peak position (θ_2);

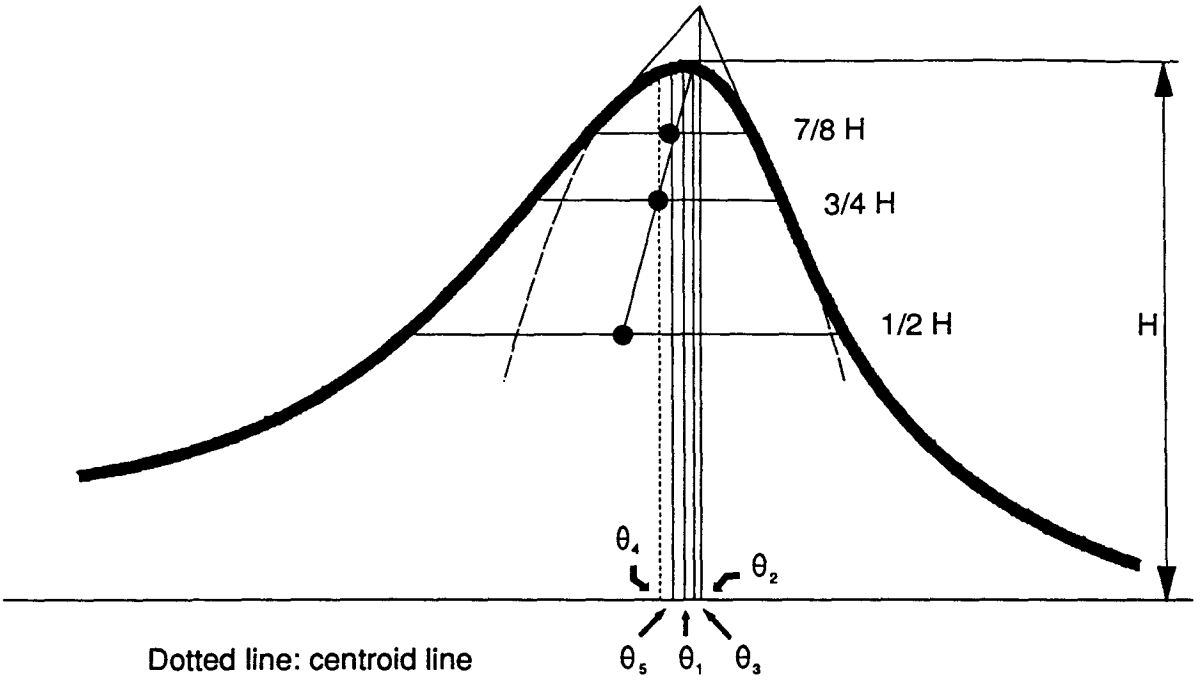

Figure 15 Methods to determine X-ray diffraction peak positions

3) Extrapolating the center at 1/2, 3/4, 7/8,····· peak heights and taking the intersection point of the extrapolation line and the peak profile as the peak position (θ_3);

4) Use of centroids (θ_4);

5) Constructing and refining a parabolic equation with a vertical axis by using several points on the profile of a peak, and taking the axis of the parabola as the peak position (θ_5);

6) Use of peak-hunting software.

The methods 1-5 are illustrated in Figure 15. Mathematically, method 4 is the most precise. Since most of the JCPDS powder diffraction cards were established by using method 3[77], method 3 was employed in this study.

By taking a combination of the above experimental routines, an accuracy of ±0.01° for measuring 2θ was reached. A USGS computer program (courtesy of the Department of Geological Science, UBC) using an iterative least square solution was then employed to calculate the lattice parameters and their standard deviations from the measured 2θ values. After 9 cycles of iteration, the final values were normally accurate to within 4 decimal places for lattice parameters a and b, and 3 decimal places for lattice parameter c.

2.5 Electrical Property Measurements

2.5.1 T_c Measurement

The critical temperature (T_c) of the samples were determined by a standard DC four-lead technique measuring the resistance as a function of temperature. The apparatus used is shown in Figure 16. Two leads touching a cylindrical sample (~ϕ9.5×3 mm) carry a known constant DC current, 10 mA here, into and out of the samples, and the other two leads measure the potential drop between two equipotential surfaces resulting from the current flow. Electrical contacts were prepared with a silver paint. A diode temperature sensor was used to measure the temperature of the sample. The sample was spring-load connected to a superconductor resistance bridge (Department of Physics, UBC).

The measurements were done in the temperature range between room temperature and liquid nitrogen temperature. During measurements, a quartz tube containing the sample was gradually lowered into a liquid nitrogen bath. The quartz tube was also filled with

nitrogen in order to obtain good heat transfer and keep the sample away from water to ensure good electrical contact between leads and electrical contacts. Both temperature and resistance were recorded by a chart recorder (Goerz Metrawatt SE780). The chart recorder was zeroed with respect to the temperature and resistance before each experiment. The accuracy of temperature (ΔT) was ± 0.5 K.

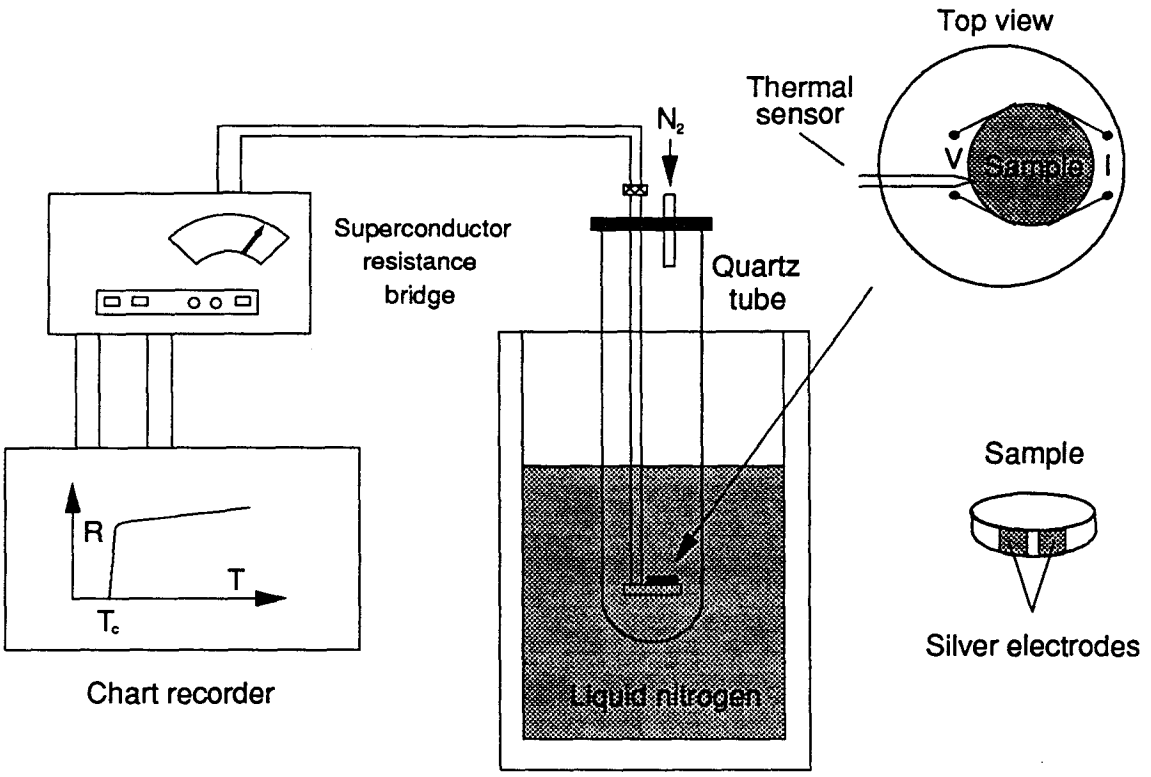

Figure 16 Schematic diagram of the Sample and apparatus for T_c measurements

2.5.2 Normal State Resistance

Quality of superconductors can also be determined by their normal state electrical properties[46]. To describe electrical properties independently of the sample shape, resistivity (ρ) is normally used. In this study, because the samples were not perfectly cylindrical, a

normalized resistance, which is the ratio of the resistances at 295K and 100K (R_{295K}/R_{100K}), was used instead of the resistivity ratio. Data were taken from the extrapolation of the linear parts of the curves obtained in T_c measurements, and the resistance data obtained directly from the plots were also used.

2.5.3 J_c Measurement

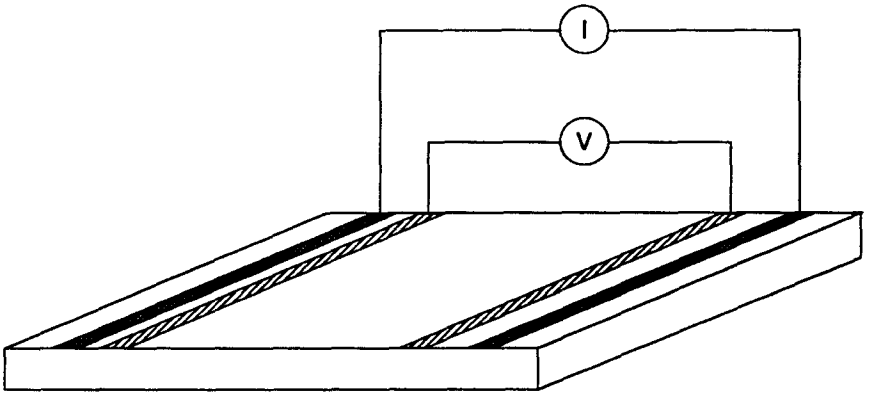

Figure 17 The geometry of the sample used for J_c measurement

Critical current density (J_c) measurements were performed at a temperature of 4.2K using liquid helium as the cryogen by the Department of Physics, UBC. The four-lead technique was also employed here. Rectangular samples (~10×5×1 mm) were used so that the dimensions of the samples could be measured more precisely. The measurements were performed without a magnetic field. The geometry of the sample used for J_c measurements is shown in Figure 17. A voltage *versus* current was obtained in each experiment. The current value at 1 μV/cm was used to compute the critical current density, J_c, of the sample measured.

3 RESULTS

3.1 X-ray Diffraction Phase Identification

Sintered pellets with various compositions and post-sintering heat treatment conditions (annealing or quenching) were reground into powders separately. These powders were characterized qualitatively with respect to the phases present by a Phillips X-ray powder diffractometer operated at 36 kV/20 mA. A normal scanning speed of $2\theta=1^\circ$ per minute was used. Room temperature X-ray diffraction spectra between 2θ values of 14 and 70° for annealed samples, and 14 and 60° for quenched samples were obtained. All samples were tested under identical experimental conditions. The major phase was identified as orthorhombic $YBa_2Cu_3O_x$ in annealed samples whereas that of quenched samples was tetragonal $YBa_2Cu_3O_x$ which has a lower x value. Some typical X-ray diffraction spectra which were reproduced are shown in Figures. 18-25. A trace amount of Y_2BaCuO_5 phase, which was conventionally called 211 or green phase (due to its color), was detected in all samples containing silver. But this green phase was not found in pure $YBa_2Cu_3O_x$ samples. Metallic silver phase was not found in samples containing 1% or less silver in annealed samples. Silver phase was difficult to detect in quenched samples because the strongest peak of silver, (111), is at $2\theta=38.12^\circ$ which overlaps the (005) peak of tetragonal $YBa_2Cu_3O_x$ at 38.20°. It seemed that the apparent solid solubility of silver in $YBa_2Cu_3O_x$ was between 1 and 1.5%. But this may be an overestimation since it is close to the detection limit, which is 1 to 2% for most materials,[78] by the X-ray diffraction method.

Comparing the X-ray diffraction spectra, one feature can be noted. The diffraction intensities of the orthorhombic $YBa_2Cu_3O_x$ phase of silver doped samples are always apparently lower than that of pure $YBa_2Cu_3O_x$ sample even if the amount of silver dopant is as small as

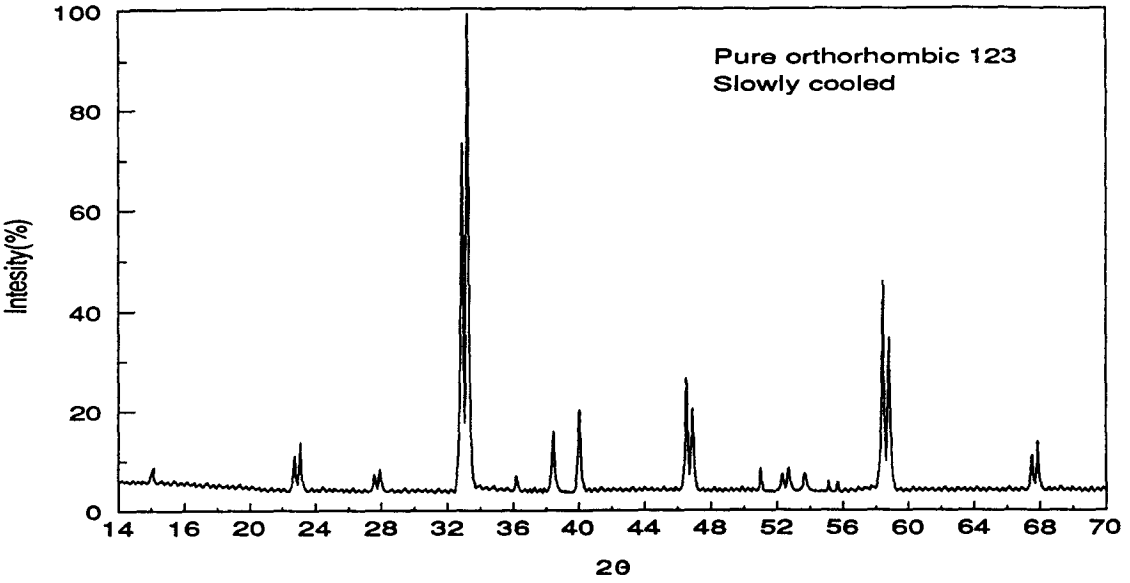

Figure 18 Diffraction pattern of pure orthorhombic $YBa_2Cu_3O_x$

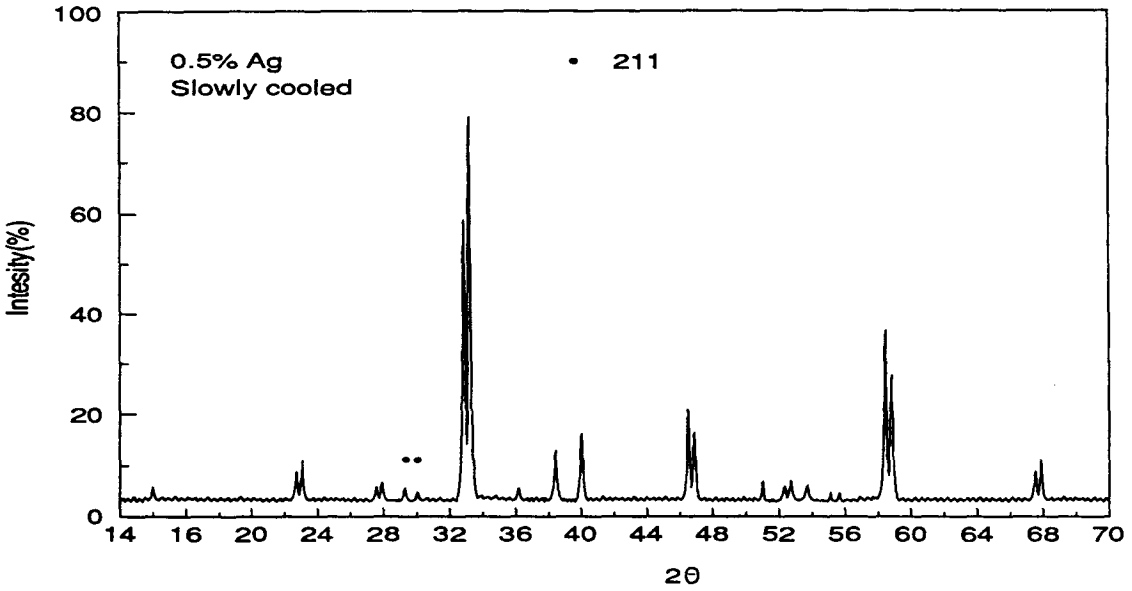

Figure 19 Diffraction pattern of orthorhombic $YBa_2Cu_3O_x$+0.5%Ag

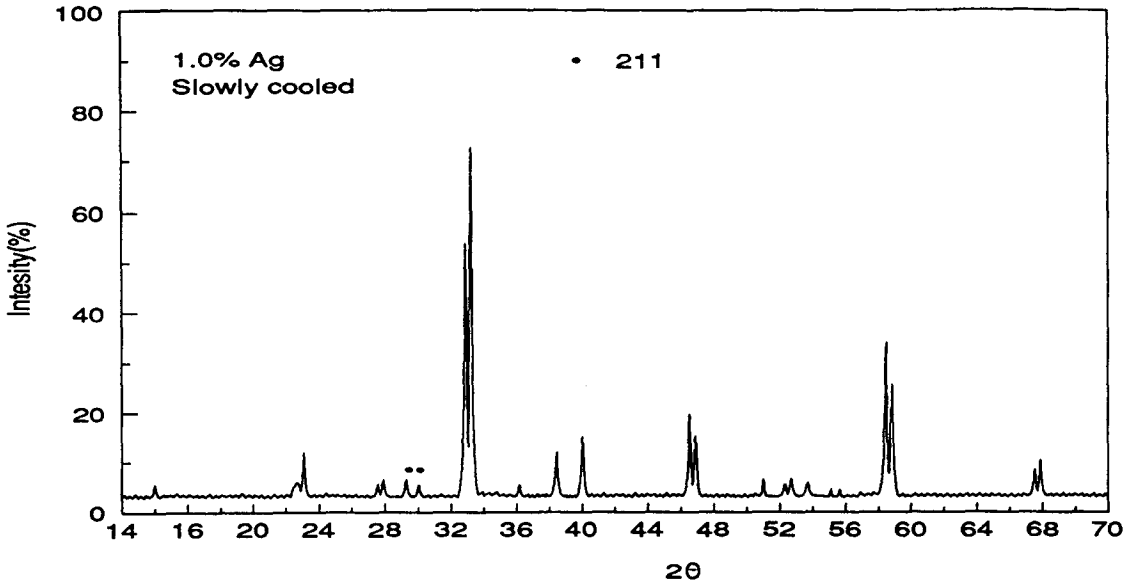

Figure 20 Diffraction pattern of orthorhombic $YBa_2Cu_3O_x$+1.0%Ag

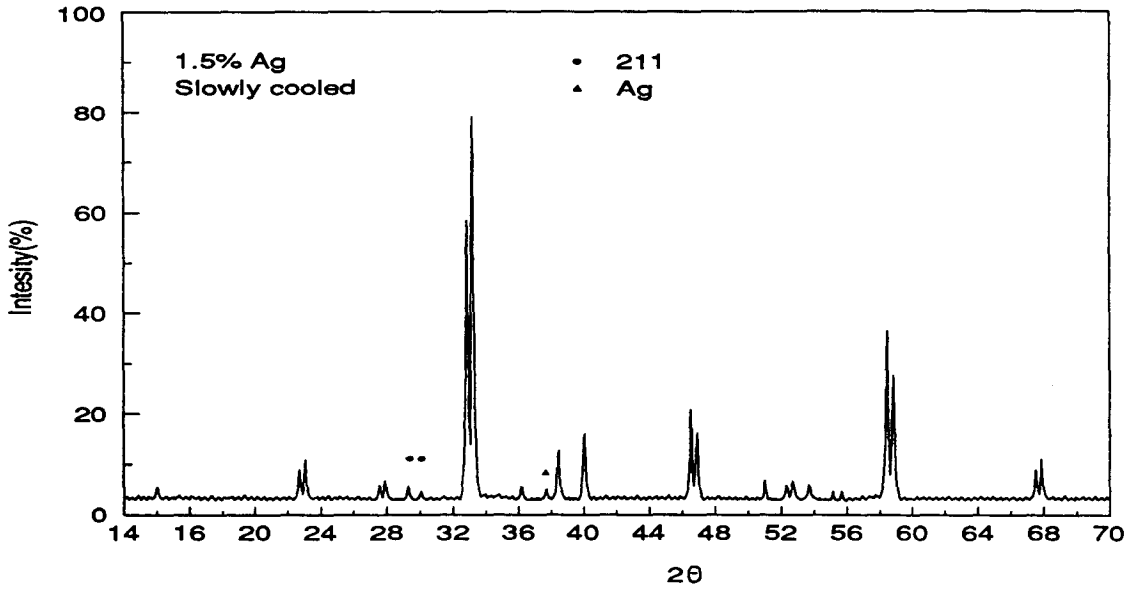

Figure 21 Diffraction pattern of orthorhombic $YBa_2Cu_3O_x$+1.5%Ag

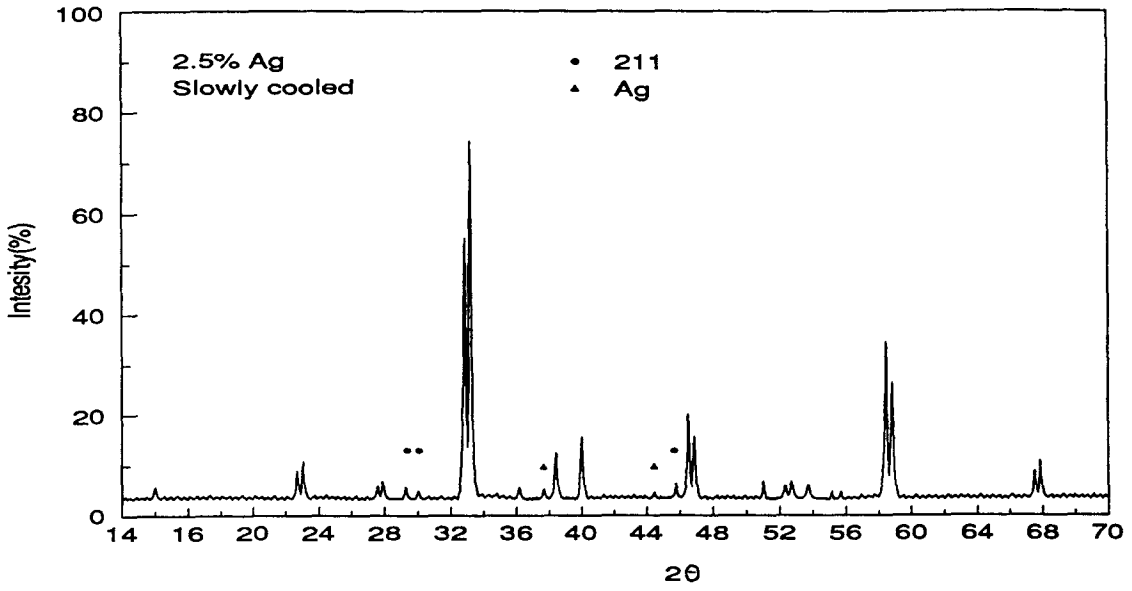

Figure 22 Diffraction pattern of orthorhombic $YBa_2Cu_3O_x$+2.5%Ag

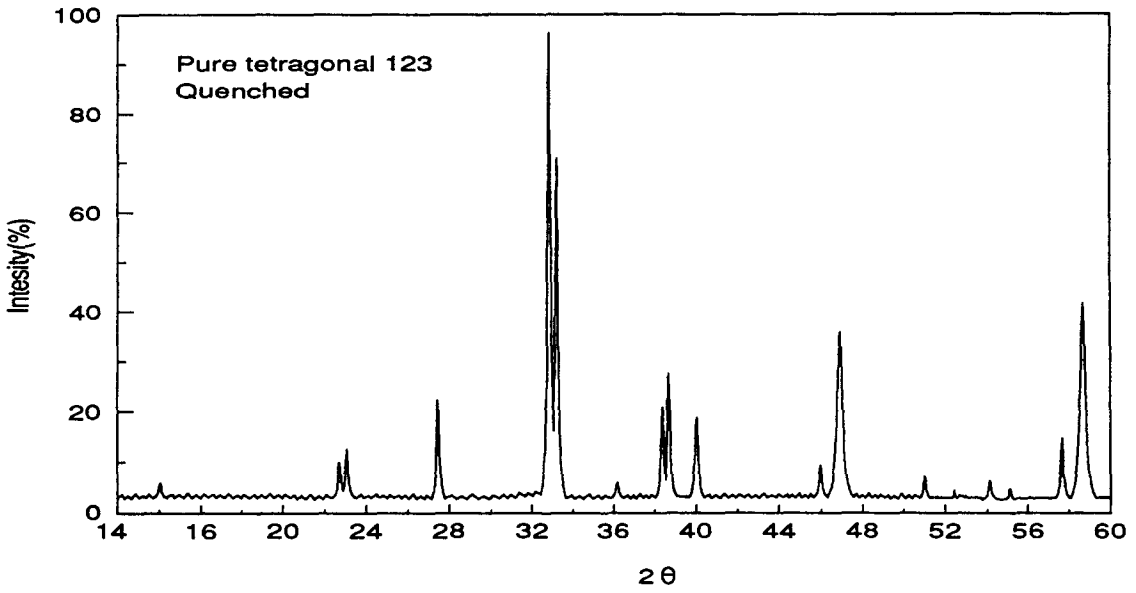

Figure 23 Diffraction pattern of pure tetragonal $YBa_2Cu_3O_x$

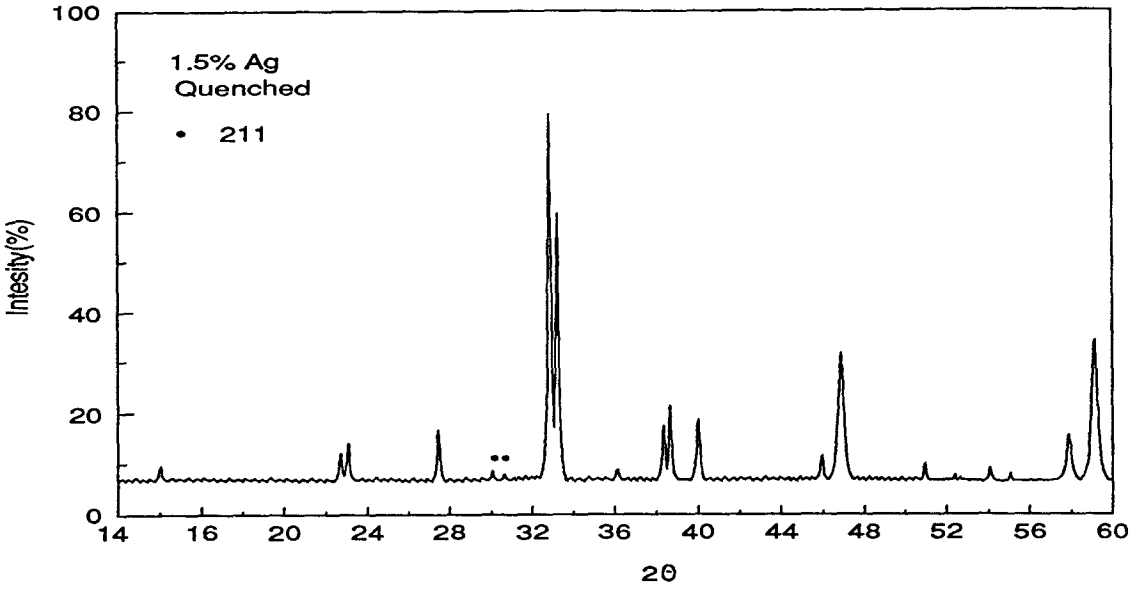

Figure 24 Diffraction pattern of tetragonal $YBa_2Cu_3O_x$+1.5%Ag

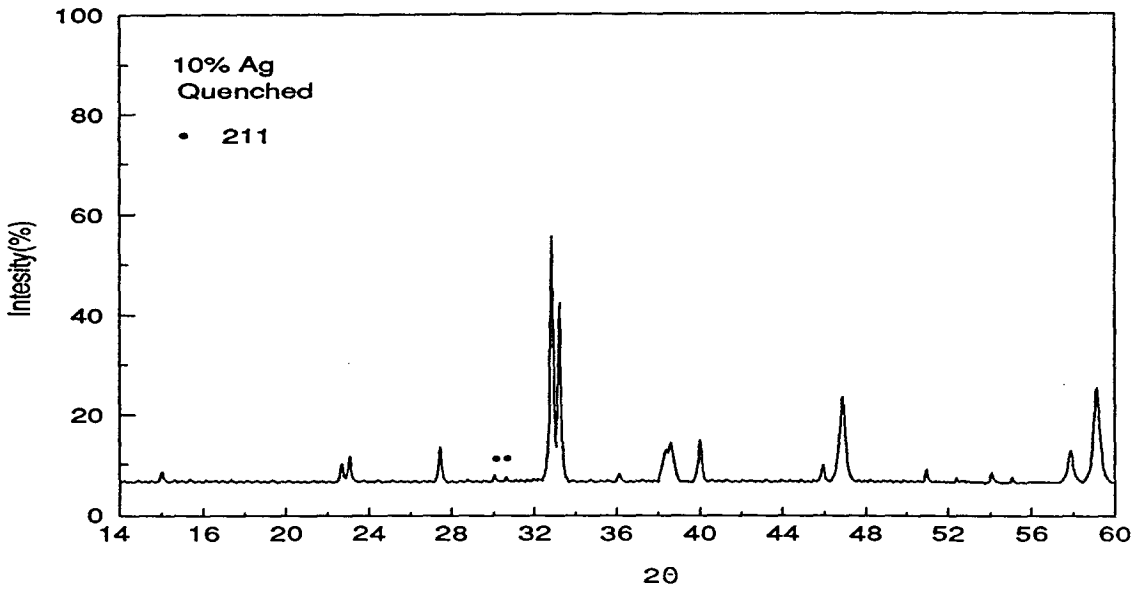

Figure 25 Diffraction pattern of tetragonal $YBa_2Cu_3O_x$+10%Ag

0.5%. By assuming that a linear relationship between the amount of phase present and the diffraction intensity of the phase exists and ignoring the presence of Y_2BaCuO_5, the normalized heights of the strongest peak of orthorhombic $YBa_2Cu_3O_x$ were obtained after deducting the corresponding background counts. The peak is a combination of (103) and (110) lines. The results are listed in Table 5. Although it is difficult to make a quantitative judgement here, the difference is obvious. There are several factors, *e.g.* absorption and scattering of X-rays, which affect the diffraction intensity for the diffractometer method. The most sensitive one is the structural factor. Detailed analysis of an absolute diffraction intensity is very laborious without the help of a computer software due to the complex crystal structure of $YBa_2Cu_3O_x$. No such an attempt has been made in this study. But the change of the diffraction intensity of $YBa_2Cu_3O_x$, at least, provided the information that the crystal structure of $YBa_2Cu_3O_x$ had been changed, even if minutely, after the introduction of silver. It was possible that a $YBa_2(Cu, Ag)_3O_x$ solid solution had been formed.

Table 5 Intensities of the Strongest Peak of Orthorhombic $YBa_2Cu_3O_x$ Phase in Ag+Y-$Ba_2Cu_3O_x$ Samples

Nominal Ag content(%)	0	0.5	1.0	1.5	2.5	5.0	10
Normalized heights of the strongest peak of orthorhombic $YBa_2Cu_3O_x$(%)	100	76	73	82	82	78	79

3.2 Microstructure Studies

3.2.1 Optical Metallographic Examination

Both annealed and quenched samples were polished and viewed in a reflected polarized optical microscope. Optical micrographs of samples with various nominal silver concentrations and heat treatment conditions are shown in Figure 26a to 26h.

In these pictures $YBa_2Cu_3O_x$ grains exhibit needle-like shapes. Following ASTM Standard E112-80, *Estimating the Average Grain Size of Metal*, no attempt was made to determine the average grain size of this type of elongated grain. For most $YBa_2Cu_3O_x$ grains, the thickness was in a range between 5 and 10 μm and the aspect ratio was about 4 to 6. Liquid phase, which appears in bright contrast, can be easily seen at grain boundaries. In slowly cooled and annealed samples, fine twin structures can be clearly seen within $YBa_2Cu_3O_x$ grains because these grains underwent the tetragonal-orthorhombic phase transformation around 650°C during cooling. Twin structure is the distinct feature of the orthorhombic phase. $YBa_2Cu_3O_x$ material is relatively weak compared to other ceramic materials. The samples tend to crumble on polishing, leading to a poor finish. Therefore some irregular voids can been seen in these micrographs because of pull-out of grains while pores left behind during sintering are a more spherical shape. Similar to the X-ray diffraction examination, no silver phase can be readily seen for samples containing 1.5% silver or less.

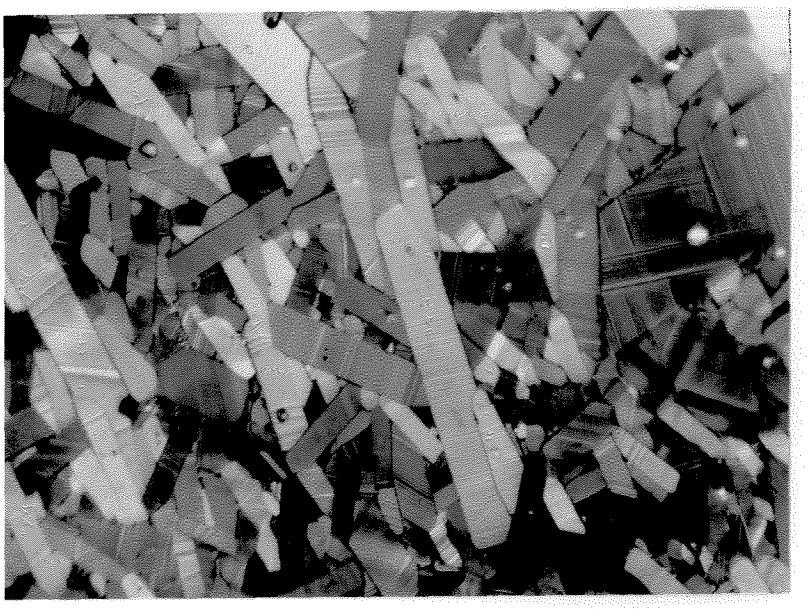

Figure 26a Pure $YBa_2Cu_3O_x$, annealed (bar=20μm).

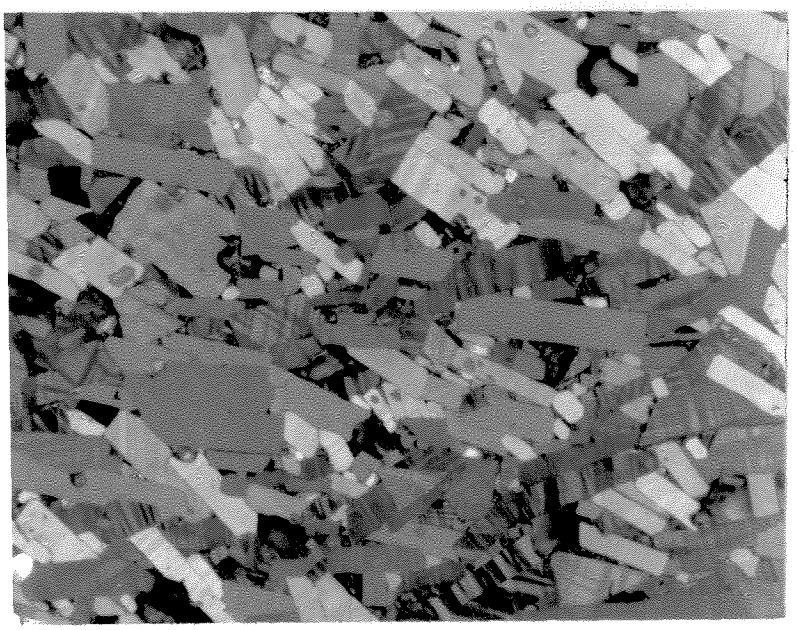

Figure 26b $YBa_2Cu_3O_x$+0.5%Ag, annealed (bar=20μm).

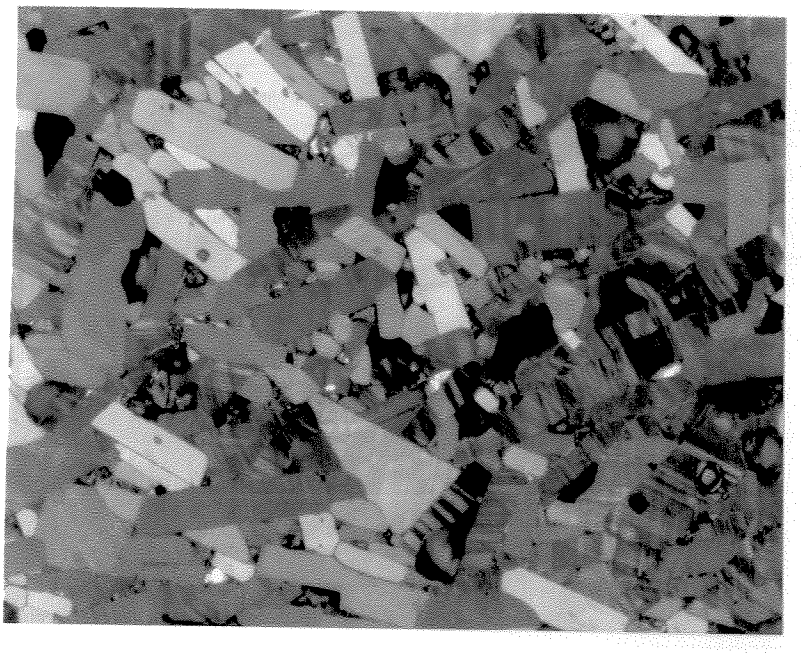

Figure 26c $YBa_2Cu_3O_x$+1.0%Ag, annealed (bar=20μm).

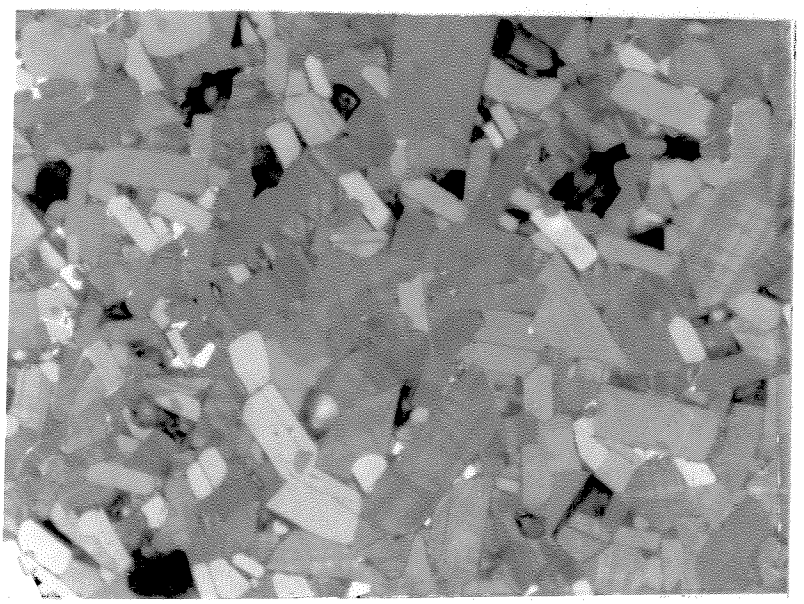

Figure 26d $YBa_2Cu_3O_x$+1.5%Ag, annealed (bar=20μm).

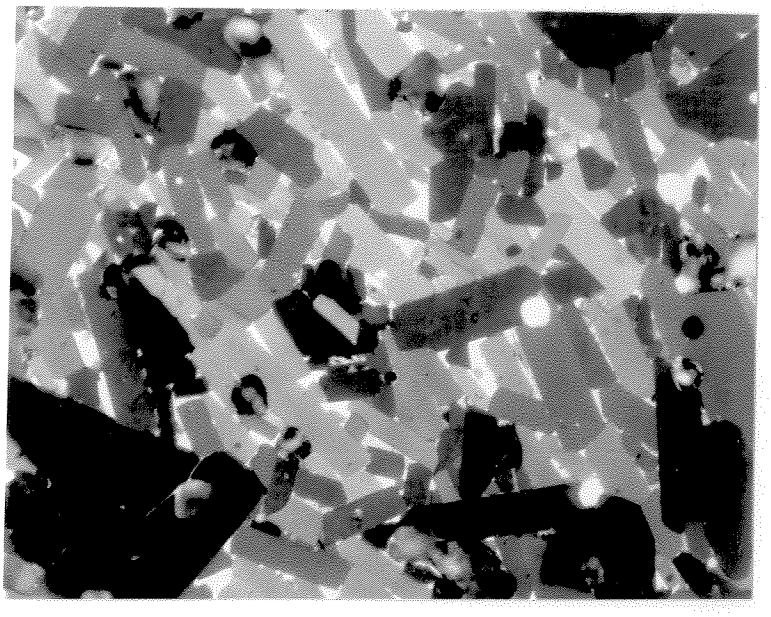

Figure 26e $YBa_2Cu_3O_x$+1.5%Ag, quenched (bar=20μm).

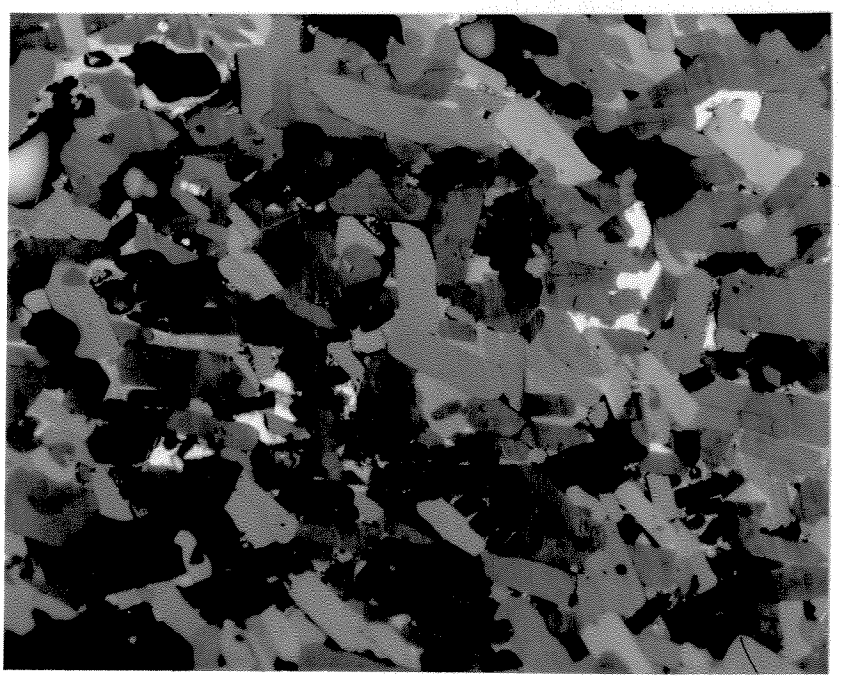

Figure 26f $YBa_2Cu_3O_x$+2.5%Ag, annealed (bar=20μm).

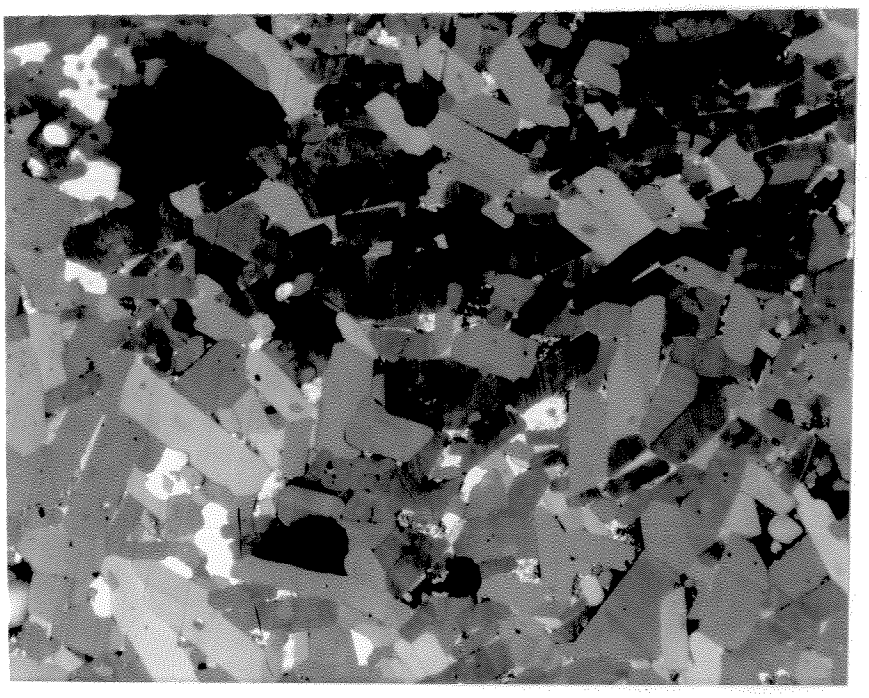

Figure 26g $YBa_2Cu_3O_x$+5%Ag, annealed (bar=20μm).

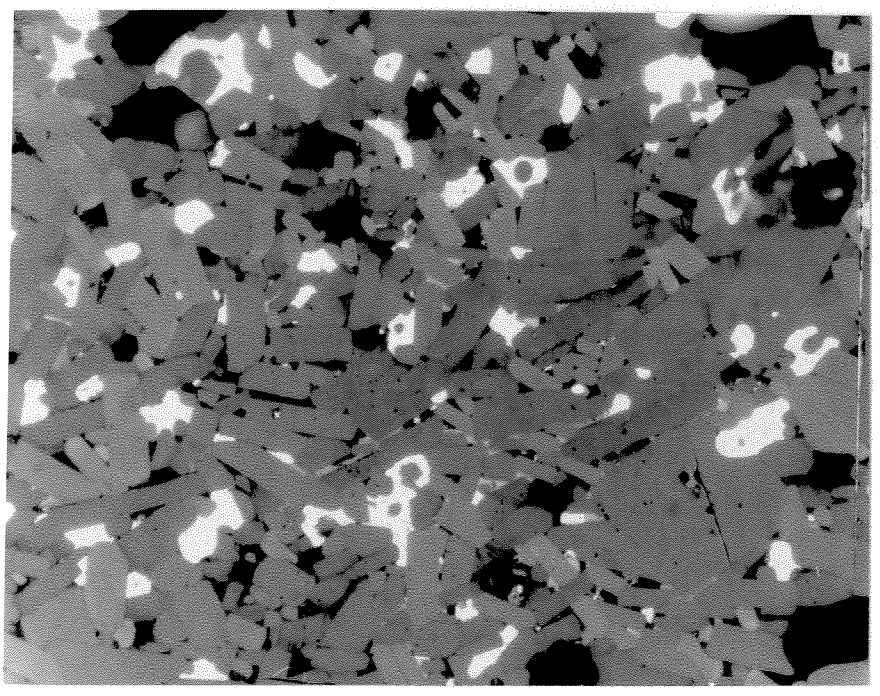

Figure 26h $YBa_2Cu_3O_x$+10%Ag, quenched (bar=20μm).

3.2.2 Electron Metallographic Examination

Since 1.5% would be below the detectability of the optical metallographic method, these samples were coated with a thin layer of carbon and observed under a scanning electron microscope. The accelerating voltage used was 20 kV. To produce a more striking contrast between silver and other phases, the backscattered electron imaging (BEI) method was employed. Selected pictures obtained from the electron metallographic observation are shown in Figure 27a to 27e.

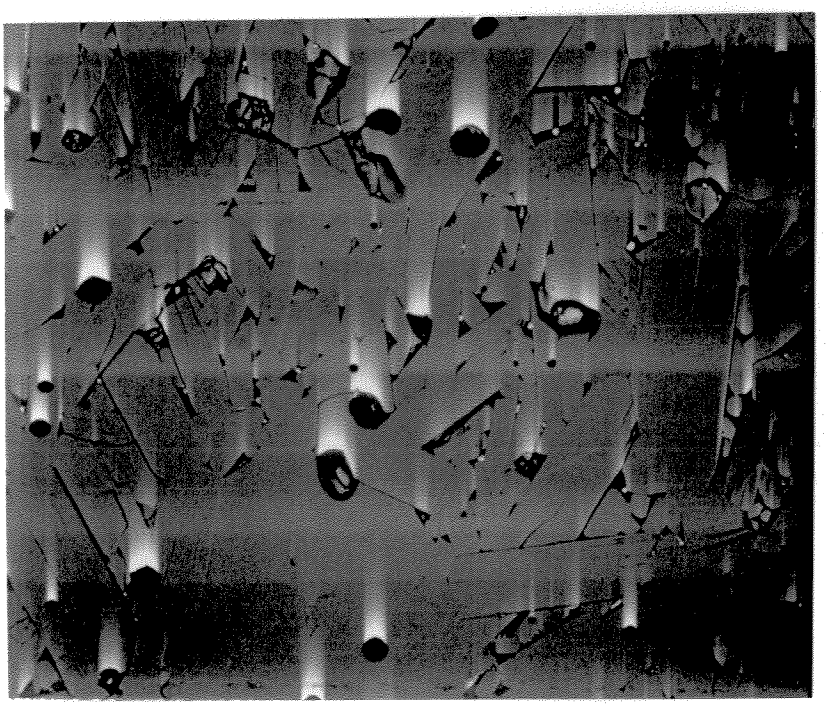

Figure 27a $YBa_2Cu_3O_x$+0.5%Ag, annealed (bar=20μm).

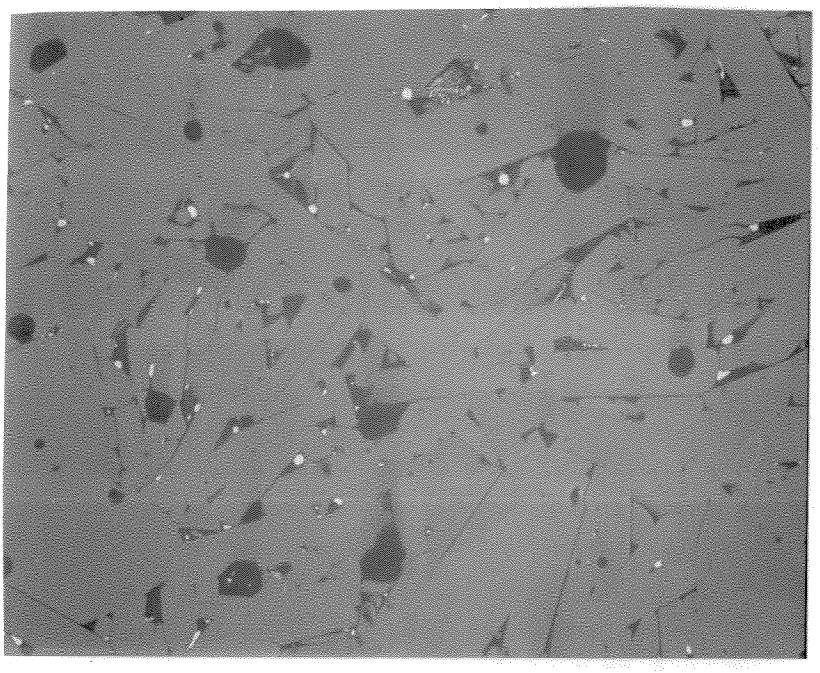

Figure 27b $YBa_2Cu_3O_x$+1.0%Ag, quenched (bar=20μm).

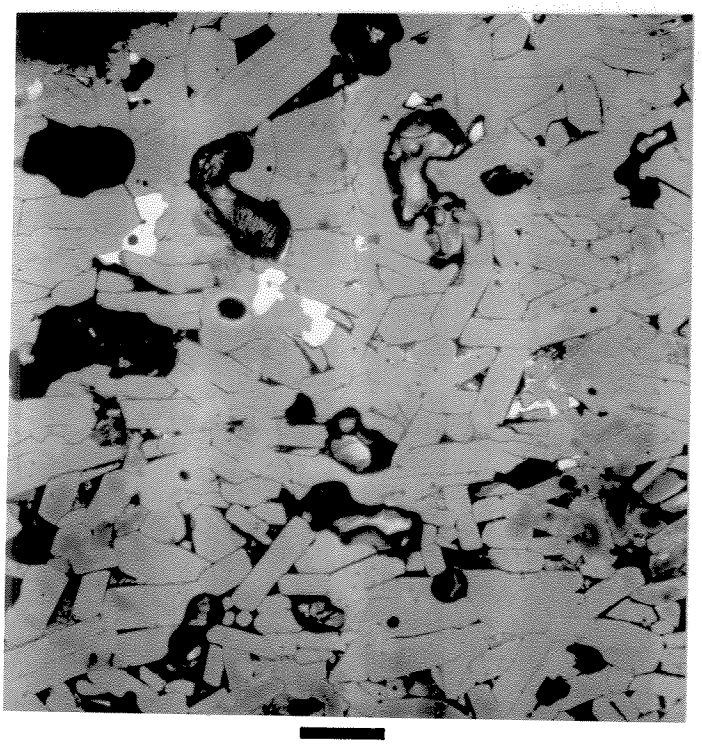

Figure 27c $YBa_2Cu_3O_x$+2.5%Ag, annealed (bar=20μm).

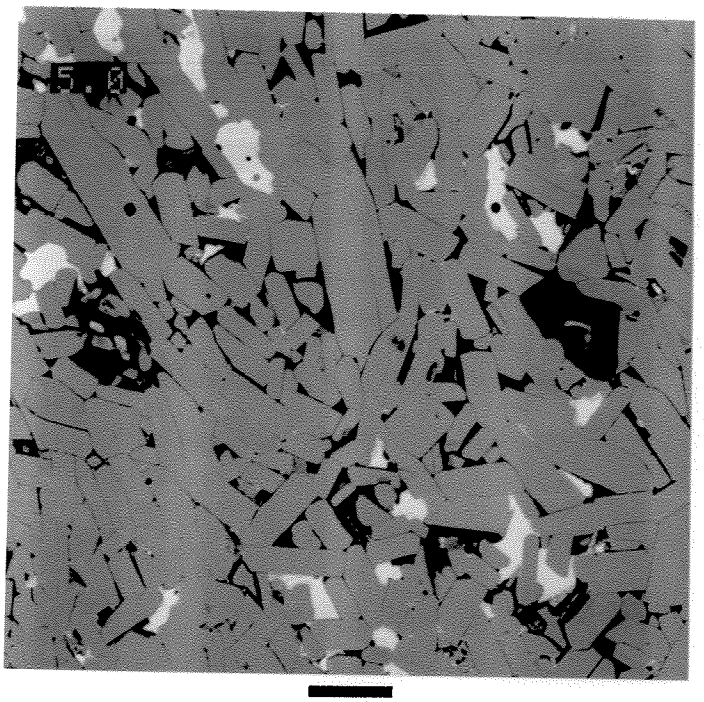

Figure 27d $YBa_2Cu_3O_x$+5.0%Ag, annealed (bar=20μm).

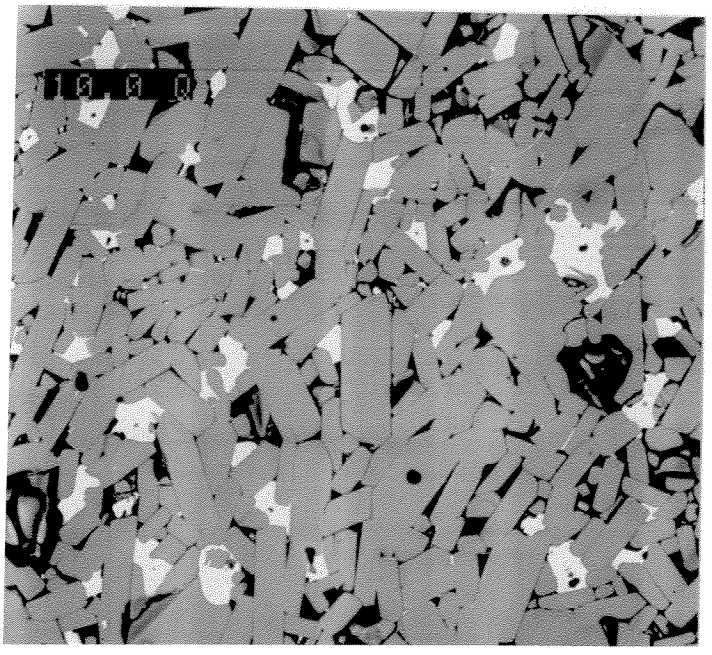

Figure 27e $YBa_2Cu_3O_x$+10%Ag, quenched (bar=20μm).

It can be evidently seen from these BEI pictures that bright particles are present at grain boundaries and triple grain junctions in all samples containing silver. Energy dispersive X-ray spectroscopic (EDX) analyses revealed that these particles were pure silver particles. An EDX spectrum from one of the particles is given in Figure 28. For samples with higher nominal silver concentrations, silver grains are of comparable grain size to that of $YBa_2Cu_3O_x$ grains. The fact that a significant number of silver particles was detected in samples containing even only 0.5% nominal silver suggests that the solid solubility of silver in $YBa_2Cu_3O_x$, if any, is very low.

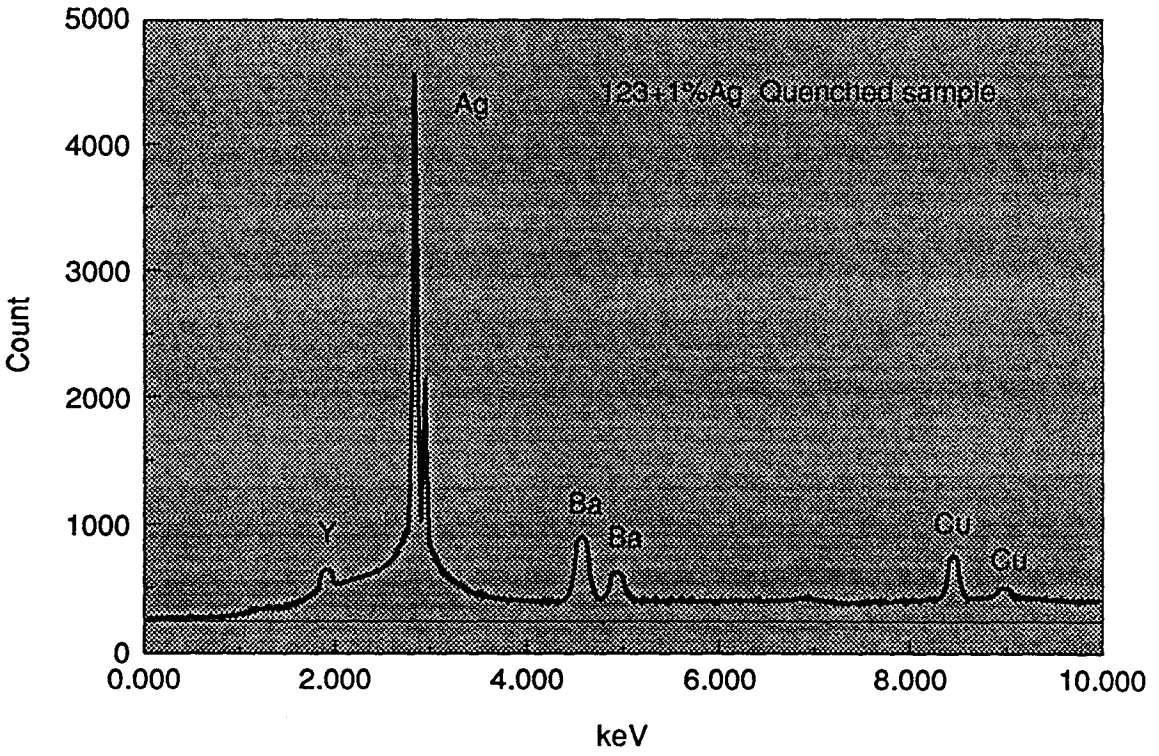

Figure 28 Energy dispersive X-ray spectrum taken from a bright particle at the grain boundary of a quenched $YBa_2Cu_3O_x$ sample containing 1% Ag.

A notable discovery is that a few tiny silver particles were spotted within $YBa_2Cu_3O_x$ grains in annealed samples at a higher magnification. One of them is shown in Figure 29. These particles may be the silver which precipitated within the grains during cooling. This indicated that the solubility would be higher at higher temperatures.

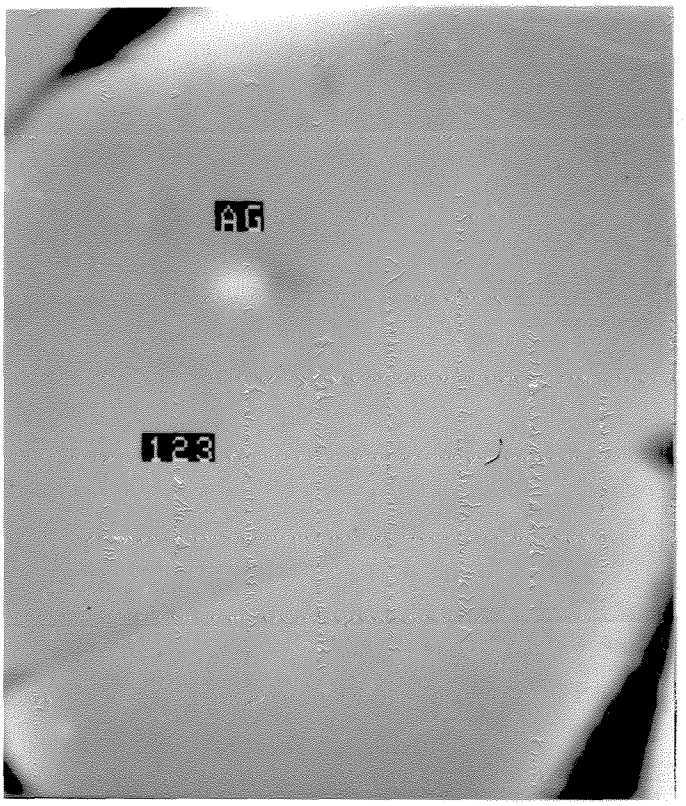

Figure 29 Scanning electron micrograph of an annealed $YBa_2Cu_3O_x$+5%Ag sample. The white spot marked AG is a silver precipitate detected by EDX (bar=1μm).

3.3 Secondary Ion Mass Spectroscopic Study

To confirm the existence of silver within $YBa_2Cu_3O_x$ grains, a secondary ion mass spectrometer was employed using $^{89}Y^+$ as the internal standard. Since SIMS is not a quantitative technique as the ion yield is strongly affected by the matrix,[80] the SIMS examination was a preliminary study. Selected samples were examined and the spectra were digitized and reproduced. Every precaution was taken to avoid the grain boundary. Only large grains were analyzed for detecting the silver within the grain. Some reproduced positive SIMS spectra are shown in Figure 30. As seen from the spectra, both $^{107}Ag^+$ and $^{109}Ag^+$ isotopic peaks are present in the samples under examination. These results confirmed that silver was definitely present within $YBa_2Cu_3O_x$ grains.

3.4 Quantitative WDX Analysis

Quantitative wavelength dispersive X-ray spectroscopic (WDX) analyses were carried out on both annealed and quenched samples to probe the extent that silver goes into $YBa_2Cu_3O_x$ grains. A large number of $YBa_2Cu_3O_x$ grains with different morphologies were analyzed. The selection of grains was random. The results are listed in Table 6. In addition, Y, Ba and Cu in all $YBa_2Cu_3O_x$ grains were analyzed and found to be in the atomic ratio of 1:2:3. Deviations from the ratio were never exceeded by more than 10%.

The intragranular silver concentrations detected by WDX against the nominal silver concentrations are plotted in Figure 31. By assuming Cu is substitued by Ag and x=7, weight percent of the intragranular concentration is converted to the y of $YBa_2Cu_{3-y}Ag_yO_x$. The y-value scale is also included in the WDX plot. An unexpected feature of the WDX results is that no matter how low the original silver concentration is, only a small amount of silver can go into

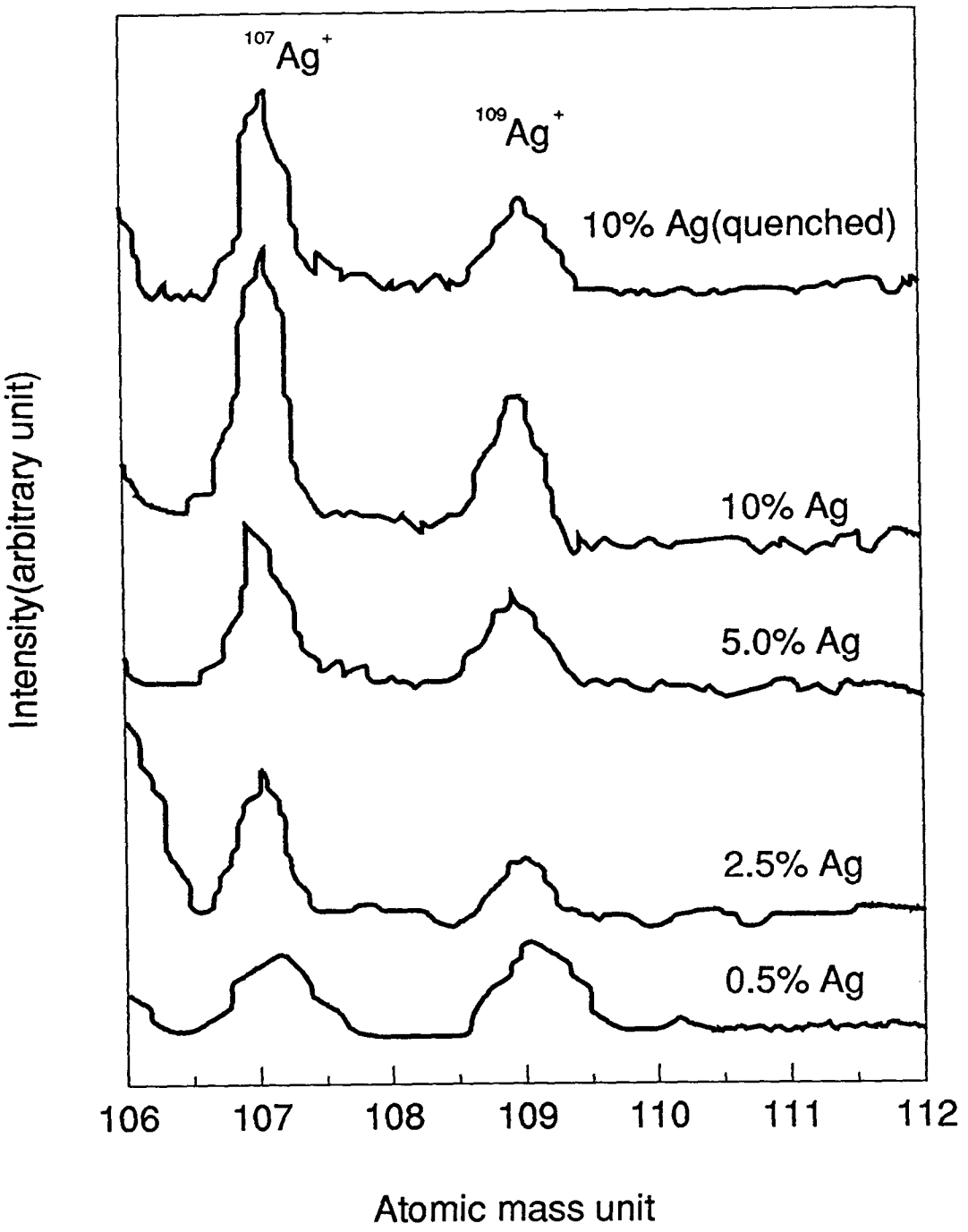

Figure 30 Positive SIMS spectra of $YBa_2Cu_3O_x$ samples containing silver.

$YBa_2Cu_3O_x$ grains. The intragranular concentration of silver increases linearly with the increase of the nominal concentration but reaches a saturation level after the nominal concentration is over 2.5%. As predicted by electron microscopic observations, at the same nominal concentration level, quenched samples always have higher intragranular concentration of silver than the annealed samples. The saturation suggests that the amount of silver that can be dissolved in $YBa_2Cu_3O_x$ has a maximum value. Neglecting the precipitation of silver, this value would be the silver solubility in $YBa_2Cu_3O_x$. The room temperature and 950°C solubilities are estimated to be 0.37% and 0.42%, respectively (as can be seen from the figure).

Table 6 Intragranular Silver Concentrations Obtained from WDX Analyses

Nominal Ag (%)	Intragranular Ag(%)			
	Annealed samples			Quenched samples
	Batch #1	Batch #2	In-house made powders	
0.5	0.12(4)	0.14(3)	0.15(5)	0.15(2)
1.0	0.15(3)	0.16(2)	0.17(4)	0.20(3)
1.5	0.26(3)	0.32(4)	0.28(3)	0.28(4)
2.5	0.32(5)	0.30(4)	0.35(6)	0.42(5)
5.0	0.37(4)	0.41(5)	0.39(4)	0.41(4)
10	0.37(6)	0.35(4)	0.40(10)	0.42(5)

Note: The bracketed numbers indicate the standard deviations of the last decimal.

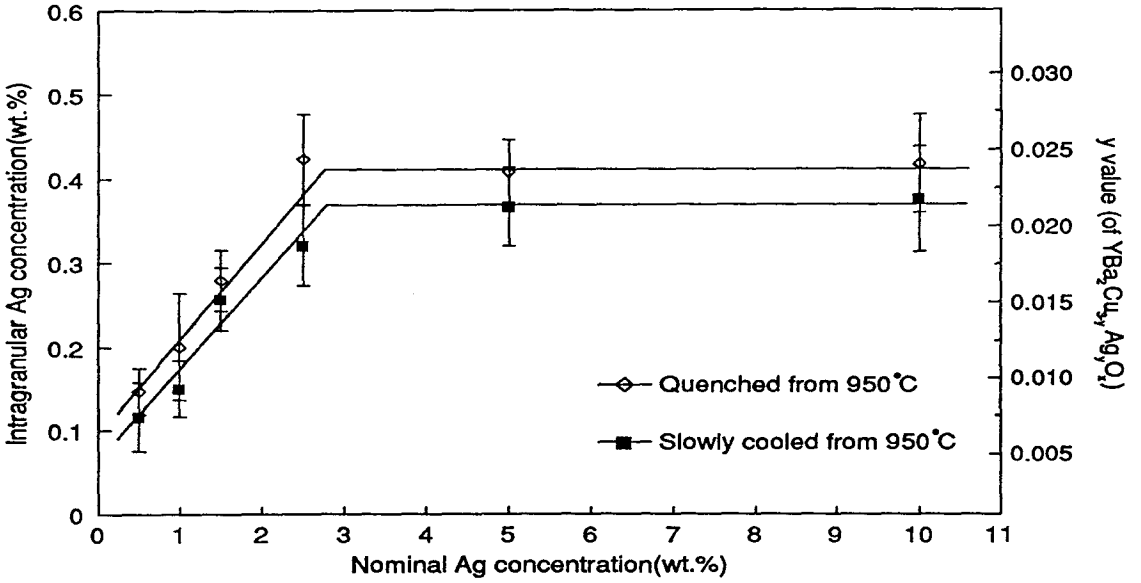

Figure 31 Intragranular vs nominal silver concentrations

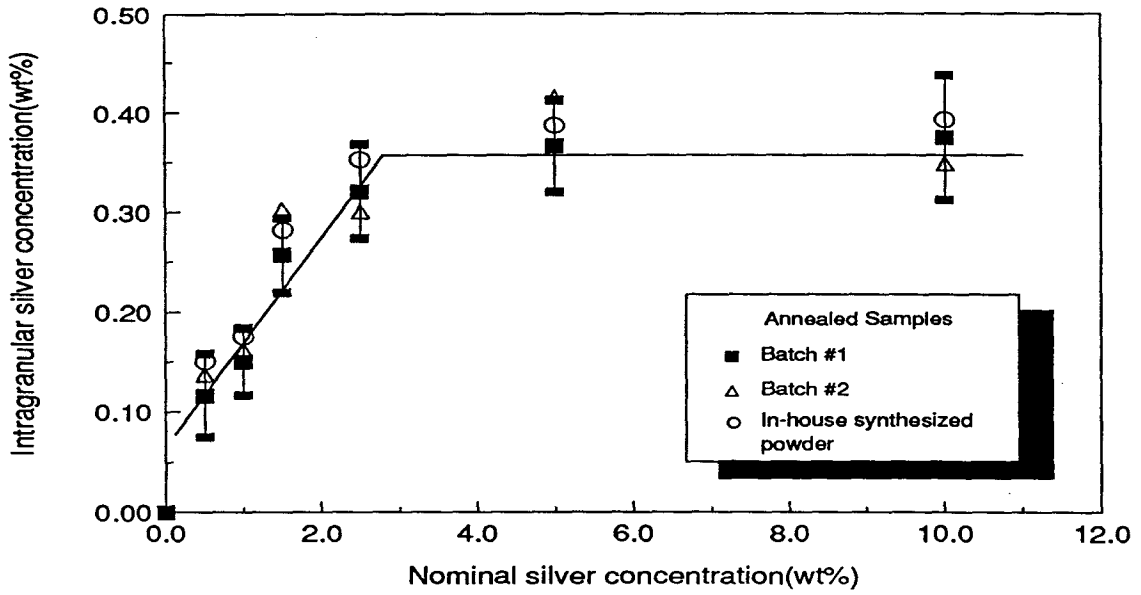

Figure 32 Reproducibility of WDX data for determining the intragranular silver concentrations

To check the reproducibility of WDX data, another batch of annealed samples was prepared and analyzed. Nearly the same results were yielded as shown in Figure 32. Next, a separate set of samples containing 0.5, 1.5 and 5% nominal silver was heat-treated two days each at 950, 800, 600, 400 and 200°C. The WDX results from these samples did not produce a statistical difference from those processed with normal annealing procedures. Uncertainties resulting from kinetic problems could, therefore, be eliminated.

3.5 Precise Determination of Lattice Parameters

As stated earlier, silver in a $YBa_2Cu_3O_x$ grain could be in solid solution as well as in the form of precipitates. The size of these possible precipitates could be very tiny and therefore invisible in a scanning electron microscope. The formation of a solid solution between silver and $YBa_2Cu_3O_x$, possibly in a substitutional type of $YBa_2(Cu, Ag)_3O_x$, will change the dimensions of the unit cell because size of silver ion is much larger than that of copper ion. To ascertain if the silver within the $YBa_2Cu_3O_x$ phase is really incorporated within the lattice, experiments were performed to determine lattice parameters of the orthorhombic $YBa_2Cu_3O_x$ phase by the method detailed in section 2.4. As mentioned in section 2.1, two batches of the samples were made for the purpose of testing the reproducibility of experimental data. Powder samples from both batches were tested and the data were averaged. Some selected 2θ values measured from the experiments and used for the calculations of the lattice parameters are listed in the Appendix. The resulting lattice parameters are listed in Table 7. The bracketed numbers indicate the standard deviations of the last digit.

For the orthorhombic $YBa_2Cu_3O_x$ phase in annealed samples, plots of lattice parameters *versus* nominal silver concentrations are shown in Figures 33, 34 and 35. It can be seen that lattice parameters a and c increased with the nominal silver concentration and appeared to reach

constant values at high silver concentrations. Also, as shown in Figure 36, the unit cell volume calculated from the lattice parameters of the orthorhombic $YBa_2Cu_3O_x$ increased with the silver concentration. These results are in agreement with the WDX results indicating that copper ions were partially substituted by silver ions and the substitution has a upper limit level. The lattice parameter b remained relatively unchanged within the statistical deviations of the measurements. The information provided by the lattice parameter measurements implied that the dissolved silver ions occupied some specific crystallographic positions in the lattice and modified slightly the crystallographic parameters of the lattice in such a way that only the a and c parameters are significantly altered but not the b parameter. A possible explanation is offered in the discussion section.

Table 7 Lattice Parameters of Orthorhombic $YBa_2Cu_3O_x$ Phase from X-ray Diffraction

Nominal Ag(%)	a(Å)	b(Å)	c(Å)	V(Å^3)
0	3.8195(5)	3.8894(5)	11.670(1)	173.36(6)
0.5	3.8225(4)	3.8892(4)	11.676(1)	173.58(5)
1.0	3.8229(8)	3.8894(8)	11.676(2)	173.61(9)
1.5	3.8231(5)	3.8901(5)	11.681(1)	173.72(6)
2.5	3.8227(7)	3.8904(7)	11.679(1)	173.69(6)
5.0	3.8240(10)	3.8900(10)	11.681(3)	173.76(13)
10	3.8247(8)	3.8888(8)	11.681(2)	173.74(10)

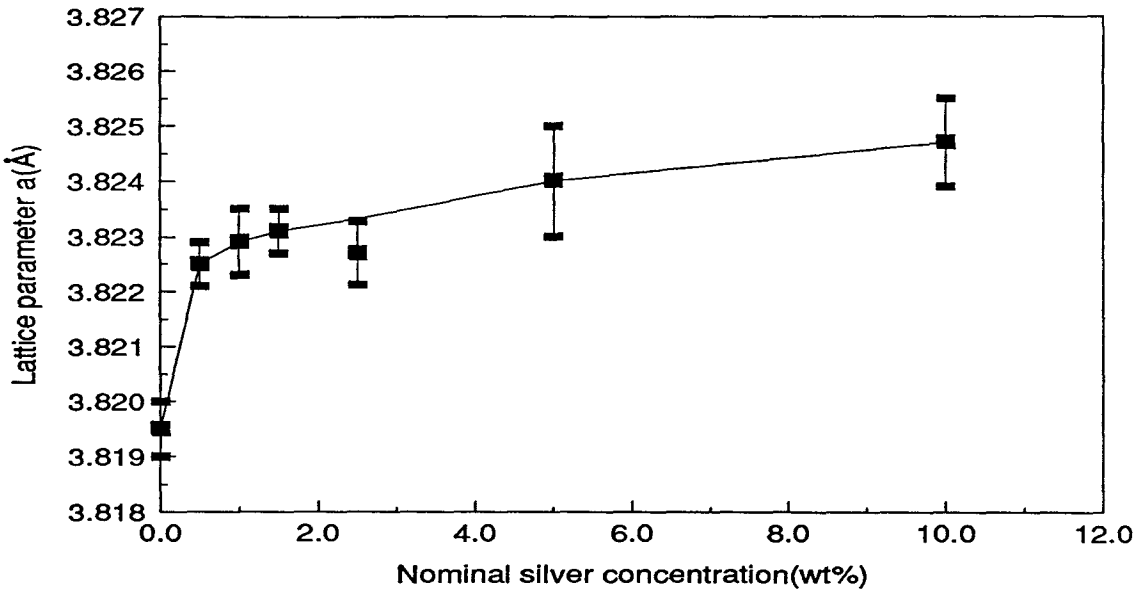

Figure 33 Lattice constant a of orthorhombic $YBa_2Cu_3O_x$ vs nominal silver concentration

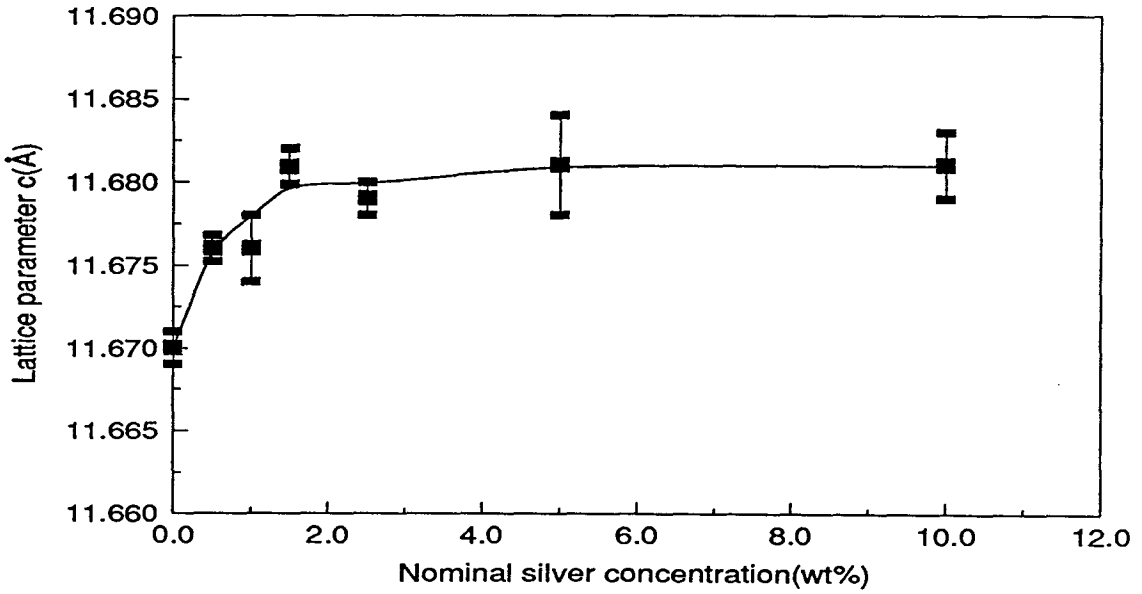

Figure 34 Lattice constant c of orthorhombic $YBa_2Cu_3O_x$ vs nominal silver concentration

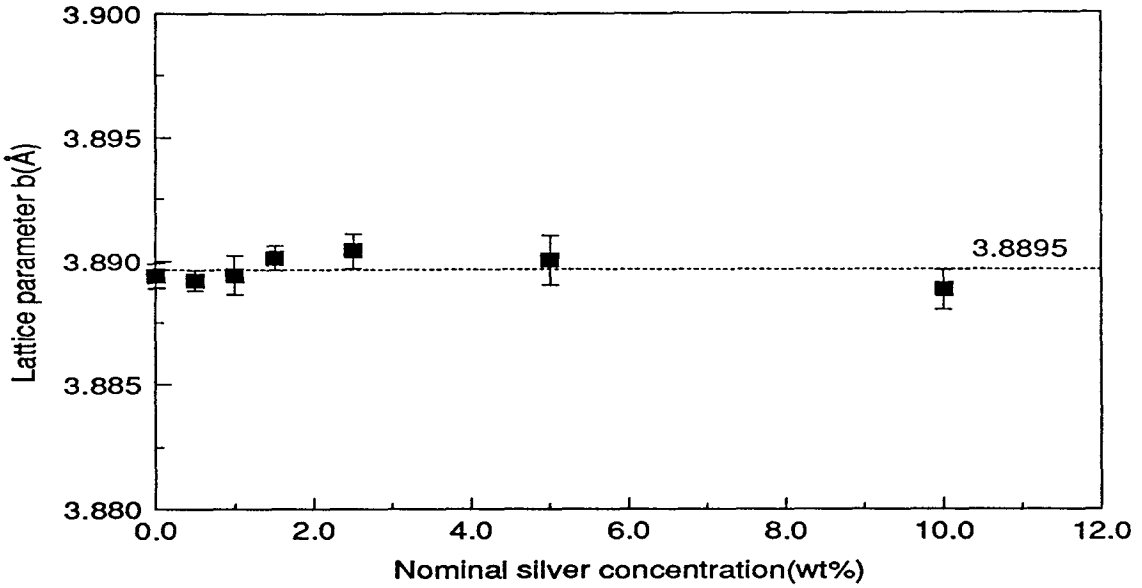

Figure 35 Lattice constant b of orthorhombic $YBa_2Cu_3O_x$ vs nominal silver concentration

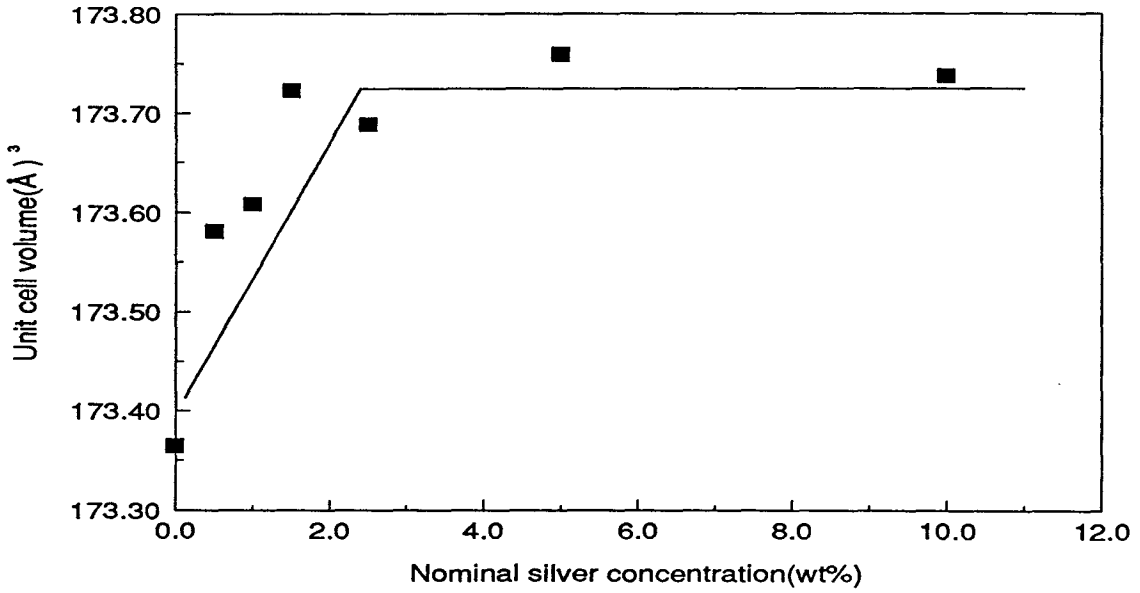

Figure 36 Unit cell volume of orthorhombic $YBa_2Cu_3O_x$ vs nominal silver concentration

3.6 Electrical Property Measurements

As mentioned in section 2.1, in-house synthesized $YBa_2Cu_3O_x$ powders were used to prepare samples for electrical property measurements, instead of the commercial $YBa_2Cu_3O_x$ powders. These samples were also examined by WDX and the data are included in Figure 32. No statistical discrepancy of intragranular silver contents between these samples and that of the samples made by the commercial powders was found.

Figure 37 shows typical resistance *versus* temperature curves. From these curves mid-point superconducting transition temperatures (T_{cm}) were determined and are included in Table 8. T_{cm} values are similar for all $YBa_2Cu_3O_x$ samples containing silver. It should be noted that in all cases the transition from normal to superconducting state remained sharp. Overall, silver does not have much influence on the transition temperature.

It is thought that the introduction of silver within the lattice (in the place of Cu) may alter the inherent resistance of the system. As the substitution of silver into the $YBa_2Cu_3O_x$ lattice reached a constant value, the change with resistivity may also reflect this effect of the solubility limit.

The normal state resistance of silver doped $YBa_2Cu_3O_x$ compound was investigated by using the resistance as obtained directly from the plots and by extrapolating the linear portion of the resistance *versus* temperature curve to determine the resistances at 295K and 100K. The normalized resistance ratio, R_{295}/R_{100}, *versus* nominal silver concentration was plotted in Figure 38. It was found that the behavior of normalized resistance had a similar behavior to those of the lattice parameters and intragranular silver concentration. Though there is a significant scatter in the data, R_{295}/R_{100} increased linearly with increasing silver concentration and then reached a

constant value at high silver concentration. The results also strongly suggest that it was the intragranular, not the intergranular, silver that might be playing a more important role in changing the electrical properties of $YBa_2Cu_3O_x$ compounds.

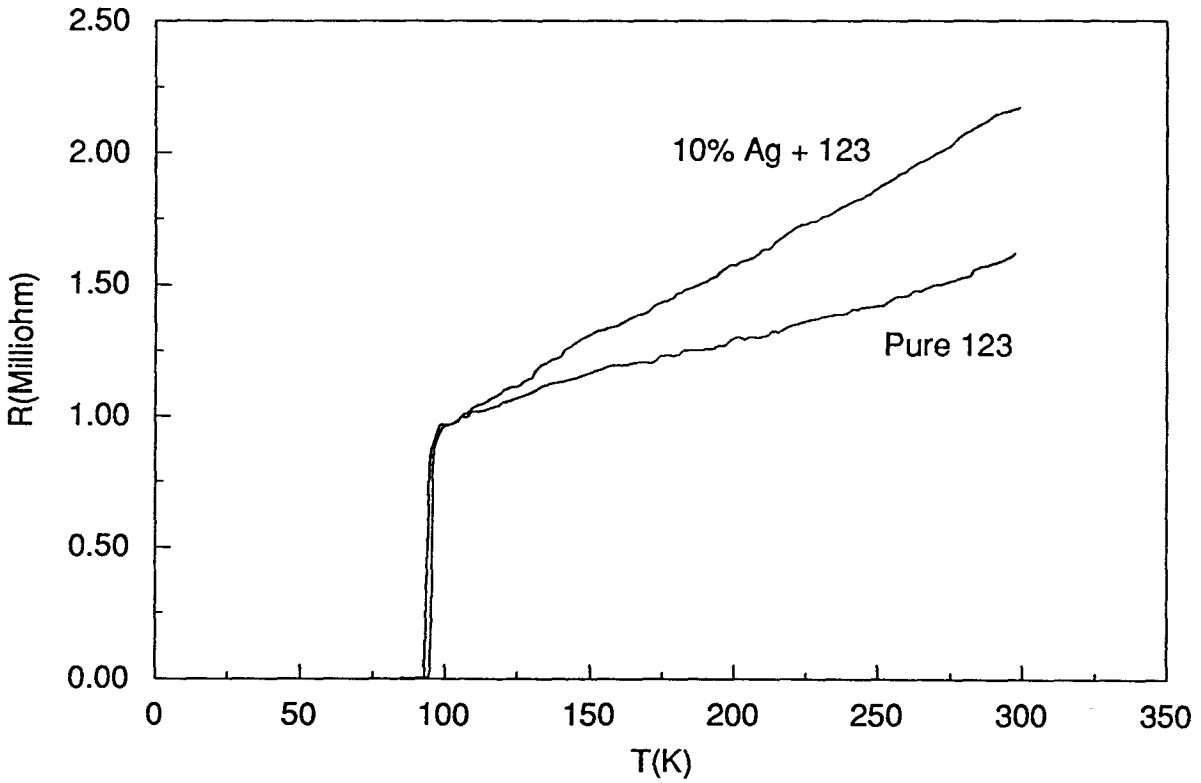

Figure 37 Resistance of $YBa_2Cu_3O_x$ as a function of temperature

Typical plots from the J_c measurements are shown in Figure 39 and 40. J_c data at 1 μV/cm are also contained in Table 8. Silver reduced J_c values in all cases except the nominal silver concentration of 0.5%. The J_c values were determined by the Physics Department, UBC.

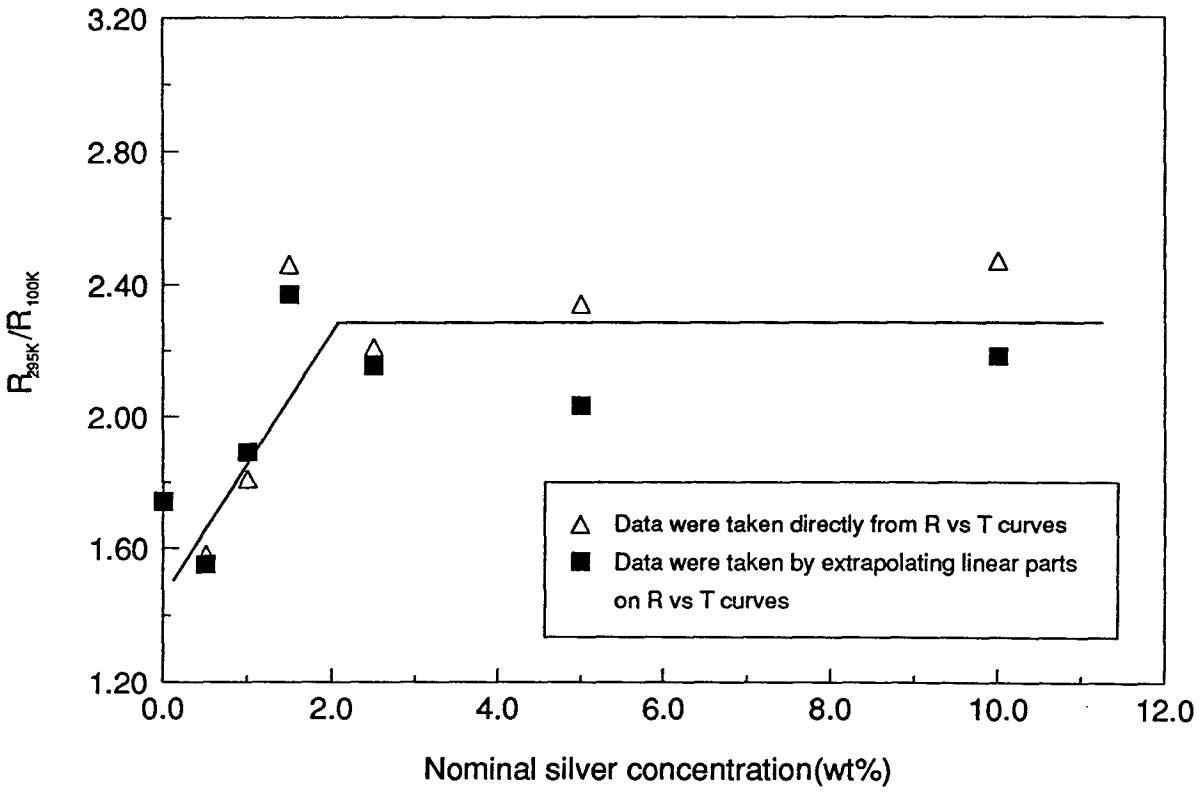

Figure 38 Normalized resistence of $YBa_2Cu_3O_x$+Ag as a function of nominal silver concentration

Table 8 Electrical Properties of Pure and Silver Doped $YBa_2Cu_3O_x$ Compounds

Nominal C_{Ag}(%)	Intragranular C_{Ag}(%)	T_{cm}(K)	J_c(A/cm^2)	R_{295K}/R_{100K}
0	0	90	88	1.74
0.5	0.12	91	92.3	1.70
1.0	0.15	92	42	1.89
1.5	0.26	88	-	1.99
2.5	0.32	89	28	2.15
5.0	0.37	91	72.3	2.03
10	0.37	92	86.3	2.18

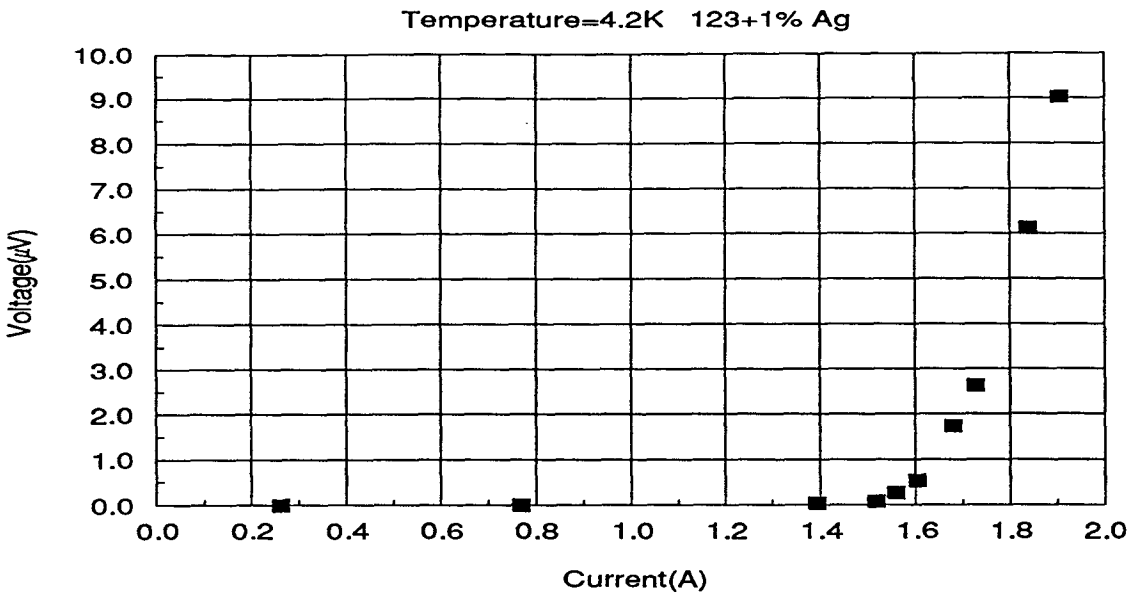

Figure 39 Voltage as a function of electric current of $YBa_2Cu_3O_x$+1.0%Ag

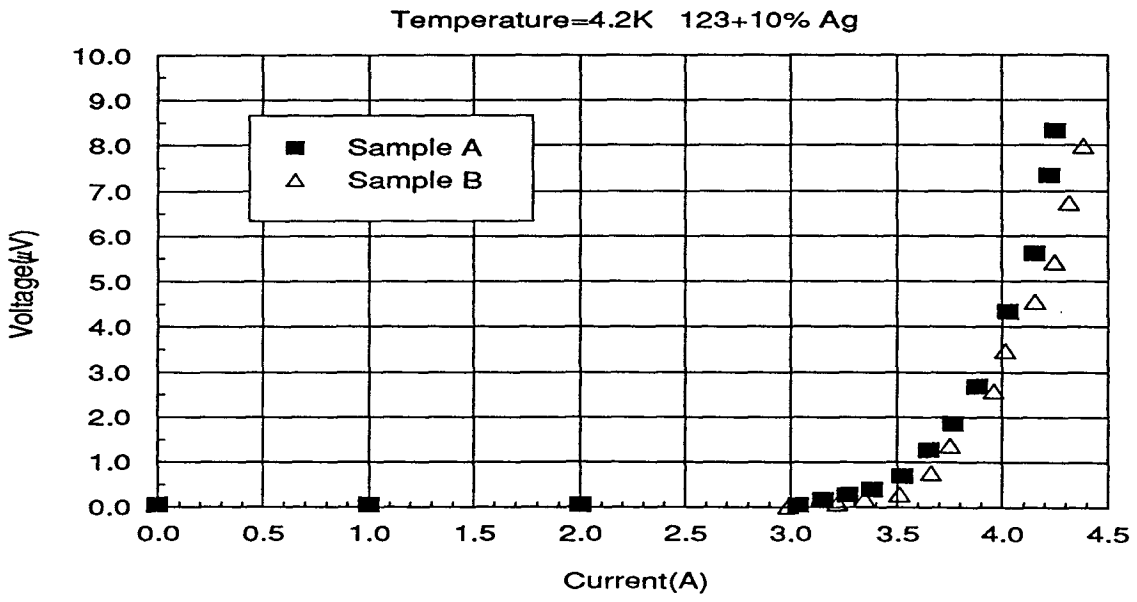

Figure 40 Voltage as a function of electric current of $YBa_2Cu_3O_x$+10%Ag

4 DISCUSSION

4.1 The Preferential Site of Silver Substitution

There is no doubt that silver ions are present within the $YBa_2Cu_3O_x$ lattice, as has been confirmed by the change of the lattice parameters, although the levels of the concentration are very low. The maximum concentration of silver in the $YBa_2Cu_3O_x$ compound is found to be about 0.37 wt% at room temperature. Figure 31 is re-plotted as Figure 41 using the atomic fraction (y) of silver (of $YBa_2Cu_{3-y}Ag_yO_x$). The maximum y value is about 0.023 at room temperature. There are two possible ways that the solid solution may be formed: interstitial or substitutional solid solutions.

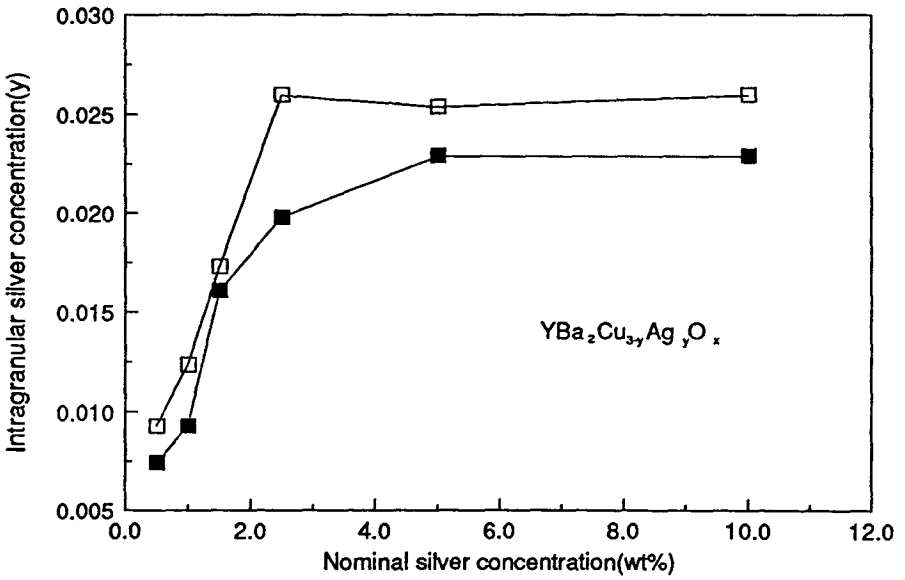

Figure 41 Analyzed silver content as a function of the nominal silver content

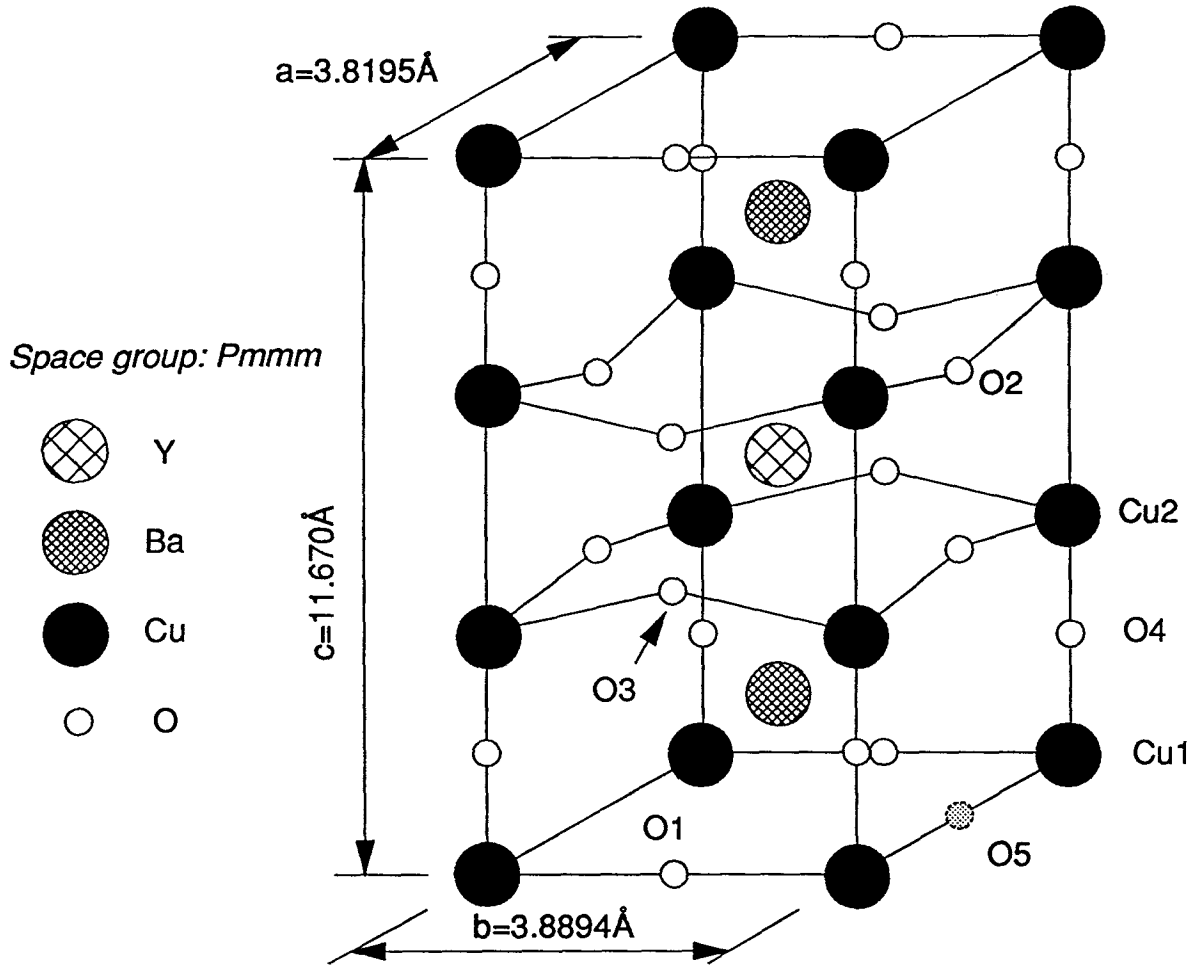

Figure 42 Crystal structure of orthorhombic $YBa_2Cu_3O_7$.

It has been confirmed that the superconductivity of $YBa_2Cu_3O_x$ compound is directly related to its specific crystal structure. Since all doped samples demonstrate clear superconducting properties in the T_c and J_c measurements, the dissolved foreign atoms or ions should not significantly modify the crystal structure of $YBa_2Cu_3O_x$ lattice. The $YBa_2Cu_3O_x$ is derived from the perovskite structure, *i.e.* O^{2-} along with Y^{3+} and Ba^{2+} are close-packed. All equivalent oxygen octahedral interstitial sites are already filled by copper ions and tetrahedral intersititial

sites are empty. The ionic radii (tetrahedral coordination) of silver are 0.89 to 1.14Å, depending on valence and that of oxygen is 1.24Å. By comparing the radius ratio of silver and oxygen ions, it is obvious that if interstitial solid solution were formed, the crystal structure would be totally changed because the oxygen tetrahedra can not accommodate such large silver ions or, at least, the increase of the lattice parameters would be much larger than that has been observed in this study. The radius ratio of the tetrahedral and octahedral sites within oxygen ion packing are 0.225 and 0.414. Therefore the likelihood of silver occupying the interstitial sites is negligible.

For a substitutional solid solution, several possibilities exist. As can be seen in Figure 42, there are four crystallographically distinct cationic sites in a $YBa_2Cu_3O_x$ lattice: Y, Ba, Cu(1) and Cu(2). At the Cu(1) site the valence of the copper ion is +3 with a square coordination (C.N.=4), whereas it is +2 with a pyramidal (C.N.=5) coordination at the Cu(2) site.

Silver has a similar outer shell electron configuration to copper (Ag: $4d^{10}5s^1$ and Cu: $3d^{10}4s^1$) and both of them tend to lose the single electron in the outermost shell to form an ionic bond and may use the s, p and d orbitals of that shell to form co-linear sp, tetrahedral sp^3 or square dsp^2 hybrid bonds. But in spite of the general similarity in the electron structures of their atoms, silver and copper differ very considerably in their chemical behavior.[81] First, the valences exhibited in their common compounds are: Cu, 1 and 2, and Ag, 1. Second, the most stable ion of Cu is the Cu^{2+} ion, whereas that of silver is Ag^+. Both Cu and Ag may be oxidized to the higher valences Cu^{3+}, Ag^{2+} and Ag^{3+}. Unlike Cu, the Ag^{2+} state can only exist in a very strong electrophilic environment, such as in fluorides, *e.g.* AgF_2 in which the Ag^{2+} has an octahedral coordination (C.N.=6). Oxides with Ag^{2+} are rarely found in naturally occurring minerals. This is because Ag^{2+} has a stronger tendency to disproportionate to Ag^+ and Ag^{3+} than

Cu^{2+}. The oxide AgO is actually a $Ag^{I}Ag^{III}O_2$. In AgO, Ag^{I} has two co-linear O neighbors while Ag^{III} has four co-planar O neighbors. This is in contrast with CuO in which all Cu atoms have 4 co-planar O neighbors, *i.e.* square coordination.

As silver is rarely found in the +2 formal valence state in oxides, the probability that silver substitutes Ba^{2+} and/or Cu^{2+} in $YBa_2Cu_3O_x$ lattice is very low. This is coincident with the fact that the only coordinations of Ag^{2+} which have been found are co-planar square (C.N.=4) and octahedral (C.N.=6) whereas the coordination numbers of Ba^{2+} and Cu^{2+} in $YBa_2Cu_3O_x$ are 10 and 5, respectively. Hence, it is reasonable to conclude that the silver ions in the $YBa_2Cu_3O_x$ lattice are trivalent. The preference for square coordination of trivalent Ag makes it very unlikely that Ag/Y substitution will occur. From the above analyses, based on structural chemistry, it can be speculated that if silver substitution occurs anywhere in the $YBa_2Cu_3O_x$ lattice it chooses the Cu(1) site, because of not only the chemical similarity of silver and copper but also, and more importantly, the same coordination environment exists for both silver and copper ions at the Cu(1) site.

This speculation is consistent with the results of the precise determination of lattice parameters in this study. First, the occupancy of oxygen in the orthorhombic phase at O(5) sites on the a axis is very low, only about 0.06[82] and this site is usually thought to be empty for the orthorhombic phase. Therefore, in $YBa_2Cu_3O_7$ the equilibrium distance between Cu(1) ions along a axis, *i.e.* the length of lattice parameter a, is mainly balanced by the coulombic force between these two Cu(1) ions. As Ag^{3+} occupy the Cu(1) sites instead of Cu^{3+}, the increased repulsion force due to larger ion size of Ag^{3+} (0.81Å for Ag^{3+} and 0.68Å for Cu^{3+} with square coordinations[83]) pushes the Ag^{3+} ions apart until a new balance is reached, resulting in an enlargement of the lattice parameter a. Second, it can be found from Table 9 that the Cu(1)-O(4) bond along the c axis is the shortest Cu-O bond in the lattice. This may imply that Cu(1) and

O(4) are strongly bonded and there is little room in this direction to allow any larger substitutional ion. The introduction of larger Ag^{3+} ions might not be completely accommodated and therefore causes a slight increase in the c direction of the lattice whereas these larger ions could be readily accommodated by the O(1) ions on the b axis without significantly changing the bond length. It has been observed[82] that the O(1) is most easily lost upon heating which indicates Cu(1)-O(1) bonds are the weakest. The maximum increase of the lattice parameter c observed in this study is only 0.011Å compared to the bond length difference between Cu(1)-O(1) and Cu(1)- O(4) of 0.11Å. This may suggest that the space along the b direction of the unit cell is big enough to accommodate the Ag-O(1) bonds. Moreover, the facts that at high temperature O(1) ions are completely removed resulting in the tetragonal phase of $YBa_2Cu_3O_6$ and Cu^+ at the Cu(1) site with two-fold coordination, which was found in the isostructure of Ag_2O and Cu_2O, also support the agreement that Cu(1) ions are substituted by silver.

Table 9 Bond Length in $YBa_2Cu_3O_7$[84]

Bond	Length(Å)
Cu(1)-O(1)	1.941
-O(4)	1.831
Cu(2)-O(4)	2.285
-O(2)	1.931
-O(3)	1.955
Ba-O(1)	2.891
-O(2)	2.976
-O(3)	2.963
-O(4)	2.747
Y-O(2)	2.404
-O(3)	2.383

4.2 Impurity Phase and Its Effect on the Electrical Properties

As mentioned earlier, it has been reported[67] that an Ag-O eutectic liquid forms above 931°C, which is lower than the sintering temperature of 950°C used in this study, and dissolves copper from $YBa_2Cu_3O_x$ phase leading to the decomposition of $YBa_2Cu_3O_x$ into the Y_2BaCuO_5 phase. In this study, the Y_2BaCuO_5 phase was detected in all samples containing silver and the amount of the Y_2BaCuO_5 phase increased with increasing nominal silver content. This is also evident from the microstructural observation of this study. Significant amounts of liquid phase can be seen in the quenched samples under the optical microscope(*e.g.* Figure 26e). The non-superconducting liquid and Y_2BaCuO_5 phases accumulated at the grain boundaries and therefore considerably degraded the transport supercurrent at high silver levels resulting in low critical current densities which are observed in this study. Unlike J_c, which is mainly the function of microstructure of a bulk material, critical temperature, T_c, is primarily an intrinsic property and sensitive only to the crystal structure of the superconducting phase. These results suggest that silver can be used beneficially only for low levels of addition.

4.3 Previously Reported Results of Silver Addition to $YBa_2Cu_3O_x$ Compounds

As referred in the introduction, Gangopadhyay and Mason[56] have determined the silver solubility in $YBa_2Cu_3O_{6+x}$. The trend of their EPMA results are similar to the WDX results of this study except that all the analyzed silver contents in their study are higher than those of this study at any given nominal silver content. However, it is worth noting that in both studies the saturation of silver substitution occurs at the nominal concentration of about 3 wt%. The small grain size in their samples may be responsible for the discrepancy. The "average grain size"

reported in their study was in the range between 2 and 6 μm. The authors did not specify the method to determine the "average grain size". It has been well documented that $YBa_2Cu_3O_x$ grains have rectangular cross sections with the (001) plane parallel to the long edge. If the linear intercept method was used as is the usual practice, the average width of these grains would be even smaller depending on the aspect ratio of the grains. Since the effective probe sampling area of electron microanalysis is approximately 1μ in diameter, it is most likely that the incident electron beam hit the grain boundaries surrounding and/or underneath the grain under analysis and generated signals from these silver-rich boundaries leading to exaggerated results.

Both Weinberger, *et al.*[57] and Cahen, *et al.*[84] have measured the lattice parameters of $YBa_2Cu_3O_x$ samples with and without silver doping by X-ray diffraction. The result from the former is that all three crystalline axes of the orthorhombic unit cell expand by about 0.08% for the sample $YBa_2Cu_{2.95}Ag_{0.05}O_x$, whereas the latter claimed that a and b remained constant while the lattice parameter c increases by 0.24% for the sample $YBa_2Cu_{2.977}Ag_{0.023}O_x$. Both of them used only the (200), (020) and (006) lines to calculate the lattice parameters. Lattice parameters may be precisely measured by minimum lines (1 or 2 or 3 lines, depending on the symmetry of the sample to be measured) provided the lines are at a very high angle (θ>80°) and the lines can be clearly resolved.[78] However, (200), (020) and (006) lines of the orthorhombic $YBa_2Cu_3O_x$ phase lie in the range of θ between 22 and 24°. Also, the (006) and (020) peaks are seriously overlapped in the orthorhombic $YBa_2Cu_3O_x$ phase. For example, the 2θ values are 46.633 and 46.725° for (006) and (020) planes in $YBa_2Cu_3O_7$ at room temperature.[85] It is very difficult to separate them by an ordinary X-ray scanning method. Therefore the method employed by these authors to estimate the lattice parameters may not be very accurate.

The similar behaviors of intragranular silver concentration, lattice parameters a and c, volume of the unit cell, and the normalized normal state resistance with the increasing nominal silver concentration observed in this study strongly support that silver is dissolved into $YBa_2Cu_3O_x$ lattice. The different changes in the lattice parameters a, b and c favor that the dissolved silver substitutes copper at the Cu(1) site. The substitution is limited by the large size difference between silver and copper (~19%). The maximum solubility is about 0.37 wt% or 2.3 atomic percent, *i.e.* at that level, the chemical formula of 123 grains is $YBa_2Cu_{2.977}Ag_{0.023}O_x$.

5 SUMMARY AND CONCLUSIONS

1. At a lower level of nominal silver addition, the concentration of silver in the $YBa_2Cu_3O_x$ compound increases with increasing the nominal concentration.
2. Quenched samples always have higher silver contents than annealed samples for all nominal silver concentrations.
3. The solid solubility of silver in $YBa_2Cu_3O_x$ has a saturation level, ~0.37 wt% at room temperature and ~0.41 wt% at 950°C, corresponding to y values 0.023 and 0.025 of $YBa_2Cu_{3-y}Ag_yO_x$, respectively.
4. No matter how low the nominal silver addition is, silver could not be completely dissolved into the $YBa_2Cu_3O_x$ lattice.
5. Lattice constants a and c, as well as the unit cell volume, increase as intragranular silver content increases and have reached constant values at high silver concentration levels. Lattice constant b remains relatively unchanged for all silver concentrations.
6. It is confirmed for the first time by experiments that the dissolved silver ions favorably occupy specific crystallographic sites in the lattice i.e. Cu(1) sites and only Cu^{3+} ions are substituted by dissolved silver ions.
7. Normalized normal state resistance is improved as nominal silver content increases. It also has reached a constant value at high nominal silver concentration levels.
8. Silver addition has little effect on the critical temperature, T_c. The critical current density, J_c is slightly affected. Only small amounts of silver addition can be used beneficially for the improvement of the bulk electrical properties.

6 REFERENCES

1. J.G. Bendnorz and K.A. Müller, 'Possible High T_c Superconductivity in the Ba-La-Cu-O System', *Z. Phys.*, **B64**, 189(1986).

2. M.K. Wu, *et al.*, 'Superconductivity at 93K in a New Mixed-Phase Y-Ba-Cu-O Compound System at Ambient Pressure', *Phys. Rev. Lett.*, **58**, 908(1987).

3. J. Narayan, *et al.*, 'Microstructure and Properties of $YBa_2Cu_3O_{9-\delta}$ Superconductors with Transition at 90 and near 290K', *Appl. Phys. Lett.*, **51**, 940(1987).

4. C.W. Chu, 'Superconductivity above 90K', *Proc. Natl. Acad. Sci. USA*, **84**, 4681(1987).

5. W.H. Poisl, 'Sintering Kinetics of the Superconducting $YBa_2Cu_3O_x$ Compound', M.A.Sc. Thesis, Department of Metals and Materials Engineering, The University of British Columbia, August, 1989.

6. A.C.D. Chaklader, private communication.

7. L. Giaever, 'Energy Gap in Superconductors Measured by Electron Tunneling', *Phys. Rev. Lett.*, **5**, 147(1960).

8. S. Jin, *et al.*, 'Critical Current Density of the $YBa_2Cu_3O_{7-\delta}$ Superconductor as Affected by Microstructural Control', *Mater. Res. Soc. Symp. Proc.*, **99**, 773(1988).

9. L.M. Sheppard, 'Superconductors: Slowly Moving to Commercialization', *Ceramic Bulletin*, **70**, 1479(1991).

10. P. Chaudhari, *et al.*, 'Critical Current Measurements in Epitaxial Films of $YBa_2Cu_3O_{7-x}$ Compound' , *Phys. Rev. Lett.*, **58**, 2684(1987).

11. T.K. Wothington, *et al.*, 'Anisotropic Nature of Hihg-Temperature Superconductivity in Single-Crystal $Y_1Ba_2Cu_3O_{7-x}$', *Phys Rev. Lett.*, **59**, 1160(1987).

12. B. Oh, *et al.*, 'Upper Critical Field, Fluctuation Conductivity, and Dimensionality of $YBa_2Cu_3O_{7-x}$', *Phys. Rev. B*, **37**, 7861(1988).

13. A. Kapitulnik, 'Properties of Films of High-T_c Perovskite Superconductors', *Physica C*, **153-155**, 520(1988).

14. P. Chaudhari, *et al.*, 'Direct Measurement of the Superconducting Properties of Single Grain Boundaries in $YBa_2Cu_3O_{7-\delta}$' , *Phys. Rev. Lett.*, **60**, 1653(1988).

15. D.R. Clarke, 'Issues in the Processing of Cuprate Ceramic Superconductors', *et al., J. Am. Ceram. Soc.*, **72**, 1103(1989).

16. T. Aselage and K. Keefer, 'Liquidus Relations in Y-Ba-Cu Oxides', *J. Mater. Res.*, **3**, 1279(1988).

17. S. Mak and A.C.D. Chaklader,' High Density High-T_c Ceramic Superconductors by Hot Pressing', *J. Can. Ceram. Soc.*, **58**, 52(1989).

18. G. Bussod, *et al.*, 'Effect of Temperature and Strain Rate on the Plastic Deformation of Fully Dense Polycrystalline $Y_1Ba_2Cu_3O_{7-x}$ Superconductor', *J. Am. Ceram. Soc.*, **72**, 137(1989).

19. J.K. Tien, *et al.*, 'Hot Isostatic Pressing (HIP) Densification of Oxide Superconductors', *Proc. SPIE*, **879**, 164(1988).

20. P.K. Gallagher, *et al.*, 'Oxygen Stoichiometry in $Ba_2YCu_3O_x$', *Mater. Res. Bull.*, **22**, 995(1987).

21. J. Tarascon and B. Bagley, 'Oxygen Stoichiometry and the High T_c Superconducting Oxides', *Mater. Res. Soc. Bull.*, **14**, 53(1989).

22. P.K. Gallagher, 'Characterization of $YBa_2Cu_3O_x$ as a Function of Oxygen Partial Pressure, Part I: Thermoanalytical Measurements', *Adv. Ceram. Mater.*, **2**, 632(1987).

23. H.M. O'Bryan and P.K. Gallagher, 'Characterization of $YBa_2Cu_3O_x$ as a Function of Oxygen Partial Pressure, Part II: Dependence of the O-T Transition on Oxygen Content', *Adv. Ceram. Mater.*, **2**, 640(1987).

24. P.S. Nicholson, 'High T_c Superconductors: Principles and Progress', *J. Can. Ceram. Soc.*, **57**, December, 50(1988).

25. K.N. Tu, *et al.*, 'Diffusion of Oxygen in Superconducting $YBa_2Cu_3O_{7-\delta}$ Ceramic Oxides', *Phys. Rev. B*, **39**, 304(1989).

26. K.E. Easterling, *et al.*, 'The Processing, Properties and Applications of Y-Ba-Cu-O Superconductors', *Mater. Forum.*, **11**, 37(1988).

27. M. Tinkham, 'Critical Currents in High T_c Superconductors', *Helv. Phys. Acta*, **61**, 443(1988).

28. R.B. van Dover, 'Pinning Enhancement in $Ba_2YCu_3O_7$', *3rd Cnadian Conference on High Temperature Superconductivity*, Montreal, May 4-5, 1989.

29. A. Lusnikov, *et al.*, 'Mechanical and High-Temperature (920°C) Magnetic Field Grain Alignment of Polycrystalline $(Ho,Y)Ba_2Cu_3O_{7-\delta}$', *J. Appl. Phys.*, **65**, 3136(1989).

30. S. Jin, *et al.*, 'Melt-Textured Growth of Polycrystalline $YBa_2Cu_3O_{7-\delta}$ with High Transport J_c at 77K', *Phys. Rev. B*, **37**, 7850(1988).

31. M.M. Fang, *et al., N. R. Cryogenics*, **37**, March Supplement, 347(1989).

32. G.W. Crabtree, *et al.*, 'Fabrication, Mechanical Properties, Heat Capacity, Oxygen Diffuson, and the Effect of Alkali Earth Ion Substitution on High T_c Superconductors', *Adv. Ceram. Mater.*, **2**, 444(1987).

33. R.F. Cook, *et al.*, 'Fracture Toughness Measurements of $YBa_2Cu_3O_x$ Single Crystals', *Adv. Ceram. Mater.*, **2**, 606(1987).

34. J.P. Singh, *et al.*, 'Effect of Silver and Silver Oxide Addition on the Mechanical and Superconducting Properties of $YBa_2Cu_3O_{7-\delta}$ Superconductors', *J. Appl. Phys.*, **66**, 3154(1989).

35. T. Nishio, *et al.*, 'Superconducting and Mechanical Properties of YBCO-Ag Composite Superconductors', *J. Mater. Sci.*, **24**, 3228(1989).

36. J.P. Singh, *et al.*, 'Mechanical and Superconducting Properties of Sintered Composite $YBa_2Cu_3O_{7-\delta}$ Tape on a Silver Substrate', *Appl. Phys. Lett.*, **53**, 237(1988).

37. G. Kozlowski, *et al.*, 'Critical Current Density Enhancement in $YBa_2Cu_3O_{7-x}$-Silver Composite Superconductor', *Physica C.*, **173**, 195(1991).

38. L.S. Yeou and K.W. White, 'The Development of High Fracture Toughness $YBa_2Cu_3O_{7-x}$/Ag Composites', *J. Mater. Res.*, **7**, 1(1992).

39. Kulik and Omel'yanchuk, 'Properties of Superconducting Microbridges in the Pure Limit', *Sov. J. Low Temp. Phys.*, **3**, 459(1977).

40. V. Ambegaokar & A. Baratoff, 'Tunneling between Supeconductors', *Phys. Rev. Lett.*, **10**, 468(1963).

41. M. Sayer, *et al.*, *Quarterly Report No. 5*, CUICAC Superconductor Consortium, Queen's University, 1990.

42. C.P. Bean, 'Magnetization of Hard Superconductors', *Phys. Rev. Lett.*, **8**, 250(1962).

43. M. Sayer, *et al.*, *Quarterly Report No. 2*, CUICAC Superconductor Consortium, Queen's University, 1989.

44. Y. Hikichi, *et al.*, 'Property and Structure of $YBa_2Cu_3O_x$-Ag Composites Prepared from Nitrate Solution', *Jpn. J. Appl. Phys.*, **29**, L1615(1988).

45. Y. Shapira, *et al.*, 'Magnetization and Magnetic Suspension of $YBa_2Cu_3O_x$-AgO Ceramic Superconductors', *J. Mag. Mag. Mater.*, **78**, 19(1989).

46. M. Itoh and H. Ishigaki, 'Influence of Silver on Critical Current of the Y-Ba-Cu-O Superconductor', *J. Mater. Res.*, **6**, 2272(1991).

47. B. Dwir, *et al.*, 'Critical Current and Electronic Properties of YBCO-Ag Compound', *Physica C.*, **162-164**, 351(1989).

48. B. Dwir, *et al.*, 'Evidence for Enhancement of Critical Current by Intergrain Ag in YBaCuO-Ag Ceramics', *Appl. Phys. Lett.*, **55**, 399(1989).

49. D. Pavuna, *et al.*, 'Electronic Properties and Critical Current Densities of Superconducting $(YBa_2Cu_3O_{6.9})_{1-x}Ag_x$ Compounds', *Solid State Commun.*, **68**, 535(1988).

50. K. Salama, *Processing of High Current $YBa_2Cu_3O_x$ Superconductors*, 3rd Cnadian Conference on High Temperature Superconductivity, Montreal, May 4-5, 1989.

51. P.N. Peters, *et al.*, 'Observation of Enhanced Properties in Samples of Silver Oxide Doped $YBa_2Cu_3O_x$', *Appl. Phys. Lett.*, **52**, 2066(1988).

52. S. Jin, *et al.*, 'Large Magnetic Hysteresis in a Melt-textured Y-Ba-Cu-O Superconductor', *Appl. Phys. Lett.*, **54**, 584(1989).

53. Y. Saito, *et al.*, 'Composition Dependence of Superconductivity on Y-Ba-(Ag, Cu)-O System', *Jpn. J. Appl. Phys.*, **26**, L832(1987).

54. P. Strobel, *et al.*, 'Superconducting Properties of Substituted $YBa_2Cu_{3(1-x)}M_{3x}O_{7-\delta}$', *Solid State Commun.*, **65**, 585(1988).

55. Y. Motsumoto, *et al.*, 'Ag Doping Effect on the Superconduction of $YBa_2Cu_3O_y$ Ceramics', *Mater. Res. Bull.*, **24**, 1231(1989).

56. A.K. Gangopadhyay and T.O. Mason, 'Solubility of Ag in $YBa_2Cu_3O_{6+y}$ and Its Effect on the Superconducting Properties', *Physica C*, **178**, 64(1991).

57. B.R. Weinberger, *et al.*, 'Y-Ba-Cu-O/Silver Composites: An Experimental Study of Microstructure and Superconductivity', *Physica C*, **161**, 91(1989).

58. M. Sayer, *et al.*, *Quarterly Report No. 7*, CUICAC Superconductor Consortium, Queen's University, 1990.

59. C.Y. Huang, *et al.*, 'High Field and Microstructures Studies of Superconducting $nYBa_2Cu_3O_y$:AgO Composites', *Modern Phys. Lett. B*, **3**, 525(1989).

60. C.Y. Huang and M.K. Wu, 'Resistive Transitions of Some Superconducting 123-AgO Composites in High Magnetic Fields', *Modern Phys. Lett. B*, **3**, 805(1989).

61. O. Ishii, *et al.*, 'Reduction of the Surface Resistance of $YBa_2Cu_3O_{7-x}$ Pellets and Thick Films by Adding Ag', *Jpn. J. Appl. Phys.*, **29**, L1075(1990).

62. J.J. Lin, *et al.*, 'Superconducting Property and Structure Studies of $YBa_2Cu_3O_7$-Ag_2O Composites', *Jpn. J. Appl. Phys.*, **29**, 497(1987).

63. O. Laborde, *et al.*, 'Magnetic and Transport Properties of Superconducting $(YBa_2Cu_3O_{7-\delta})_{1-x}Ag_x$ Ceramics', *Physica C*, **162-164**, 827(1989).

64. H.K. Verma, *et al.*, 'Silver-YBCO Composites derived from Citrate Gel', *Supercon. Sci. Technol.*, **3**, 73(1990).

65. M. Miller, 'Improvement of $YBa_2Cu_3O_{7-x}$ Thick Film by Doping with Silver', *et al., Appl. Phys. Lett.*, **54**, 2256(1989).

66. G.G. Peterson, *et al.*, 'Improvement of Polycrystalline Y-Ba-Cu-O by the Addition of Silver', *J. Mater. Res.*, **3**, 605(1988).

67. Loehman, *et al.*, 'Wetting and Reactions between Silver and Bulk $YBa_2Cu_3O_{7-x}$', *Physica C*, **170**, 1(1990).

68. S. Zannella, *et al.*, 'Comparative Study between the Electric and Magnetic Properties and the Grain Boundary Structure of $YBa_2Cu_3O_{7-x}$-Ag_2O Superconductors', *Physica C*, **162-164**, 1179(1989).

69. S. Sen, *et al.*, 'Fabrication of Stable Superconductive Wires with $YBa_2Cu_3O_x/Ag_2O$', *Appl. Phys. Lett.*, **54**, 766(1989).

70. R.A. Outlaw, *et al.*, 'Oxygen Transport through High-Purity, Large-Grain Ag', *J. Mater. Res.*, **3**, 1378(1988).

71. A.C.D. Chaklader, *et al.*, *Quarterly Report No. 8*, CUICAC Superconductor Consortium, University of British Columbia, 1991.

72. R. Castaing, *Advances in Electronics and Electron Physics*, **13**, ed. L. Marton, Academic, New York, 1960, p. 317.

73. H.E. Bishop, 'A Monte Carlo Calculation on the Scattering of Electrons in Copper', *Proc. Phys. Soc.*, **85**, 855(1965).

74. S.J.B. Reed, *X-ray Optics and Microanalysis*, eds. R. Castaing, P. Deschamps and J. Philibert, Hermann, Paris, 1966, p. 339.

75. L.S. Birks, *X-ray Spectrochemical Analysis*, Interscience, New York, 1969.

76. R. Jenkins, *Modern Powder Diffrection, Review in Mineralogy*, **20**, eds. D.L. Bish and J.E. Post, Mineralogical Society of America, Washington, D.C., 1989, p. 57.

77. S.T. Li, *X-ray Diffraction and Electron Microanalysis of Metals*, Metallurgical Press, Beijing, 1980, p. 132.

78. H.P. Klug and L.E. Alexander, *X-ray Diffraction Procedures*, John Wiley and Sons, New York, 1967.

79. B.D. Cullity, *Elements of X-ray Diffraction*, Addison-Wiley, New York, 1969, p. 447.

80. Z.X. Shen, L.A. Frederick and A.C.D. Chaklader, *Superconductivity and Ceramic Superconductors, Ceramic Transaction*, **13**, eds. K.M. Nair and E.A. Giess, The American Ceramic Society, Inc., Westerville, Ohio, 1990, p. 467.

81. A.F. Wells, *Structural Inorganic Chemistry*, 4th ed., Oxford, London, 1975, p. 875.

82. J.D. Jorgensen, *et al.*, 'Oxygen Ordering and the Orthorhombic-to-Tetragonal Phase Transition in $YBa_2Cu_3O_{7-x}$', *Phys. Rev.*, **B36**, 3608(1987).

83. R.D. Shannon, 'Revised Effective Ionic Radii in Halides and Chalcogenides', *Acta Cryst.*, **A32**, 751(1976).

84. D. Cahen, *et al.*, 'Effects of Ag/Cu Substitution in $YBa_2Cu_3O_7$ Superconductors', *Mater. Res. Bull.*, **22**, 1581(1987).

85. A.M.T. Bell, 'Calculated X-ray Powder Diffraction Patterns and Theoretical Densities for Phases Encountered in Investigations of Y-Ba-Cu-O Superconductors', *Supercond. Sci. Technol.*, **3**, 55(1990).

APPENDIX

Selected X-ray Diffraction Data of the Orthorhombic $YBa_2Cu_3O_x$ Phase and the Calculated Lattice Parameters from USGS Computer Program

Table 10 Pure $YBa_2Cu_3O_x$

a=3.8196±0.0005Å	b=3.8883±0.0005Å	c=11.671±0.001Å

hkl	2θ (degree)
003	22.84
100	23.25
102	27.88
013	32.53
103	32.85
110	32.85
112	36.36
005	38.50
113	40.38
020	46.68
006	46.68
200	47.58
210	53.40
121	53.40
123	58.23
116	58.23
213	58.80
026	68.10
108	68.84
206	68.84

Table 11 $YBa_2Cu_3O_x$+0.5%Ag

a=3.8225±0.0004Å b=3.8892±0.0004Å c=11.6763±0.0009Å

hkl	2θ (degree)
002	15.17
003	22.84
100	23.25
102	27.88
013	32.52
103	32.82
110	32.82
112	36.34
005	38.51
113	40.36
020	46.67
006	46.67
200	47.54
115	51.48
123	58.21
116	58.21
213	58.77
026	68.11
108	68.78
206	68.78

Table 12 $YBa_2Cu_3O_x$+1.5%Ag

a=3.8231±0.0004Å b=3.8901±0.0005Å c=11.681±0.001Å

hkl	2θ (degree)
002	15.15
003	22.82
100	23.24
102	27.86
013	32.52
103	32.80
110	32.80
112	36.34
005	38.50
113	40.34
020	46.66
006	46.66
200	47.53
115	51.46
203	53.35
210	53.35
123	58.19
116	58.19
213	58.77
026	68.08
108	68.75
206	68.75

Table 13 $YBa_2Cu_3O_x$+10%Ag

a=3.8247±0.0008Å	b=3.8888±0.0008Å	c=11.681±0.002Å

hkl	2θ (degree)
003	22.81
100	23.21
102	27.81
013	32.53
103	32.81
110	32.81
005	38.50
113	40.33
020	46.69
006	46.69
200	47.51
115	51.41
123	58.20
116	58.20
213	58.75
026	68.08
108	68.75
206	68.75